

Spring 2021

## **Polymer Microparticles for Encapsulation and Presentation Of Anti-inflammatory Agents for Inflammatory Diseases**

Christopher Isely

Follow this and additional works at: <https://scholarcommons.sc.edu/etd>

 Part of the [Chemical Engineering Commons](#)

---

### **Recommended Citation**

Isely, C.(2021). *Polymer Microparticles for Encapsulation and Presentation Of Anti-inflammatory Agents for Inflammatory Diseases*. (Doctoral dissertation). Retrieved from <https://scholarcommons.sc.edu/etd/6229>

This Open Access Dissertation is brought to you by Scholar Commons. It has been accepted for inclusion in Theses and Dissertations by an authorized administrator of Scholar Commons. For more information, please contact [digres@mailbox.sc.edu](mailto:digres@mailbox.sc.edu).

POLYMER MICROPARTICLES FOR ENCAPSULATION AND PRESENTATION OF  
ANTI-INFLAMMATORY AGENTS FOR INFLAMMATORY DISEASES

by

Christopher Isely

Bachelor of Science  
Iowa State University, 2016

---

Submitted in Partial Fulfillment of the Requirements

For the Degree of Doctor of Philosophy in

Chemical Engineering

College of Engineering and Computing

University of South Carolina

2021

Accepted by:

Robert Michael Gower, Major Professor

Mark Uline, Committee Member

Esmail Jabbari, Committee Member

Qian Wang, Committee Member

Melissa Moss, Committee Member

Tracey L. Weldon, Interim Vice Provost and Dean of the Graduate School

© Copyright by Christopher Isely, 2021  
All Rights Reserved.

## ACKNOWLEDGEMENTS

I have to first acknowledge my major professor, Dr. Michael Gower, who has been so influential in developing my skills as a scientist, and my way of thinking critically about the world. Second, I have to acknowledge my family, my mom Mary Lee Isely, my dad Karl Isely, and my brother Kevin Isely. Without your support I wouldn't have made it through the last five years. Next, I have to acknowledge my colleagues Michael Hendley and Kendall Murphy who were with me the whole time, and whose mentorship meant so much to me. Next, the current PhD students Kido Atube, Candice Cheung and Nick Colonna, who have provided so much companionship and support. To the undergrads who I had the privilege of mentoring, Maddie Spetz, Alex Stevens and Christine Steege for helping me with so many tasks and being a sounding board for a lot of my ideas. To my friends, Joe Lopata, Charles Fricke and Greg Tate who studied with me and kept me laughing on the weekends. And to all the friends and family not named here who supported me through this process, I thank you. The last five years have had its ups and downs, but I wouldn't have done anything differently.

## ABSTRACT

Inflammatory diseases have a huge economic impact on the healthcare system. Incidence of obesity and muscle atrophy, two high-profile inflammatory diseases, continues to increase, and anti-inflammatory agents are potential therapeutics for these diseases. Resveratrol is a polyphenol that has anti-inflammatory effects; however, resveratrol suffers from low bioavailability and hasn't had impressive clinical results when delivered orally. Mannose is a monosaccharide that also has anti-inflammatory effects, however, effects are highest when mannose is presented on the surface of a support the size of a bacteria. Incorporation of resveratrol and mannose into biodegradable polymer microparticles could be a feasible approach to overcome these drawbacks for treating inflammatory diseases. The most commonly used polymer for FDA approved microparticle formulations is poly(lactide-co-glycolide) (PLG) and the most common fabrication technique is the oil in water (O/W) emulsion solvent extraction method. The objective of this work was to fabricate and optimize resveratrol-encapsulated and mannose-presenting PLG particles using the O/W emulsion solvent extraction method, and to study particle effects on cells involved in inflammation.

Here, we show resveratrol can be encapsulated in PLG microparticles to a high extent and particles decrease lipid load in adipocytes grown in culture. We found that incorporation of resveratrol in the particle formation process causes nonspherical morphology, which is notable because stable emulsions are known to form spheres. Nonspherical morphology was dependent primarily on resveratrol and cosolvent

concentration, and it was found that nonspherical morphology was unique to resveratrol among several stilbene small molecules. Nonspherical morphology of particles has been shown to have biological implications, and addition of resveratrol to oil in water emulsions could be a simple method for conveying nonspherical morphology to particles fabricated with an already FDA approved method.

Many bioactive agents, such as mannose, bind cell surface receptors, and PLG particles can act as a support for these agents to promote cell signaling. Mannose was attached to the surface of PLG microparticles using a novel process. We chemically modified poly(vinyl alcohol) (PVA) using isothiocyanate chemistry and used this PVA as the emulsifier in the fabrication system, which will spontaneously coat the surface of particles. Mannose-presenting particles bound macrophages, colocalized with the mannose receptor and directed macrophages to secrete factors that led to increased myotube formation, a key step in muscle regeneration. This process can be used as a new method for achieving surface functionalization and for treating inflammatory diseases.

Taken together, this work demonstrates the versatility of PLG as an immune modifying material. This work also demonstrates a new method for tuning morphology of polymer particles using resveratrol in the O/W emulsions, and a new method for attaching surface ligands through modifying PVA. In addition to treating obesity and muscle atrophy, adding resveratrol to PLG particles for tuning morphology and using PVA for surface functionalization are innovations that could be easily implemented in already FDA approved formulations, and could have far-reaching applications in this growing sector of the pharmaceutical industry.

## TABLE OF CONTENTS

Acknowledgements .....	iii
Abstract .....	iv
List of Tables .....	vii
List of Figures .....	viii
Chapter 1: Background and Significance .....	1
Chapter 2: Development of Microparticles for Controlled Release of Resveratrol to Adipose Tissue and the Impact of Drug Loading on Particle Morphology and Drug Release .....	10
Chapter 3: Fabrication of Biodegradable Particles with Tunable Morphologies by the Addition of Resveratrol to Oil in Water Emulsions .....	42
Chapter 4: Development of Modified PVA for Surface Functionalizing PLG Microparticles for Macrophage Targeting and Signaling .....	72
Chapter 5: Concluding Remarks and Future Directions .....	95
References .....	101
Appendix A: PLG Particle Fabrication Best Practices .....	117
Appendix B: Manuscript Permissions .....	121

## LIST OF TABLES

Table 3.1 Conditions used for resveratrol particle formulations .....	46
Table 3.2 Surface area measurements of low surface area silica standard .....	50
Table 3.3 Solvent properties .....	58
Table 4.1 Reaction trials of ITC modifiers with PVA .....	82



## LIST OF FIGURES

Figure 2.1. The effect of ethanol on particle mass yield and size.....	20
Figure 2.2. Morphology of resveratrol loaded PLG particles .....	22
Figure 2.3. The effect of resveratrol loaded particles on adipocyte lipid content .....	24
Figure 2.4. In vitro release profiles of resveratrol particles .....	25
Figure 2.5. The effect of resveratrol concentration on particle morphology .....	26
Figure 2.6. The effect of PVA concentration on particle morphology .....	27
Figure 2.7. Confocal imaging of particles made with FITC-PVA.....	28
Figure 2.8. Flow cytometry of resveratrol particles made with FITC-PVA .....	29
Figure 2.9. The effect of homogenization time and speed on particle size .....	30
Figure 2.10. Effect of particle diameter on drug loading and particle mass yield .....	31
Figure 2.11. The effect of particle size on resveratrol release .....	33
Figure 2.12. A comparison of particle size distribution using dynamic light scattering (DLS) and image analysis.....	38
Figure 2.13 Particle size analysis of polystyrene beads measured with light microscopy .....	38
Figure 2.14 Representative standard curve for resveratrol .....	39
Figure 2.15 Light microscopy of RSV particles pre and post lyophilization .....	39
Figure 2.16 Resveratrol standard curve via HPLC .....	40
Figure 2.17 Flowability of resveratrol particles.....	40
Figure 2.18 SEM image of particles fabricated with 5% PVA in the emulsion .....	41

Figure 3.1 Images from video microscopy of particle formation with corresponding SEM images .....	52
Figure 3.2 X-ray diffraction of resveratrol and PLG particles.....	53
Figure 3.3 Effect of ethanol and resveratrol on sessile drop formation .....	54
Figure 3.4 Effect of resveratrol-like molecules on particle morphology .....	56
Figure 3.5 Relative contributions of ethanol and resveratrol on particle morphology .....	57
Figure 3.6 The effect of cosolvent on particle morphology.....	59
Figure 3.7 Effect of ethyl acetate on particle morphology .....	60
Figure 3.8 Morphology of PCL and PLLA particles made with resveratrol .....	61
Figure 3.9 Coumarin 6 encapsulated crumpled particles formed with resveratrol.....	63
Figure 3.10 Nonspherical particles separated by size using differential centrifugation.....	64
Figure 4.1 Synthesis of modified poly(vinyl alcohol)... ..	82
Figure 4.2 Characterization of FITC-PVA .....	84
Figure 4.3 Characterization of MITC-PVA .....	85
Figure 4.4 Imaging of PLG particles made with modified PVA .....	87
Figure 4.5 Binding of MITC particles by RAW 264.7 cells.....	88
Figure 4.6 Colocalization of MR with MITC-PVA particles.....	89
Figure 4.7 Effect of conditioned media on myotube formation.....	90
Figure B.1 Copyright permissions for publications reprinted in this dissertation .....	121

# CHAPTER 1

## BACKGROUND AND SIGNIFICANCE

### 1.1 Inflammatory Diseases

Inflammation is associated with a vast array of conditions, including cardiovascular disease, type 2 diabetes, cancer, obesity and muscle atrophy<sup>1</sup>. Inflammatory states can potentiate the disease itself, such as in the case of obesity and muscle atrophy<sup>2,3</sup>. It is still not completely understood why inflammation is associated with these diseases<sup>1</sup>, but it is recognized that anti-inflammatory therapies can be beneficial in treating obesity and muscle atrophy, which are highly prevalent in the U.S.

Obesity is an inflammatory disease that is a comorbidity to many of the leading causes of death in the U.S.<sup>4</sup>. Obesity is defined as a body mass index over 30 and is considered an epidemic in the United States according to the CDC<sup>5</sup>. The healthcare costs of treating the disease were \$147 billion in 2008. By 2017 and 2018 42.4% of the American population was obese, which was an increase of 36% from as recently as 2014<sup>5</sup>. New treatment methods and approaches are needed for this public health crisis. Obesity is characterized by an increase in size and number of fat cells (adipocytes) in body fat (adipose tissue) and also inflammation which potentiates the disease<sup>6</sup>. Treatment strategies for obesity currently include diet and exercise, prescription medication, and invasive surgery -- in that order depending on the severity of the case<sup>4</sup>. Each of these treatments suffers from downsides: diet and exercise changes typically suffer from low compliance;

prescription medications so far have resulted in bad side effects; and invasive surgery is typically considered a last resort. As such, new strategies are being developed to address some of these drawbacks<sup>7,8</sup>. Treating the adipose tissue with anti-inflammatory drugs may have positive outcomes in obesity. However, many anti-inflammatory drugs are hydrophobic molecules that have low solubility and low bioavailability<sup>8</sup>. New methods are needed for delivering anti-inflammatory drugs to the adipose tissue.

Muscle atrophy, the loss of muscle mass, is also a condition that is characterized by inflammation<sup>9</sup>. Sarcopenia is the type of muscle atrophy associated with aging<sup>10</sup>. An often-cited report suggested sarcopenia cost the U.S. \$18 billion in 2000 which was 1.5% of total healthcare costs<sup>11</sup>. Muscle injuries have increased over the last 20 years, especially as the U.S. population ages and more elderly patients require healthcare services<sup>12</sup>. Current treatment strategies for muscle atrophy include exercise and several supplements such as Vitamin D<sup>13</sup>. Few treatment strategies exist beyond exercise and supplements, and when they fail there are not many options. Therefore, muscle atrophy is a condition that needs more attention and treatment strategies.

## **1.2 Macrophages and inflammatory diseases**

Macrophages play vital roles in almost all tissues in terms of regulating inflammation, hormone levels and general homeostasis<sup>14</sup>. They are incredibly plastic and functionally diverse, owing to their need to be phagocytic in some cases and regenerative in others<sup>15</sup>. In some inflammatory disease states it is thought that an effective treatment could be to induce macrophages to become more anti-inflammatory<sup>16</sup>.

Many methods have been studied for inducing anti-inflammatory phenotype in macrophages, primary among them is treatment with Interleukin 4 (IL-4)<sup>17</sup>. However, IL-

4 treatment is not a very translatable approach, as recombinant IL-4 (and other cytokines) are expensive and bolus injections of proteins are metabolized quickly and can have toxic effects<sup>18,19</sup>. A simple option is to administer anti-inflammatory small molecules that have similar effects as IL-4. Another method for inducing an anti-inflammatory phenotype in macrophages is activating the mannose receptor (MR) (also known as CD206)<sup>20</sup>. MR is activated by the monosaccharide mannose, and MR clustering was shown to promote anti-inflammatory cytokine secretion in macrophages<sup>21</sup>. “Reprogramming” macrophages into an anti-inflammatory phenotype using anti-inflammatory compounds for treatment of diseases such as obesity and muscle atrophy is a concept that could have promise but has not been fully studied.

One such anti-inflammatory compound that could benefit inflammatory diseases is resveratrol. Resveratrol is a natural polyphenol found in wine, grapes and peanuts<sup>22</sup>. It is thought to be the compound that gives wine beneficial properties<sup>23</sup>. Resveratrol is an anti-inflammatory and antioxidant compound, and it has also recently been shown to be an exercise mimetic<sup>24,25</sup>. Resveratrol was shown to reduce body fat and improve glucose tolerance in mice<sup>26</sup>. It has also had delipidating effects in adipocytes grown in vitro<sup>27</sup>. However, resveratrol has problems with low bioavailability in humans and has required large doses in clinical trials<sup>28,29</sup>. Walle et al. found that after a 25 mg dose of resveratrol was consumed, only 5 ng/mL of resveratrol could be detected in the plasma. New methods are needed to achieve therapeutic levels of resveratrol in the target tissues for treatment of inflammatory diseases.

### **1.3 Biodegradable Polymer Microparticles for Biomedical Applications**

Biodegradable polymer microparticles were developed as drug delivery vehicles in the 1970s to improve the delivery of drugs with low solubility, low bioavailability, toxic effects and other barriers to oral administration<sup>30</sup>. In these systems, a drug is encapsulated in a biocompatible, biodegradable polymer that breaks down in the body, and the drug is released in a controlled manner<sup>31</sup>. At the time of their development, long-term (months to years) controlled release of drugs was out of reach, and these particles were some of the first to show that it was possible<sup>32</sup>. Since then, the drug delivery field has exploded with interest in polymer particles, and new formulations and methods of fabrication are developed every year<sup>33</sup>. The global advanced drug delivery systems market was estimated to be \$178 billion as of 2015 and estimated to grow to \$227 billion as of 2020<sup>34</sup>. Interest in these systems is expected to grow further, as the population ages and new treatment technologies are needed every year. This platform has proven itself useful and clinically relevant. The work presented in this dissertation focuses on delivery of resveratrol and mannose for therapeutic applications such as obesity and muscle atrophy, along with some innovations to polymer microparticle morphology and functionality.

Poly lactic acid (PLA) and poly glycolic acid (PGA) were some of the most successful and early polymers to be used as polymer microparticle delivery vehicles<sup>35,36</sup>. These polymers had found earlier uses as resorbable medical devices such as sutures, stents and structural meshes<sup>37</sup>. As a result, some groups repurposed them as drug delivery vehicles<sup>38</sup>. PLA, PGA and their copolymer poly(lactide-co-glycolide) PLG were found to be biocompatible and could degrade in water, allowing them to be used when a biomaterial is needed for a period of time, but after a while could be resorbed by the body and not

require surgical removal<sup>39</sup>. These, and other polyesters, degrade via hydrolysis of the ester bond, and their degradation patterns have been well established<sup>40–42</sup>. PLG microparticle formulations for drug delivery advanced to clinical trials during the 1980s, and Lupron Depot was FDA approved in 1989<sup>43</sup>. Since then, around 20 PLG-based microparticle formulations have achieved FDA approval<sup>44</sup>. Although 20 PLG-based formulations is impressive, one review article suggests this number should be much higher, as there are many more than 20 drugs that could benefit from PLG encapsulation<sup>44</sup>. Although encapsulation of drugs in polymer particles is a fairly simple concept, producing microparticles with desired effects is challenging<sup>45–47</sup>.

Many particle characteristics need to be considered and controlled in order to make reproducible and optimized particles. For example, previous work has shown that particle size<sup>48</sup>, particle shape<sup>49</sup>, polymer composition<sup>41</sup>, molecular weight<sup>42</sup>, degradation rate<sup>39</sup> and drug release rate<sup>50</sup> are all very important response variables in particle production. To achieve control over these response variables, parameters of fabrication techniques need to be tuned in precise ways. Many efforts have been made to improve control of many of these variables, such as size and drug release, where complicated fabrication methods were required for precise control<sup>46,51</sup>.

#### **1.4 Oil in Water (O/W) emulsion solvent extraction method**

There are many ways to fabricate polymer microparticles for drug delivery, such as emulsion-based formation, spray drying, phase separation and solvent casting<sup>52,53</sup>. Among these, the O/W emulsion solvent extraction/evaporation method is the most commonly used for drugs with low water solubility<sup>45,54,55</sup>. The O/W emulsion solvent extraction/evaporation method involves dissolving the polymer in an organic solvent

(dispersed phase) and an emulsifier in water (continuous phase). These two phases are homogenized at high speed and a primary emulsion is formed. This emulsion is added to the aqueous phase, which extracts the organic solvent and, in some cases, promotes evaporation of the organic solvent. This causes the polymer to precipitate into microparticles, stabilized by an emulsifier. These particles can then be lyophilized into a powder and stored in dry conditions for long periods (months to years) before delivery. FDA-approved particles such as Vivitrol and Lupron Depot use this fabrication method for injectable microparticles for systemic delivery of agents<sup>56,57</sup>. As a result, this method has a track record of FDA approval, and new concepts for particle design could build off the O/W emulsion solvent extraction technique and receive a smoother approval process. Many drugs have been encapsulated with this method in the literature<sup>54,58</sup>, but there are still many drugs that have not been studied.

### **1.5 Opportunities for innovation on biodegradable polymer microparticles**

Although biodegradable polymer particles were initially conceived as drug delivery vehicles, they can be useful for other purposes as well. They can be used as supports for presenting bioactive agents or ligands to the surface of cells<sup>59</sup> and have also been used as novel vaccine carriers<sup>31,60</sup>. In this dissertation, the focus will be on their usefulness as drug delivery vehicles and as supports for ligand-receptor interactions. Morphology and surface functionality are two parameters of polymer particles that have been shown to be of importance to the cell-material interaction of particles in the body. Morphology and surface functionality are also addressed closely in this dissertation.

Morphology of particles can affect the host response to biomaterials<sup>61</sup>. Despite this, relatively few studies fabricating PLG particles have taken into account the effect of the



morphology of the particles on biological responses<sup>49,62</sup>. The default morphology of a polymer particle is a smooth sphere due to the way the particle is formed in the O/W emulsion system. In an emulsion, a sphere is the shape that is thermodynamically favorable and other shapes are difficult to achieve without disrupting the stability of the emulsion<sup>63</sup>. Some other methods have been employed to produce particles of varying morphologies. Flow lithography was used to produce particles with wrinkled morphology, and these particles were tested in vitro for their interaction with cells. It was found the wrinkled particles interacted more readily than spherical particles<sup>64</sup>. This suggests that morphology is a key parameter of interest in particle-cell interactions.

Surface functionality is also an aspect of polymer particles that has a large effect on cell-material interactions. Efforts to modify the surface of PLG particles came about not long after the first PLG particles were designed<sup>65</sup>. Attaching surface ligands to PLG particles was proposed as a way to target cells of interest or even to promote cellular signaling through receptor activation<sup>66</sup>. Most methods for surface ligand attachment require many steps and harsh chemicals. Methods that involve one-step reactions and milder chemistry may result in more readily FDA approved formulations.

Taken together, there are many areas in the field of polymer microparticle formation to be optimized, including testing new drugs such as resveratrol for their effect on adipose tissue, and importance of developing methods to tune morphology and surface functionality using components in FDA approved systems.

#### *1.5.1 Aim 1: Develop microparticles for resveratrol delivery to adipose tissue*

Previous groups have encapsulated resveratrol to improve bioavailability<sup>28,67</sup>, but none have, to our knowledge, considered delivering resveratrol in microparticles to the

adipose tissue. We propose that PLG particle delivery of resveratrol to the adipose tissue could improve the bioavailability, and that these particles can be easily tuned for size using parameters of the oil in water emulsion solvent extraction method. Our hypothesis was that PLG microparticles could be loaded with resveratrol to a high extent, and that the resveratrol would be bioactive and cause delipidation in adipocytes. In this aim we find that not only can resveratrol be loaded into PLG particles to a high extent, it is also bioactive in that it causes lipid mobilization in adipocytes grown in culture. We also show that resveratrol causes morphology changes in PLG particles dependent on resveratrol and emulsifier concentration<sup>68</sup>.

#### *1.5.2 Aim 2: Understand the impact of resveratrol on morphology of PLG particles*

In this aim our objective was to study the effect on morphology of PLG particles using resveratrol as a secondary emulsifier. We find that adding resveratrol to O/W emulsions affects the morphology of PLG particles<sup>68</sup>. Morphology is a poorly studied but, by all accounts, impactful aspect of particle-based drug delivery to cells and tissue<sup>49,69</sup>. Particles have been shown to adhere more readily to wrinkled particles<sup>64</sup>. Particles with distinct morphologies are shown to elicit different immune responses<sup>70</sup>. In this aim we show that resveratrol causes distinct effects on the morphology of PLG particles after being added to the emulsion, and that this is cosolvent and resveratrol concentration dependent<sup>71</sup>.

### **1.6 Using modified PVA for surface functionalization of PLG particles for macrophage targeting**

Many methods for functionalizing the surface of PLG particles have been studied in the literature<sup>72,73</sup>. Simple adsorption processes for attaching ligands have been used, as well as complex chemistries. Most chemical modifications involve modifying PLG after

particle fabrication. Utilizing the concept of PVA adsorption on the surface of PLG microparticles<sup>74</sup>, we sought to chemically modify PVA, and use modified PVA in the PLG particles fabrication process. A major benefit of this process is that characterization of the product is simpler, as characterization occurs prior to forming the particle.

*1.6.1 Aim 3: Designing functionalized PLG particles to induce anti-inflammation in macrophages for treatment of muscle atrophy*

Mannose is a ligand for mannose receptor in macrophages that has potential use as a targeting moiety in polymer particles<sup>75</sup> and that can also cause cell-signaling events<sup>76</sup>. In fact, many groups have used mannose as a surface functionalizing group to target and signal to macrophages in vitro and in vivo<sup>77-80</sup>. We proposed that modifying PVA for functionalizing PLG particles would be a simpler and milder approach for surface presentation of ligands such as mannose.

We hypothesize that PLG particles can be functionalized using mannose modified PVA to induce anti-inflammation for treatment of muscle atrophy. In this aim we show that PLG particles can be successfully functionalized with modified PVA via NMR analysis and confocal microscopy. We also show that mannose attached to PLG particles is functional and that it induces mannose receptor colocalization. In addition, media conditioned with macrophages treated with mannose functionalized particles induced myotube fusion in vitro. The work in this aim demonstrates the potential in PVA modification for surface functionalizing PLG particles and mannose receptor activation as a potential treatment option for muscle atrophy.

## CHAPTER 2

# DEVELOPMENT OF MICROPARTICLES FOR CONTROLLED RELEASE OF RESVERATROL TO ADIPOSE TISSUE AND THE IMPACT OF DRUG LOADING ON PARTICLE MORPHOLOGY AND DRUG RELEASE<sup>1</sup>

### 2.1 Introduction

Resveratrol is a polyphenolic compound occurring in various plants, including grapes, berries, and peanuts<sup>22</sup>, as a defense mechanism against environmental stresses such as infections and ultraviolet radiation<sup>81</sup>. A remarkable range of biological functions are attributed to this molecule. For example, it acts as a cancer prevention agent<sup>82</sup>, an anti-inflammatory<sup>83</sup>, and an antioxidant<sup>84</sup>. More recently, it has been identified as an anti-obesity compound<sup>26,85</sup>. It exerts this effect by activating signaling pathways in fat cells that are also activated by energy restriction (i.e. dieting)<sup>26</sup>. The result is an increase in lipolysis and fatty acid oxidation that leads to a reduction in body fat<sup>86</sup>. Unfortunately, resveratrol suffers from poor bioavailability, requiring large and frequent doses, thereby hampering its vast therapeutic potential<sup>29,87</sup>.

---

<sup>1</sup> Isely, C., Hendley, M.A., Murphy, K.P., Kader, S., Annamalai, P., Jabbari, E., and Gower, R.M. 2019. *International Journal of Pharmaceutics*. 568: 118469. Reprinted here with permission of publisher.

Resveratrol is generally administered orally, but extensive first pass metabolism results in the molecule's low concentration in the systemic circulation and accumulation in tissues<sup>88</sup>. To address this issue, we are developing biodegradable microparticles as drug depots for controlled release of resveratrol within fat tissue. Goals for this study were maximizing drug loading to decrease the mass of carrier delivered, limiting particle size to a range above 5 microns to inhibit phagocytic clearance, and producing drug release profiles with a duration expected to sustain resveratrol at levels observed in the adipose tissue in rats fed a diet laced with resveratrol<sup>89</sup>. While microcarriers have been investigated for controlled release of resveratrol previously, they were designed to release resveratrol quickly to the gut<sup>90</sup>, skin<sup>91</sup>, or nasal mucosa<sup>92</sup>. In those previous studies, total drug release occurs in hours to days, which is too short for our applications. In effort to extend release duration, we have selected a relatively high molecular weight poly(lactide-co-glycolide) copolymer that is 75% lactide as the drug carrier. We have extensive experience with this polymer formulation and know that it integrates well with the adipose tissue<sup>93-95</sup>. Single emulsion/solvent evaporation was utilized to encapsulate resveratrol within the polymer matrix.

Herein, we describe surprising effects of resveratrol on particle morphology and demonstrate how resveratrol loading and release can be controlled by changing particle size. Finally, we report a simple approach, with mild chemistry, to functionalize poly(vinyl alcohol) with fluorescein, which enabled visualization of resveratrol's impact on particle surface chemistry.

## 2.2 Materials and Methods

### 2.2.1 Materials

75:25 poly (D,L-lactide-co-glycolide) with a lauryl ester end group and an inherent viscosity of 0.79 dL/g was purchased from Evonik. Dichloromethane, resveratrol, poly (vinyl alcohol) (Mw 13,000-23,000, 87-89% hydrolyzed), and fluorescein isothiocyanate were purchased from Sigma (St. Louis, MO). 200 proof ethanol was purchased from Decon Laboratories (King of Prussia, PA). Dimethyl sulfoxide (DMSO) was purchased from Fisher (Hampton, NH). Ultrapure water was obtained from a Thermo Scientific Barnstead Nanopure system. 3T3-L1 mouse embryonic fibroblasts (CL-173) were purchased from ATCC (Manassas, VA). Dulbecco's Modified Eagle's Medium (DMEM) with 4.5 g/L glucose and L-glutamine was purchased from Corning Cellgro (Corning, NY). Trypsin with 0.25% EDTA, Fetal Bovine Serum (FBS) and Pen/Strep were purchased from Fisher (Hampton, NH). Super Calf Serum was purchased from GemCell (Sacramento, CA). Insulin (bovine), dexamethasone, and methylisobutylxanthine (IBMX) were purchased from Sigma (St. Louis, MO).

### 2.2.2 Resveratrol Loaded PLG Particle Fabrication

Poly(lactide-co-glycolide) (PLG) particles were prepared using a single oil-in-water emulsification/solvent evaporation method as described previously with modifications<sup>95</sup>. Briefly, PLG was dissolved in dichloromethane (DCM) at 6% (weight/weight, hereafter labeled as 6%) and resveratrol (Sigma) was dissolved in 100% ethanol at 40 mg/mL. The organic phase, which consisted of varying volume ratios of ethanol and DCM, was added to an aqueous solution of polyvinyl alcohol (PVA) at 1 or 2% (weight/volume, hereafter labeled as 1 or 2%) in a 1:7 volume ratio and homogenized

using a Kinematica PT3100D homogenizer. The emulsion was then added to an aqueous solution of PVA and stirred for 5 hours, allowing the DCM and ethanol to evaporate and the particles to harden. The volume of PVA solution in the solvent evaporation beaker was 5 times greater than the emulsion mixture. The particles were then passed through a 40  $\mu\text{m}$  filter, collected via centrifugation, and washed 4 times in ultrapure water. Particles were frozen at  $-20^{\circ}\text{C}$  and lyophilized overnight. Particles were then stored protected from light, under vacuum, at room temperature.

### *2.2.3 Scanning Electron Microscopy and Light Microscopy*

Carbon adhesive tape was attached to aluminum SEM stubs and particles were spread onto the stubs. Compressed air was applied briefly to the particles to create a monolayer on the carbon tape. Particles were sputtered with gold 3 times for 60 seconds in a Denton Desk II Vacuum sputter coater. Images were taken using a TESCAN Vega3 Scanning Electron Microscope at 10kV.

Light microscopy images were taken on an EVOS FL microscope at 20x. Particles were prepared in ultrapure water and suspended at a concentration of 0.25 mg/mL. 400  $\mu\text{L}$  of these suspensions was added to a 48-well plate and allowed to settle prior to image acquisition.

### *2.2.4 Measurement of Particle Size Distribution*

Particle size distribution for each batch of particles was determined by analyzing light microscopy images with ImageJ software. Briefly, three representative images were acquired and converted to binary. The ImageJ Particle Analysis plugin-in was used to measure particle diameter. The size data was then plotted as a histogram with a 5  $\mu\text{m}$  bin-width. We report the mean particle diameter and the coefficient of variation (CV%), which

is the standard deviation divided by the mean. We validated our image analysis method with dynamic light scattering (Figure 2.12) and with monodispersed polystyrene particles that were obtained from Duke Standards (Figure 2.13).

#### 2.2.5 Mass Yield, Resveratrol Loading, and Encapsulation Efficiency

Particle mass yield was calculated according to equation 1.

$$\text{Mass Yield (\%)} = \left( \frac{M_{PT}}{M_{PLG} + M_{RE}} \right) * 100 \quad (1)$$

Where  $M_{PT}$  is the mass of particles recovered from the emulsion,  $M_{PLG}$  is the mass of PLG added to the emulsion, and  $M_{RE}$  is the mass of resveratrol added to the emulsion.

Resveratrol loading was determined via UV-Vis by dissolving resveratrol particles in DMSO and measuring absorbance at 330 nm using a Spectramax 190 UV-Vis spectrophotometer. A 10-point standard curve was prepared by dissolving 1 mg of empty particles and a known mass of resveratrol in DMSO. Figure 2.14 depicts a typical standard curve. Resveratrol concentration was determined by comparing the unknown samples to the standard curve. Resveratrol loading was calculated by equation 2.

$$\text{Loading} \left( \frac{\mu\text{g}}{\text{mg}} \right) = \frac{M_R}{M_P} \quad (2)$$

Where  $M_P$  is the mass of particles dissolved in DMSO and  $M_R$  is the mass of resveratrol measured in those particles.

Efficiency of resveratrol loading into the particles was calculated by first calculating the theoretical amount of resveratrol loaded into an entire batch of particles (particle loading multiplied by the mass of particles recovered from the emulsion) and then dividing that number by the amount of resveratrol added to the emulsion as depicted in equation 3.



$$Efficiency (\%) = \left( \frac{Loading * M_{PT}}{M_{RE}} \right) * 100 \quad (3)$$

Where *Loading* is calculated by equation 2,  $M_{PT}$  is the mass of particles recovered from the emulsion, and  $M_{RE}$  is the mass of resveratrol added to the emulsion.

Resveratrol loading was also determined via HPLC. Particles were dissolved in DMSO and then precipitated by adding methanol, water and acetic acid while retaining soluble resveratrol. The final concentrations were 10% DMSO, 30% Methanol, 57.5% Water, and 2.5% Acetic Acid. After the PLG precipitated, the mixture was centrifuged at 1750xg for 10 min and the supernatant was collected for HPLC analysis. Free resveratrol was prepared in a solution of the same concentration of solvents to make a 6-point standard curve.

A Thermo Ultimate 3000 binary gradient system was used for HPLC analysis. A Chromegabond WR C18 column was used in the analysis and the flow rate was kept at 0.2 mL/min. An Agilent G1315B Diode Array UV Detector was used in the analysis at 306nm. Solvent A was water and Solvent B was acetonitrile. From 0-30min the solvent was 90% A and 10% B, from 30min to 31min the solvent was 5% A and 95% B, and from 31min on the solvent was 90% A and 10% B. The area under the curve of the chromatograms of free drug was plotted against concentration to make a standard curve shown in Figure 2.16. The amount of resveratrol in particles was calculated by interpolating this curve. Loading was calculated using Eq. 2.

#### 2.2.6 *In Vitro Release Assay*

Particles containing resveratrol were dispersed in 1 mL ultrapure water in 1.5 mL tubes and shaken at 650 rpm using an Eppendorf Thermomixer R maintained at 37°C. At the designated time point, the particles were collected via centrifugation, suspended in

ultrapure water, and centrifuged again. The particles were then frozen and lyophilized. Particles were analyzed for resveratrol loading as described in section 2.5. Resveratrol released (%) was calculated by equation 4.

$$Drug\ released\ (\%) = \left( \frac{L_0 - L_t}{L_0} \right) * 100 \quad (4)$$

Where  $L_0$  is the initial loading of the particles, and  $L_t$  is the loading at time  $t$  during the release assay.

#### *2.2.7 Ethanol Wash of Resveratrol Particles*

Particles were suspended in 100% ethanol for 1 minute. The particles were then collected via centrifugation, suspended in ultrapure water, frozen, and lyophilized. Particles were analyzed for resveratrol loading as in section 2.5. The amount of resveratrol removed by the ethanol wash was calculated by equation 5.

$$Drug\ removed\ (\%) = \left( \frac{L_0 - L_{EtOH}}{L_0} \right) * 100 \quad (5)$$

Where  $L_0$  is the initial loading and  $L_{EtOH}$  is the loading after the ethanol wash.

#### *2.2.8 3T3-L1 Adipocyte Cell Culture*

3T3-L1 fibroblasts (ATCC), were differentiated into adipocytes following ATCC's protocol, with slight modifications. Briefly, 3T3-L1 cells were seeded in 6 well plates at 80,000 cells/well and cultured in DMEM supplemented with 10% Super Calf Serum and 1% Pen/Strep. 48 hours after confluence was reached, media was exchanged with "differentiation media" consisting of DMEM supplemented with 10% FBS, 10  $\mu$ g/mL bovine insulin, 0.25  $\mu$ M dexamethasone, and 0.5 mM IBMX. 48 hours after differentiation media was added, media was exchanged for DMEM supplemented with 10% FBS and 10  $\mu$ g/mL bovine insulin. After another 48 hours, media was exchanged for DMEM

supplemented with 10% FBS. Cells were then cultured until treatment with particles, which occurred 9 days after exposure to the differentiation media.

#### *2.2.9 Particle Treatment and Oil Red O Assay*

Blank PLG particles (300  $\mu\text{g/mL}$ ), resveratrol loaded PLG particles (300  $\mu\text{g/mL}$ ), or free resveratrol (60  $\mu\text{M}$ ) was added to 3T3-L1 adipocytes 9 days after exposure to the differentiation media. 48 hours later cells were washed, fixed in 10% formalin and stained with Oil Red O as follows. Cells were washed with ultrapure water and then washed with 60% isopropanol for 2 minutes. Cells were then incubated with Oil Red O for 10 minutes at room temperature. Cells were then washed four times with ultrapure water. Images were taken on a Nikon Eclipse Ci microscope using the 4x objective. Oil Red O was extracted from the wells by incubating the cells in 100% isopropanol for 10 minutes at room temperature. Absorbance of extracted Oil Red O was measured at 500 nm using a spectrophotometer.

#### *2.2.10 FITC Labeling of PVA and Particle Fabrication*

PVA was dissolved in DMSO at 50 mg/mL. FITC and dry KOH were added to the solution at concentrations of 3.5 mg/mL and 0.5 mg/mL, respectively. This solution was stirred at room temperature for 5 hours. The solution was then dialyzed using dialysis tubing (3.5 kDa MWCO) in 3 L of ultrapure water for 3 days, replacing the water twice daily. The FITC labeled PVA (FITC-PVA) was collected, frozen, and lyophilized. This FITC-PVA was then used to fabricate PLG particles as described above.

#### *2.2.11 Confocal Microscopy*

Particles were suspended in a 50:50 mixture of ultrapure water and anti-fade mounting media, pipetted on a slide, mounted with a coverslip, and dried overnight. Images

were acquired on a Zeiss 700 confocal microscope using the 488nm laser. Particles were analyzed for fluorescence intensity using ImageJ as follows. A line was drawn through each particle and the maximum intensity of FITC on the surface was recorded using the plot profile function. 27 particles were analyzed for each condition. Data is mean  $\pm$  standard deviation of the measured surface pixel intensity.

#### *2.2.12 Flow Cytometry*

Particles were suspended in ultrapure water and analyzed with a BD FACS Aria flow cytometer for FITC fluorescent intensity. Approximately 600 particles were analyzed for each condition. Data was analyzed using FlowJo (Treestar).

#### *2.2.13 Statistical Analysis*

Statistical analysis was carried out using GraphPad Prism. Where appropriate, an unpaired t-test or one-way ANOVA followed by Tukey's multiple comparison test were carried out to compare differences between means. Error bars represent the standard deviation of the means. Linear trends were determined with a Pearson's correlation test. Specific details regarding statistical analyses carried out for each data set are described in the figure legend.

### **2.3 Results**

#### *2.3.1. The Effect of Ethanol on PLG Particle Fabrication*

We sought to produce PLG particles containing resveratrol using a single emulsion/solvent evaporation technique in which the oil phase is PLG dissolved in DCM and the aqueous phase is water containing PVA as the emulsifier. However, resveratrol is not soluble in DCM and it is well established maximal encapsulation is achieved when the drug is soluble in the oil phase<sup>54</sup>. Resveratrol is soluble in ethanol up to 50 mg/mL<sup>96</sup> and

thus, we investigated ethanol as a co-solvent to increase resveratrol's solubility in the oil phase.

Ethanol reduces the interfacial tension between water and DCM<sup>97</sup>, which favors the formation of smaller droplets during emulsification<sup>98</sup>. Therefore, we first determined ethanol's effect on particle size and mass yield in the absence of resveratrol. 6% PLG was poorly soluble in a 1:1 mixture of ethanol and DCM (Figure 2.1A) and few particles formed during the emulsion process, with a mass yield of  $11 \pm 4$  % (Figure 2.1B). In contrast, 6% PLG was soluble in a 1:2 or a 1:3 mixture of ethanol and DCM (Figure 2.1A), and particle mass yield was similar between the two conditions,  $63 \pm 3$  % for 1:2 versus  $67 \pm 7$  % for 1:3 (Figure 2.1B). Furthermore, both conditions showed similar mass yield compared to DCM alone (Figure 2.1B). Representative light microscopy images of the 1:2 and 1:3 formulations are shown in Figure 2.1C and D. We found that 1:2 particles were smaller than the 1:3 particles with an average diameter of  $5.7 \mu\text{m}$  versus  $10.5 \mu\text{m}$  (Figure 2.1E and F). In addition, the 1:3 particles had a similar size distribution to those made with DCM alone (data not shown). Thus, we selected a 1:3 volume ratio of ethanol and DCM as the oil phase in subsequent experiments.

### 2.3.2 Fabrication of Resveratrol Loaded PLG Particles

We next employed the single emulsion solvent/evaporation method to fabricate resveratrol loaded PLG particles (from here on in this chapter referred to as *resveratrol particles*). We found that a 40 mg/mL solution of resveratrol in ethanol was miscible with an 8 % solution of PLG in DCM when mixed at a 1:3 ratio and no precipitates formed (data not shown).

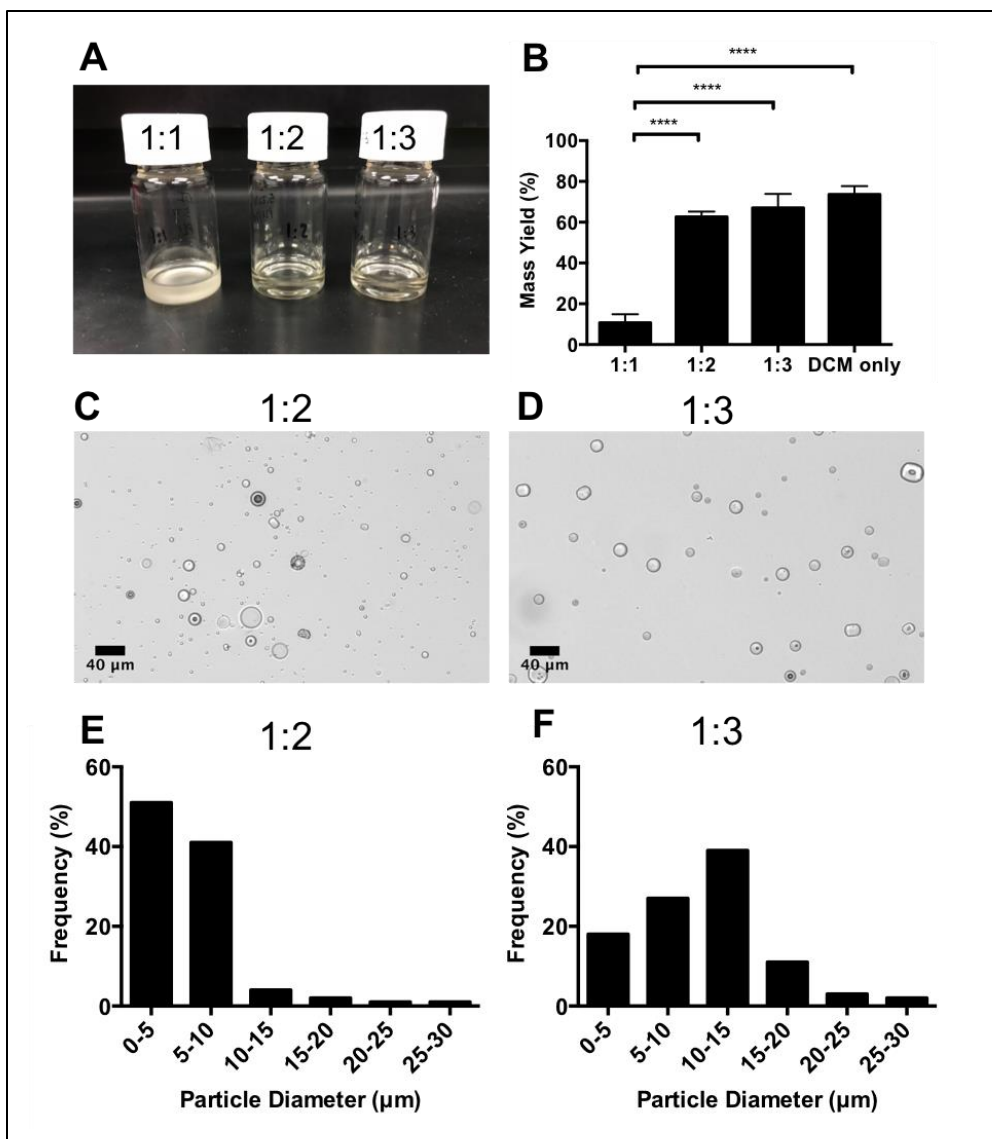


**Figure. 2.1. The effect of ethanol on particle mass yield and size.** (A) Vials containing 1:1, 1:2, and 1:3 volume ratios of ethanol and DCM with 6% PLG. (B) Mass yield of particles made with an organic phase consisting of 1:1, 1:2, 1:3 volume ratios of ethanol and DCM and DCM only. Data is the mean of three independent particle fabrications and analyzed with one-way ANOVA followed by Tukey's multiple comparisons test. \*\*\*\*  $p < 0.0001$ . (C, D) Light microscopy images and (E, F) size distribution of particles made with 1:2 and 1:3 mixtures of ethanol and DCM. Scale bar indicates 40  $\mu$ m.

We utilized this mixture for the oil phase of the emulsion, which thus contained resveratrol at 10 mg/mL and 6% PLG. This oil phase yielded particles that were irregularly shaped with ruffled surfaces (Figure 2.2A) compared to particles made with an oil phase that consisted of only DCM and 6% PLG (Figure 2.2C). Particles made using a 1:3 mixture of ethanol and DCM that lacked resveratrol were also smooth and spherical (Figure 2.2B), indicating resveratrol is responsible for the altered particle morphology. It was determined that lyophilization was not a factor in the irregular morphology through imaging resveratrol particles before and after lyophilization, seen in Figure 2.15. Loading was  $65 \pm 5$   $\mu\text{g}/\text{mg}$  for the resveratrol particles and mass yield was  $40 \pm 5$  %, which is lower than the mass yield for the other two conditions, depicted in Figure 2.1B. Furthermore, resveratrol loading measured using UV-Vis was verified using HPLC. HPLC analysis yielded a particle loading of  $69 \pm 7$   $\mu\text{g}/\text{mg}$ , which was consistent with loading found using the UV-Vis method. Therefore, UV-Vis, a simpler and more cost-effective method, was used for the remainder of the study. The HPLC standard curve is shown in Figure 2.16. Taken together, the data indicates that resveratrol can be loaded into PLG particles using the single emulsion/solvent evaporation technique, but mass yield is decreased, and morphology is altered.

In addition, it is important to note that all particles fabricated using this method resulted in flowable powders, suggesting no aggregation. Images of particles before and after spinning the tube show that particles flow and take the shape of the container, seen in Figure 2.17.

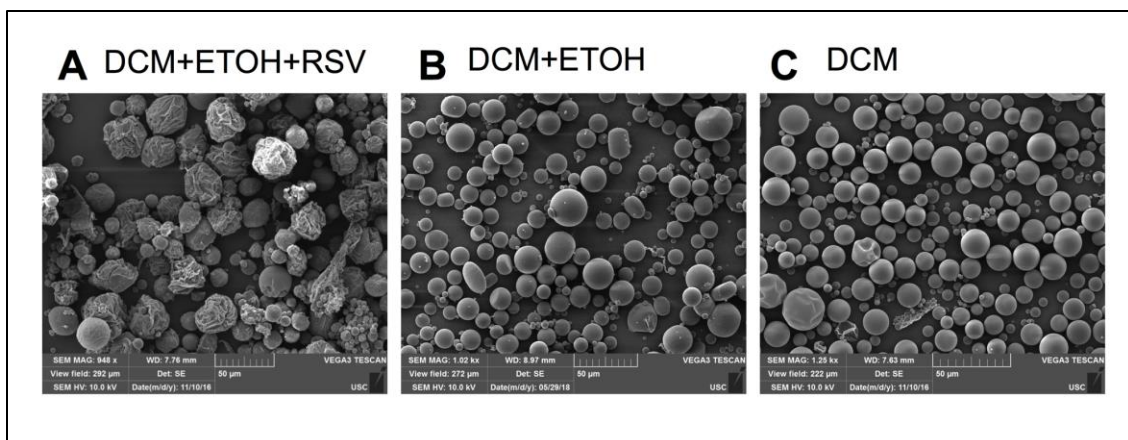


**Figure 2.2. Morphology of resveratrol loaded PLG particles.** Representative images of particles made with an oil phase consisting of (A) a 1:3 mixture of ethanol and DCM and 10 mg/mL of resveratrol, (B) a 1:3 mixture of ethanol and DCM and no resveratrol, and (C) DCM with no resveratrol or ethanol. All particles were made with an oil phase that was 6% PLG. The aqueous phase of the emulsion contained 1% polyvinyl alcohol. Scale bars indicate 50  $\mu\text{m}$ .

### 3.3 Bioactivity of Resveratrol Loaded into PLG Particles

Having successfully loaded PLG particles with resveratrol, we determined if resveratrol remained bioactive following the fabrication process. To accomplish this, we investigated the ability of the resveratrol particles to induce lipolysis in differentiated 3T3-L1 adipocytes by measuring lipid content with an Oil Red O assay. 3T3-L1 adipocytes are differentiated from 3T3-L1 fibroblasts and extensively used to model human adipocytes. Resveratrol promotes lipolysis in these cells<sup>25,27</sup>, which decreases intracellular lipid content. Lipid content can be visualized with Oil Red O, a lipophilic dye, (Figure 2.3A-F) and lipid content can be quantified by extracting the dye (Figure 2.3G) and measuring the solution's absorbance (Figure 2.3H). While the undifferentiated fibroblasts do not stain strongly with Oil Red O due to a low level of intracellular lipid (Figure 2.3A), 3T3-L1 adipocytes exhibit extensive staining throughout the monolayer (Figure 2.4B). We found that treatment of adipocytes with 300  $\mu\text{g/mL}$  of resveratrol particles decreased Oil Red O



staining to a similar level of cells treated with 60  $\mu$ M resveratrol (Figure 2.3D versus 2.3E and 2.3H). As controls, adipocytes were treated with particles that did not contain resveratrol (Figure 2.3C) and ethanol, which is a vehicle control for the resveratrol treatment (Figure 2.3F). Importantly, these treatments did not decrease Oil Red O signal. Taken together these data indicate that the resveratrol remains bioactive following its incorporation into PLG particles.

#### *2.3.4. In Vitro Release Profile of Resveratrol Particles*

Having determined that the resveratrol remains bioactive once loaded into PLG particles, we next investigated the release kinetics of resveratrol from the particles in vitro. Particles were mixed in water for 6 weeks (Figure 2.4A). Release at early time points (0.25, 1, and 3 days) was highly variable with coefficients of variation in excess of 80% at day 3. The first 14 days of the release assay was repeated once more, however large variability in release was still observed (Figure 2.4B). We hypothesized that irregular morphology was responsible for the release profile's high variability and set out to produce resveratrol particles with smooth surfaces and spherical geometry in effort to decrease variability in drug release.

#### *2.3.5. The Effect of PVA and Resveratrol on Particle Morphology*

Our SEM data (Figure 2.5) indicated that incorporation of resveratrol into the PLG particle was altering surface morphology. We speculated that resveratrol was interfering with PVA's ability to function as an emulsifier and this could lead to the ruffled surface. Since the amount of PVA on the surface of a PLG particle can be increased by increasing the PVA concentration in the aqueous phase<sup>99</sup>, we investigated if increasing the concentration of PVA in the emulsion and solvent evaporation steps would lead to smooth,

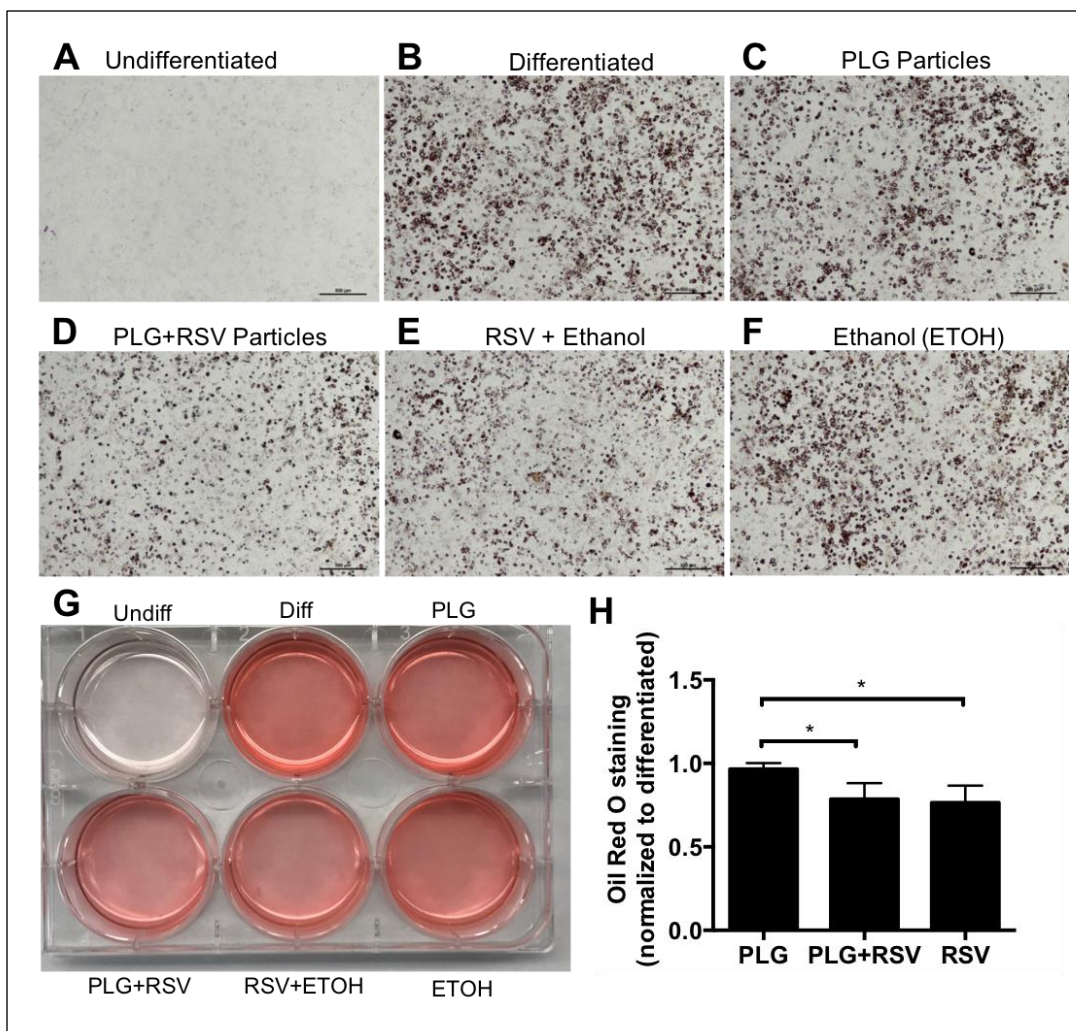


**Figure 2.3. The effect of resveratrol loaded particles on adipocyte lipid content.** (A-F) Images of cell monolayers stained with Oil Red O. Experimental groups include (A) undifferentiated fibroblasts, (B) adipocytes with no treatment, (C) adipocytes treated with 300  $\mu\text{g/mL}$  of PLG particles, (D) adipocytes treated with 300  $\mu\text{g/mL}$  of resveratrol particles (E) adipocytes treated with 60  $\mu\text{M}$  resveratrol dissolved in ethanol and suspended in DMEM at 0.05 v/v %, and (F) adipocytes treated with an equivalent amount of ethanol. (G) Image of Oil Red O extracted in isopropanol from the six experimental groups. (H) Absorbance values of Oil Red O extracted from cells using isopropanol at 500 nm. Absorbance correlates to lipid content inside the cells. Labels for (H) correspond to (C-E) in terms of treatment group. The experiment was repeated 4 times. One-way ANOVA was conducted followed by a Tukey multiple comparison test. \*  $p < 0.05$ . Scale bars indicate 500  $\mu\text{m}$ .

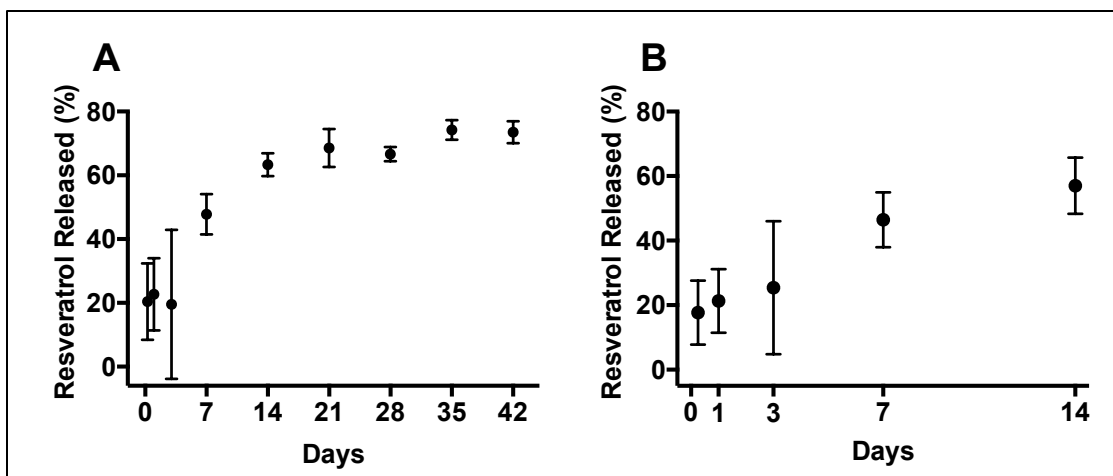


**Figure 2.4. In vitro release profiles of resveratrol particles.** (A) Six-week resveratrol release profile. Data are mean  $\pm$  standard deviation from one experiment with three replicates per time point. (B) Two-week resveratrol release profile. Data is plotted as mean  $\pm$  standard deviation from two independent experiments with three replicates per time point.

spherical particles. We found that doubling the PVA concentration in the emulsion step (from 1 to 2%) and increasing PVA in the solvent evaporation step (from 0 to 1%) did not improve particle morphology (Figure 2.5A). In fact, we increased the concentration of PVA in the emulsion step to 5%, but the particles still exhibited irregular morphology (Figure 2.18). As an alternative approach, we incrementally decreased the concentration of resveratrol in the oil phase from 10 mg/mL to 4 mg/mL by changing the volume ratio of the ethanol solution (containing 40 mg/mL resveratrol) and DCM from 1:3 to 1:9. A stark change in morphology was observed when the resveratrol concentration decreased from 5 mg/mL to 4 mg/mL, with the latter yielding spherical particles with smooth surfaces (Figure 2.5).

Having determined conditions that yield smooth, spherical particles, we investigated the impact of PVA concentration, in both the emulsion and solvent evaporation steps, on morphology. We found that a PVA concentration of 2% in the

emulsion step and 1% in the solvent evaporation was necessary to maintain the smooth, spherical morphology as decreasing PVA in either step led to irregular morphology (Figure 2.6). Furthermore, we found that resveratrol loading nearly doubled (from 5.3 to 9.6  $\mu\text{g}/\text{mg}$ ) as we decreased PVA concentration from 2% to 1% in the emulsion step and from 1% to 0% in the evaporation step. Taken together, the data suggest that PVA and resveratrol compete for incorporation into the particle and when present at high enough levels, resveratrol alters particle morphology.

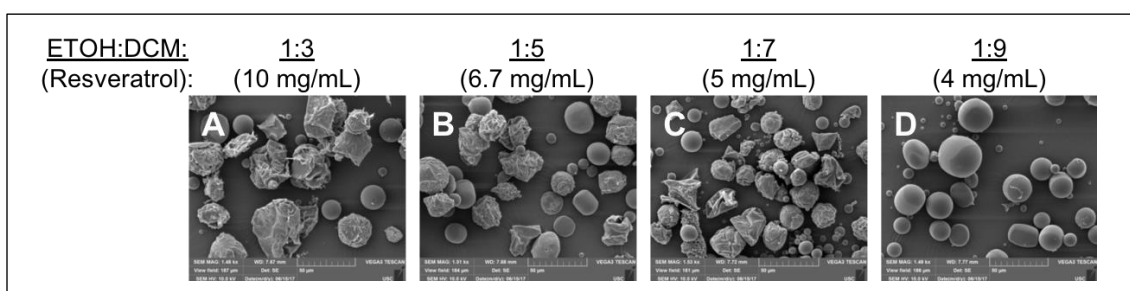


**Figure 2.5. The effect of resveratrol concentration on particle morphology.** (A-D) Images of resveratrol loaded particles made with decreasing concentrations of resveratrol in the oil phase (shown in parentheses), which was achieved by decreasing the volume ratio of ethanol to DCM, which is depicted as ETOH:DCM ratio above each image. 6% PLG was used in the emulsion. The PVA concentration was 2% in the emulsion step and 1% in the evaporation step. Scale bars indicate 50  $\mu\text{m}$ .

#### 2.3.6. The Effect of Resveratrol on the Particle's PVA Content

To further investigate if resveratrol was interfering with PVA's ability to associate with the particle's surface, we measured how PVA content and distribution changes with resveratrol loading by utilizing FITC-labeled PVA (FITC-PVA). Confocal microscopy of spherical particles indicated that FITC-PVA was present on the surface of the particle and evenly distributed (Figure 2.7 A-C). This was the case whether or not resveratrol was incorporated into the particle as long as the spherical morphology was preserved; however,

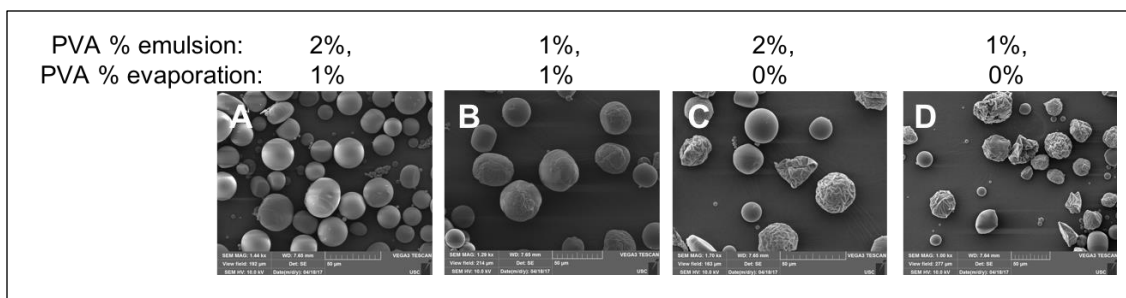


**Figure 2.6. The effect of PVA concentration on particle morphology. (A-D)** Images of resveratrol particles made with an oil phase consisting of a 1:9 mixture of ethanol to DCM and containing 4 mg/mL resveratrol and 6% PLG. PVA concentrations in the emulsion step and solvent evaporation step are indicated above the image as emulsion % (w/v) and evaporation % (w/v), respectively. Scale bars indicate 50 µm. Loading values were as follows: 5.3 µg/mg (A) 5.4 µg/mg (B) 7.1 µg/mg (C) 9.6 µg/mg (D).

particles made with a high resveratrol loading (65 µg/mg), which leads to the ruffled surface morphology, exhibited an altered FITC signal that suggested PVA was not evenly distributed over the particle's surface (Figure 2.7D). While not strongly apparent in the confocal images by eye, image analysis revealed that the FITC signal at the surface of the spherical particles was decreased when resveratrol was encapsulated into the particle (Figure 2.7E). To confirm the confocal data, we conducted flow cytometry of the particles made with FITC-PVA (Figure 2.8). Congruent with the confocal data, the FITC signal is decreased on resveratrol particles. Taken together, the data suggests that resveratrol incorporation into the particle decreases the amount of PVA that associates with the particle's surface, suggesting that resveratrol accumulates at the particle surface.

### 2.3.7. The Effect of Particle Size on Resveratrol Loading

Based on our findings up to this point, we suspected some fraction of the resveratrol incorporated into a particle was loaded on its surface. If this was the case, particle size would impact resveratrol loading because specific surface area increases as particle size

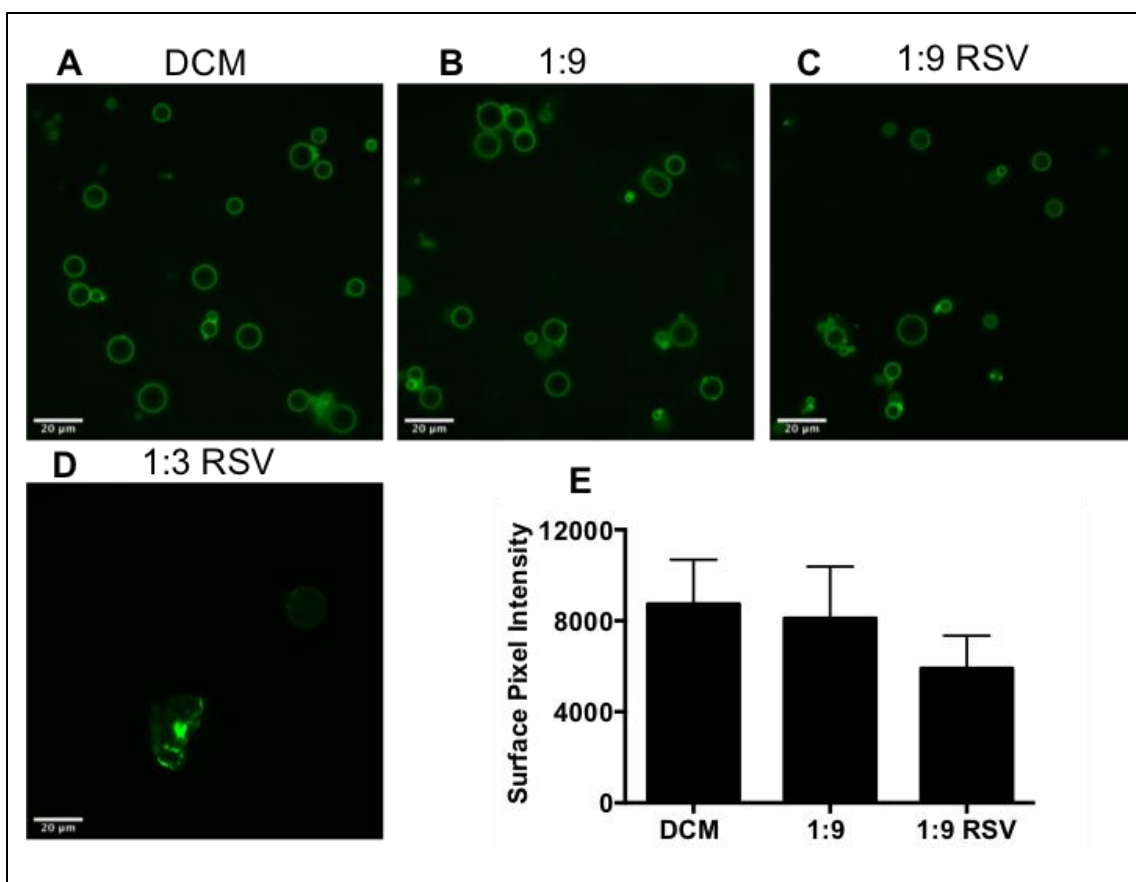


**Figure 2.7. Confocal imaging of particles made with FITC-PVA.** Fluorescent images of particles made with oil phases consisting of 6% PLG in (A) DCM (B) 1:9 ethanol:DCM, (C) 1:9 ethanol:DCM containing 4 mg/mL resveratrol, and (D) 1:3 ethanol:DCM containing 10 mg/mL resveratrol. FITC signal intensity was quantified using ImageJ and is depicted in panel (E) as mean  $\pm$  standard deviation for 27 particles per group. Scale bar is 20  $\mu$ m.

decreases. To investigate the effect of particle size on resveratrol loading, we produced particles with diameters ranging from 5 to 13  $\mu$ m by changing the emulsion's homogenization time and speed. We found that increasing homogenization time narrowed the size distribution and increasing homogenization speed decreased particle size, but all particles exhibited spherical morphologies (Figure 2.9). After producing several additional batches of particles, we determined that 11,000 RPM for 5 minutes was best for producing

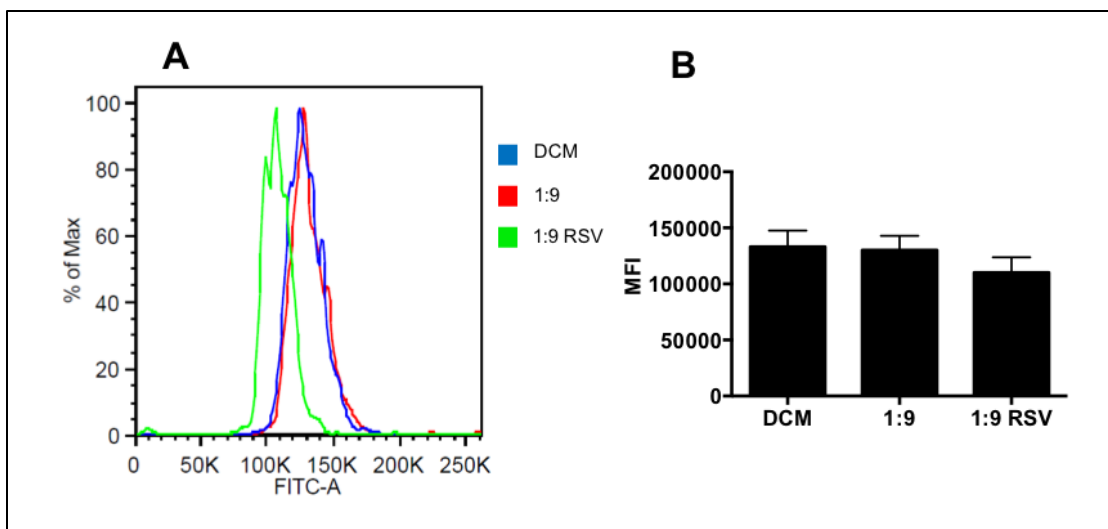


**Figure 2.8. Flow cytometry of resveratrol particles made with FITC-PVA. (A)** Histograms depicting FITC fluorescence intensity of particles made with oil phases consisting of 6% PLG in DCM (blue), 1:9 ethanol:DCM (red), and 1:9 ethanol:DCM containing 4 mg/mL resveratrol (green). **(B)** Mean fluorescence intensity (MFI) and standard deviation of data from panel (A). 600 particles were analyzed for each group.

smaller particles, which had a diameter of  $5.2 \pm 0.9 \mu\text{m}$  and a loading of  $4.9 \pm 0.4 \mu\text{g/mg}$ , while 7,000 RPM for 30 seconds was best for producing larger particles, which had a diameter of  $10.3 \pm 1.9 \mu\text{m}$  and a loading of  $2.5 \pm 1.2 \mu\text{g/mg}$  (Figure 2.10A, blue dots and red dots). Congruent with the idea that some of the resveratrol is surface loaded, there was a negative correlation between resveratrol loading and particle diameter (Figure 2.10A). Also, because there is no impact of particle size on mass yield, drug encapsulation efficiency also increased with decreased particle diameter (Figure 2.10 B and C).

#### 2.3.8. The Effect of Particle Size on Resveratrol Release

Having established that particle size impacts resveratrol loading, we next investigated the effect of particle size on resveratrol release. We found that  $4 \mu\text{m}$  particles with a drug loading of  $4.7 \mu\text{g/mg}$  exhibited a different release profile compared to  $11 \mu\text{m}$  particles with a drug loading  $2.5 \mu\text{g/mg}$  (Figure 2.11). Specifically,  $4 \mu\text{m}$  particles released

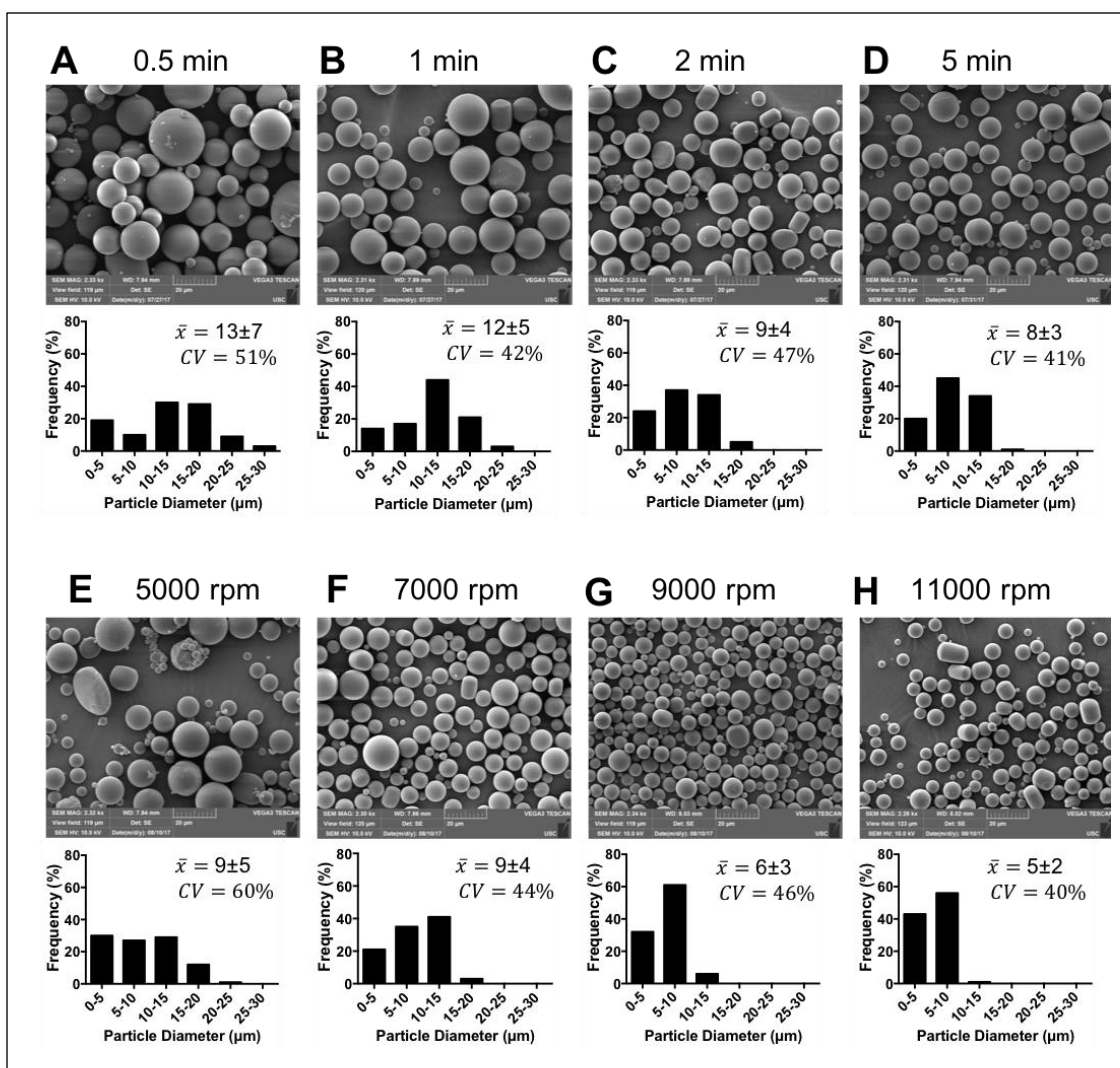


**Figure 2.9. The effect of homogenization time and speed on particle size.** Images and size distributions for particles homogenized at 7000 rpm for increasing amounts of time (A-D) and homogenized for 5 minutes at increasing homogenization speeds (E-H). Particles were produced with a 1:9 mixture of ethanol to DCM containing 4 mg/mL resveratrol. The PVA concentration is 2% in the emulsion step and 1% in the evaporation step. Scale bars indicate 20 μm.  $\bar{x}$  is mean ± standard deviation. CV is coefficient of variation. RPM is rotations per minute and indicates the speed of the homogenizer tip.

60% of their resveratrol in the first 24 hours, after which time no more resveratrol was released, but resveratrol still remained in the particles (Figure 2.11A). In contrast, 11 μm particles released 20% of their resveratrol in the first 24 hours and then continued to release



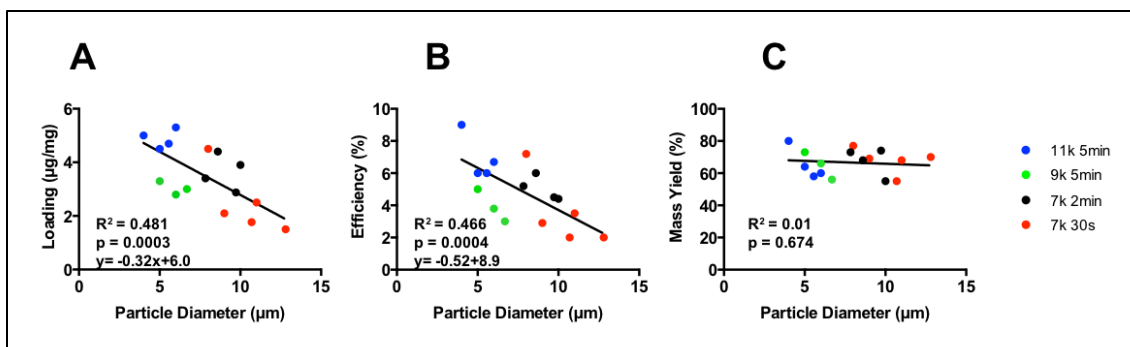


**Figure 2.10. Effect of particle diameter on drug loading and particle mass yield.** Plots of particle diameter versus (A) drug loading, (B) drug encapsulation efficiency, and (C) particle mass yield for several batches of particles. Pearson correlation coefficients and associated P values were calculated to determine the extent of a linear correlation between variables.

drug for 14 days. In addition, the 11  $\mu\text{m}$  particles exhibited lower variation in the amount of drug released at early time points compared to the 4  $\mu\text{m}$  particles.

Following the release assay, we suspected the burst release exhibited by the 4  $\mu\text{m}$  particles was due to resveratrol associated with the surface of the particle, which requires 24 hours to be released, possibly due to its poor solubility in water. To investigate this, we washed particles in 100% ethanol for one minute and then measured the residual resveratrol loading. We found that the ethanol wash removed approximately the same amount of resveratrol as was released during the first 24 hours of the release assay for large (9 and 11  $\mu\text{m}$ ) and small (4 and 5  $\mu\text{m}$ ) particles (Figure 2.11A versus 2.11B). Importantly, submerging the 9 or 5  $\mu\text{m}$  particles in water for one minute did not remove any resveratrol (data not shown). While it would have been optimal to use the same batch of particles for both experiments in Figure 2.11, this was not possible because of the mass of particles required for the release assay. However, this technicality does not prevent us from concluding that when loading particles with resveratrol, a certain amount of the drug is weakly associated with the surface and releases over a 24 hours period in our assay. For

particles in the range of 4 to 5  $\mu\text{m}$ , the surface associated resveratrol is a substantial proportion (~60%) of the total resveratrol loaded. In contrast, surface associated resveratrol makes up less than 20% of the resveratrol loaded into larger particles (9 to 11  $\mu\text{m}$ ), allowing them to exhibit a more sustained release profile.

We suspected that the surface area to volume ratio played a role in the increase in loading and burst release in the smaller particles. Looking at the surface area to volume ratio (SA/V), the small particles had a SA/V of 1.5 and large particles had a SA/V of 0.6. This is about a 3-fold increase in SA/V from small to large particles. The burst release after 24 hours increases by about 3-fold (20 to 60%) which matches this calculation. The ethanol wash showed an increase of at least 4-fold between the smaller and large particles (20-80%), which is higher than expected. This could be because the ethanol is washed for 1 minute and there may be some internal resveratrol washed out as well.

## **2.4. Discussion**

Our goal was to develop PLG microparticles for the controlled release of resveratrol. Our initial approach was to utilize a single emulsion/solvent evaporation protocol that maximized resveratrol's solubility in the oil phase by using ethanol as a co-solvent. We achieved PLG particles with a loading of 65  $\mu\text{g}/\text{mg}$  and resveratrol remained bioactive. Interestingly, the particles had ruffled surfaces atypical of particles produced by emulsion, which have a smooth surface to minimize interfacial free energy<sup>100</sup>. We believe the irregular morphology is due to interfacial instabilities that arise at the oil/water interface as the solvents diffuse out of the oil droplet. We propose that during solvent removal, the decrease in interfacial surface area of the shrinking droplet leads to an interfacial excess of resveratrol, which decreases surface tension and causes droplet expansion. The expansion

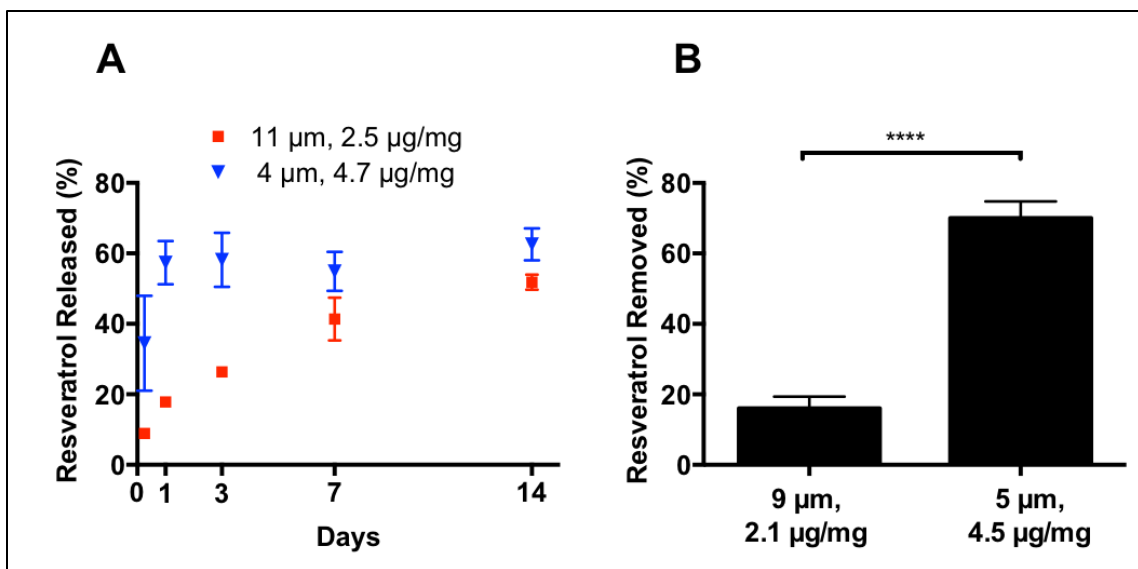


**Figure 2.11. The effect of particle size on resveratrol release.** (A) A comparison of release profiles for 4 and 11  $\mu\text{m}$  particles with drug loadings of 4.7 and 2.5  $\mu\text{g}/\text{mg}$ , respectively. (B) Resveratrol removed from particles after submersion in ethanol for 1 minute. Two batches of resveratrol particles were assayed: 9  $\mu\text{m}$ , 2.1  $\mu\text{g}/\text{mg}$  and 5  $\mu\text{m}$ , 4.5  $\mu\text{g}/\text{mg}$ . All measurements were carried out in triplicate. Data is mean  $\pm$  standard deviation. Resveratrol removed was analyzed with an unpaired t-test. \*\*\*\* indicates p-value < 0.0001.

manifests as folding and deforming of the interface that does not reverse prior to the polymer's phase transition when the particle hardens. In support of our explanation, surface ruffling was described for a similar system in which polystyrene, chloroform, and n-hexadecanol were emulsified in an aqueous solution of sodium dodecyl sulfate<sup>101</sup>. By increasing the concentration of n-hexadecanol or the rate of solvent evaporation, both of which promote interfacial excess of n-hexadecanol, the authors tuned the surface topography of the polystyrene particles from smooth to ruffled.

While the irregular shaped particles had the highest drug loading (65  $\mu\text{g}/\text{mg}$ ), they also exhibited variable drug release at early time points. We sought to improve drug release by producing smooth, spherical particles. By decreasing resveratrol and increasing PVA in the emulsion we achieved smooth particles, but the cost was a 15 to 25-fold decrease in

drug loading depending on particle size. In addition, resveratrol was still present on the surface of these particles, which caused 5  $\mu\text{m}$  particles to release 60% of their payload in 24 hours compared to 20% for larger, 10  $\mu\text{m}$  particles. The impact of particle size on loading and release for small molecules encapsulated in PLG has been studied by several groups<sup>102–105</sup> and our findings are consistent. To summarize, drug loaded on the microparticle's surface contributes to burst release, and when there is substantial surface loading of the drug, small particles have higher drug loading due to their greater specific surface area relative to large particles. Interestingly, none of the small molecules in these studies (dexamethasone, piroxicam, gefitinib) impacted particle morphology. We hypothesize that resveratrol exhibits greater surface activity in our emulsion compared to the other molecules in their emulsions.

An interesting finding was that resveratrol and PVA compete for the surface of the particle during its formation. We observed this phenomenon indirectly in two ways: (i) a decrease in resveratrol loading with increasing concentrations of PVA in the aqueous phase and (ii) a decrease in fluorescence intensity of resveratrol particles emulsified with FITC-PVA, indicating a decrease in PVA on the particle surface. PVA acts as an emulsifier in our system and prevents coalescence of the oil droplets. The decrease in mass yield of the 1:3 particles when made with resveratrol ( $67\pm7\%$ , no resveratrol versus  $40\pm5\%$ , 10 mg/mL resveratrol) indicates a consequence of PVA displacement is partial breakdown of the emulsion before particles harden. Thus, another motivation to evenly distribute resveratrol throughout the particle is to increase mass yield of the polymer particles (i.e. the drug delivery system).

To our knowledge, we are the first to functionalize PVA with FITC and use this fluorescent emulsifier to study the surface of PLG microspheres. In the reaction, the isothiocyanate group on FITC spontaneously reacts with an alcohol group on PVA and forms a monothiourethane when stirred together at room temperature in DMSO<sup>106</sup>. This straightforward and mild chemistry should be easily employed by any lab that produces PLG particles using PVA as an emulsifier.

Currently, the resveratrol delivery rate and duration needed to induce weight loss and affect other aspects of adipose tissue function have not been extensively investigated; however, a study involving rats provides some guidelines<sup>89</sup>. Oral administration of resveratrol at 30 mg/kg/day for six weeks decreased body fat in rats fed a high fat diet and resveratrol metabolites were present in fat tissue at a concentration of  $2.66 \pm 0.55$  nmol/g. Unchanged resveratrol was not detected, likely due to its short half-life, which is 9.2 hours in humans when administered orally<sup>29</sup>. Assuming humans would require 3 nmol/g of resveratrol delivered to visceral adipose tissue per day and given that an adult male has 500 g of visceral fat<sup>107</sup>, a drug delivery system would need to release 345  $\mu$ g/day. The time averaged delivery rate for the 65  $\mu$ g/mg particles was 1.2  $\mu$ g/mg/day over six weeks. 345  $\mu$ g/day would require less than 300 mg of particles distributed throughout 500 g of fat tissue. There is precedence for delivering this amount of polymer to humans. For example, a typical dose of VIVITROL microspheres, which are naltrexone encapsulated into 75:25 PLG, is 1 g injected intramuscularly<sup>108</sup>. Thus, we believe it is warranted to begin investigating the therapeutic efficacy of the ruffled particles in pre-clinical models of obesity; however, we will simultaneously work towards developing particles with higher resveratrol loadings and optimal drug release rates.

To develop particles for optimal resveratrol delivery, it will be necessary to understand why resveratrol accumulates at the surface of PLG particles in the emulsion. One possibility is that ethanol may have enhanced resveratrol's surface activity by promoting its accumulation at the oil/water interface. We speculate that due to ethanol's high miscibility with water compared to DCM, it may have diffused out of the particle more quickly without a large impact on polymer viscosity because PLG is not soluble in ethanol. Due to resveratrol's poor solubility in both DCM and water, it accumulated at the oil/water interface leading to surface loading.

We think that the ability of the drug to deposit on the surface of the microparticles is governed by its surface activity in the emulsion used to make the particles, with higher surface activity leading to more surface deposition. While we do not know the orientation of resveratrol when it inserts at the oil-water interface, we speculate that it orients perpendicular to the interface with the benzene-1,3-diol in the aqueous phase and the phenol group in the oil phase because we expect the benzene-1,3-diol to be more hydrophilic than the phenol group. Thus, we think the number of hydroxyl groups and their orientation relative to each other on the stilbene impacts surface activity, with orientations that increase the hydrophilicity at one end of the molecule relative to the other resulting in a molecule with higher surface activity. Pinosylvin, with a benzene-1,3-diol and a benzene ring on either end of the double bond is expected to exert more surface activity, while trans-stilbene, with no hydroxyl groups is expected to exhibit lower surface activity than resveratrol. Trans-4-hydroxy stilbene may exhibit similar surface activity if the phenol group exerts a sufficient level of hydrophilicity and it is difficult to predict piceatannol's activity since either end of the molecule boasts two hydroxyl groups. However, we

recognize that the way these molecules will interact with other molecules at the interface (i.e. water, ethanol, dichloromethane, poly(vinyl alcohol)) is difficult to predict, and future studies that involve molecular modeling may be necessary to truly understand this. Future studies will also investigate if a single-solvent oil phase can improve resveratrol loading while preserving a smooth particle surface and controlling drug release.

## **2.5. Conclusion**

We demonstrate that resveratrol, a molecule that is not soluble in DCM but soluble in ethanol, can be encapsulated into PLG microspheres using an oil-in-water emulsion/solvent evaporation technique with ethanol as a co-solvent. Increasing the volume fraction of ethanol in the oil phase increases resveratrol's solubility and subsequent loading in the particle. Some of the resveratrol loads onto the particle surface, which may be a property inherent of resveratrol, due to the presence of ethanol, or some combination thereof. Nevertheless, there is a point where resveratrol's density on the particle surface leads to ruffling. Particles with this morphology exhibit variable drug release at early time points. By decreasing resveratrol and increasing PVA in the emulsion, smooth particles are produced, and drug release is controlled by particle size; however, drug loading is low. Future work will design a particle with high drug loading and low variability in drug release.

Broadly, this work serves as a cautionary tale that inclusion of a co-solvent in the oil-in-water emulsion/solvent evaporation technique may impact drug distribution and, possibly, particle morphology. On the other hand, we demonstrate that bioactive payloads can be used to tune surface roughness of their drug delivery vehicle, which may afford greater control over drug delivery by modulating biomaterial-tissue interactions.

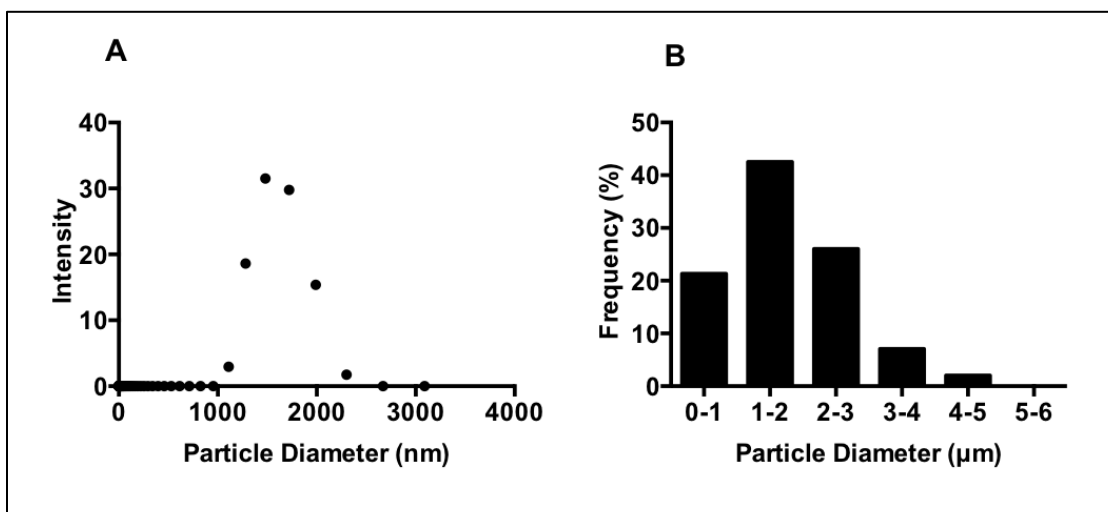


**Figure 2.12. A comparison of particle size distribution using dynamic light scattering (DLS) and image analysis.** (A) Particle size distribution for a batch of PLG particles measured with Malvern Zetasizer (a DLS instrument). DLS analysis yielded an average particle diameter of 1.72  $\mu\text{m}$  with a PDI of 0.225. (B) Size distribution of the same particles using light microscopy and image analysis described in section 2.2.4. Image analysis yielded an average particle diameter of  $1.81 \pm 0.9 \mu\text{m}$ .

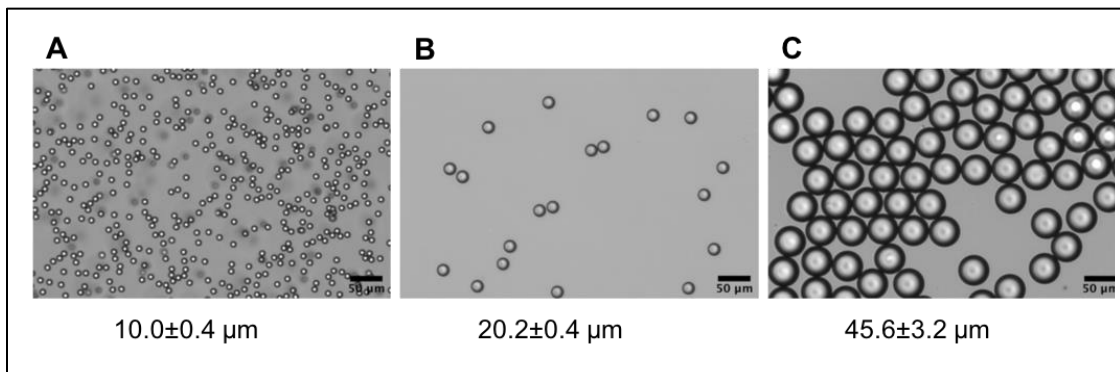


**Figure 2.13. Particle size analysis of polystyrene beads measured with light microscopy.** (A) 10  $\mu\text{m}$ , (B) 20  $\mu\text{m}$  and (C) 50  $\mu\text{m}$  polystyrene beads purchased from Duke standards. The mean particle size and standard deviation measured using light microscopy and image analysis methods in described section 2.2.4 is listed below the image.



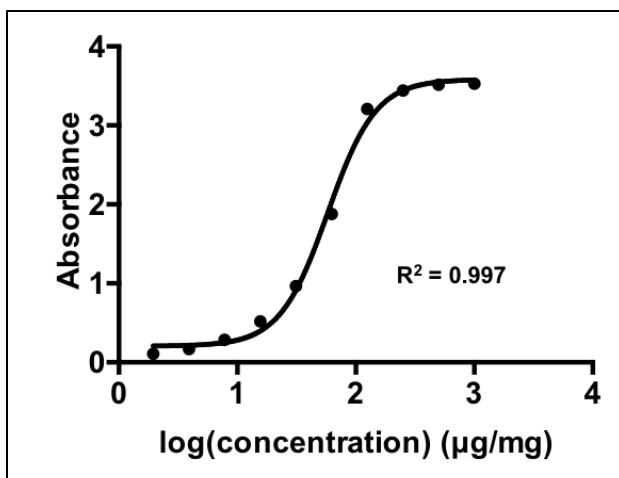


**Figure 2.14.** Representative standard curve for resveratrol dissolved in DMSO containing PLG at 1 mg/mL.

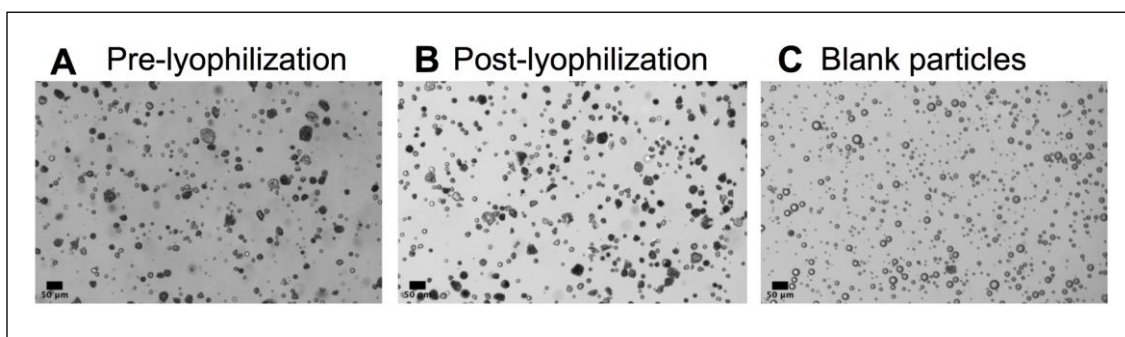


**Figure 2.15. Light microscopy of RSV particles** depicted in Figure 2.2A before (A) and after (B) lyophilization. Particles with no resveratrol (C) have spherical shapes, suggesting lyophilization does not cause irregular particle formation.

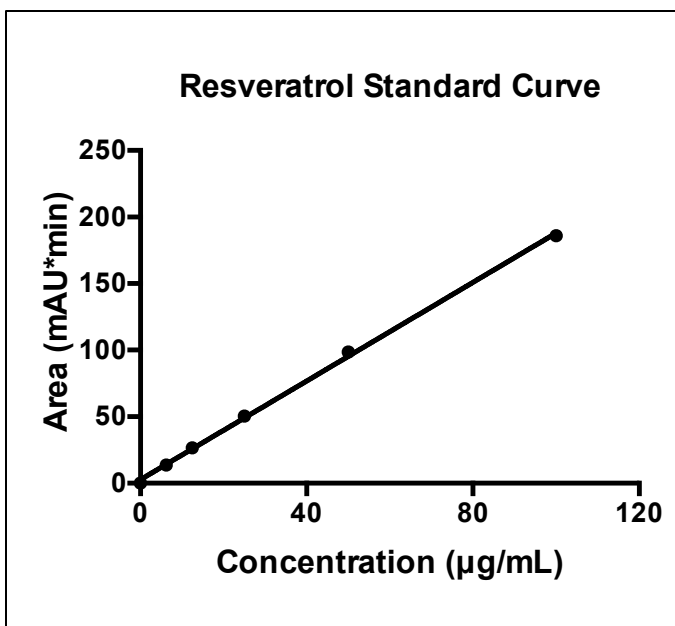


**Figure 2.16. Resveratrol Standard Curve via HPLC.** Validation of UV-Vis analysis was done via HPLC of resveratrol loading of irregular particles shown in Figure 2.2A. Loading of resveratrol was found to be  $69 \pm 7$  ug/mg, which was very close to  $65 \pm 5$  ug/mg found via UV-Vis.

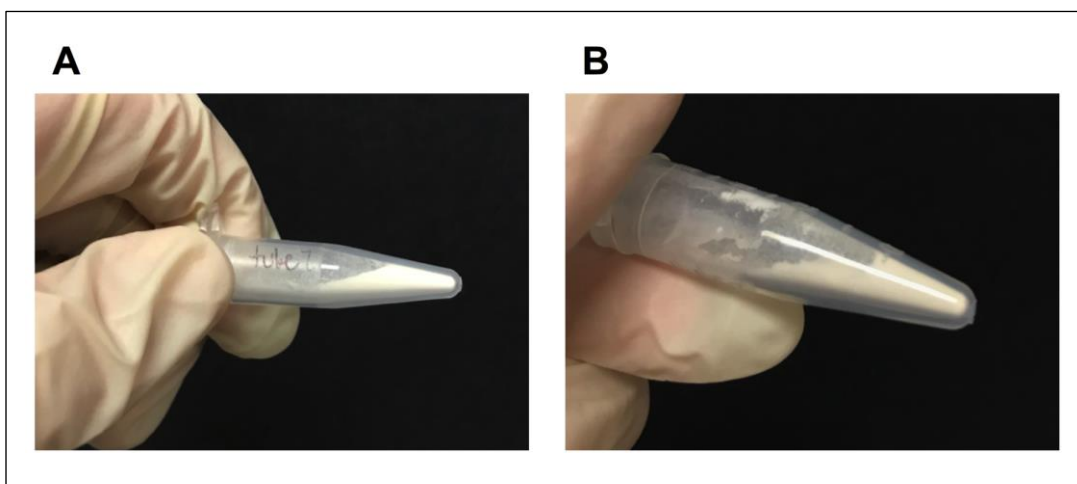


**Figure 2.17. Flowability of particles.** Particles in an Eppendorf tube before (A) and after (B) spinning on the axis. Particles flow and take the shape of the container.

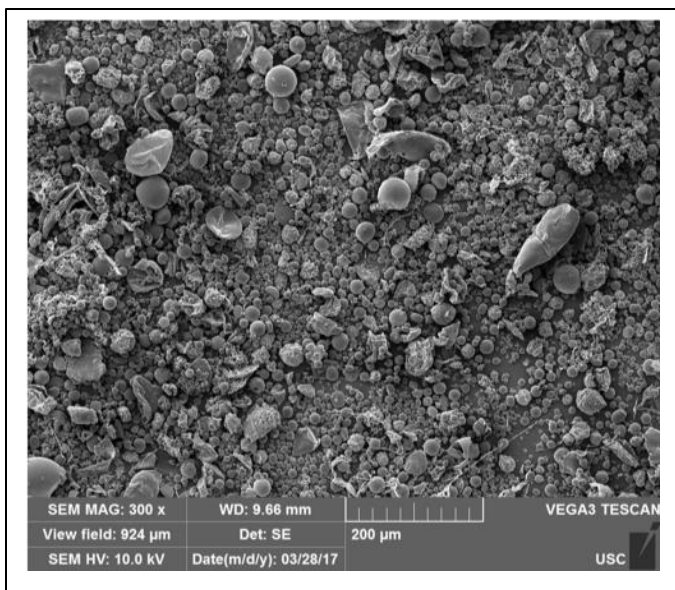


**Figure 2.18. SEM image of particles fabricated with 5% PVA in the emulsion.** Conditions used were 1:3 ethanol to DCM, 10ug/mg resveratrol, 7000 rpm for 30 seconds, and 5% PVA in the emulsion step and 0% PVA in evaporation step.

## CHAPTER 3

# FABRICATION OF BIODEGRADABLE PARTICLES WITH TUNABLE MORPHOLOGIES BY THE ADDITION OF RESVERATROL TO OIL IN WATER EMULSIONS.<sup>2</sup>

### 3.1 Introduction

The oil in water (O/W) emulsion/solvent extraction technique for making biodegradable polymer particles involves dissolving a polymer in an organic solvent (typically dichloromethane, DCM) and homogenizing in an aqueous solution of an emulsifier (typically polyvinyl alcohol, PVA). The two phases are immiscible, and spherical droplets are produced because this geometry minimizes interfacial energy. The emulsion is then added to a large volume of aqueous solution and the organic solvent is extracted from the dispersed phase, which results in the polymer precipitating and hardening into particles. The particles are then recovered through centrifugation. This technique is one of the most studied and utilized for producing polymer particles because of its versatility and scalability, and it is used for several FDA approved polymer-based, controlled-release therapies such as Vivitrol<sup>57</sup>, Lupron Depot<sup>109</sup>, and Risperdal<sup>110</sup>. The O/W emulsion/solvent extraction technique allows for tuning of many particle properties including, size, drug release rate, and surface chemistry<sup>54,58</sup>. However, altering particle

---

<sup>2</sup> Isely, C., Stevens, A.C., Tate, G.L., Monnier, J.R., and Gower, R.M. 2020. *International Journal of Pharmaceutics*. 590: 119917. Reprinted here with permission of publisher.

morphology is challenging because of the tendency of this emulsion system to form spheres<sup>62</sup>. Tuning particle morphology is of interest because it impacts cell-material interactions and subsequent biological responses<sup>49</sup>. Cells interact differently with nonspherical particles than spherical ones<sup>61,64,111</sup>. For example, macrophages internalize ellipsoidal particles in an orientation dependent manner. The long end of the ellipsoid is internalized more readily than the flat side<sup>61</sup>. Additionally, fibroblasts attach more readily to particles with a wrinkled surface than those that are smooth<sup>64</sup>. Finally, nonspherical particles cause maturation of dendritic cells to a greater extent than spherical particles<sup>111</sup>. Particle fabrication techniques used in these studies include particle film stretching<sup>61</sup>, photopolymerization<sup>64</sup>, and microfluidics<sup>111</sup>. While these methods are elegant, they are technically challenging and do not have a history of implementation in GMP manufacturing<sup>54,112</sup>. Thus, while these studies demonstrate the importance of particle morphology on the biological response, the particle fabrication techniques employed may be difficult to adapt to the pharmaceutical industry<sup>44,113</sup>.

The scalability of the O/W emulsion technique makes it attractive for making nonspherical particles at an industrial scale. As a point of comparison, photopolymerization and lithography produce approximately  $10^6$  particles per day with constant operation; in contrast, a bench-scale O/W emulsion batch process produces  $10^9$  particles in a matter of hours and is only limited by the size of the vessel<sup>62</sup>. While nonspherical particles have been achieved using O/W emulsion systems<sup>114</sup>, they required poloxamer surfactants that have yet to be incorporated in an FDA approved polymer particle controlled release therapy<sup>44</sup>. Taken together, a methodology to modulate particle morphology that utilizes the DCM/PVA emulsion system would be highly desirable.

Recently, we investigated poly(lactide-co-glycolide) particles for delivery of resveratrol to fat tissue, a small molecule with anti-obesity properties<sup>26</sup> and an established safety profile in humans<sup>28</sup>. To accomplish this, we developed a method to encapsulate resveratrol within the particles using the DCM/PVA emulsion system by utilizing ethanol as a cosolvent in the oil phase<sup>68</sup>. Unexpectedly, we found that the incorporation of resveratrol into the particles led to a non-spherical morphology. While the previous study evaluated the particles for controlled release of resveratrol, an investigation into why the emulsion system produced non-spherical particles was not carried out. Herein, we sought to study the system by investigating the effect of cosolvent, primary solvent and type of stilbene on particle morphology. In addition, we investigate its applicability to additional polyesters used in FDA approved devices<sup>115</sup> and demonstrate an ability to encapsulate a model hydrophobic drug, coumarin 6. Taken together, the data presents a facile method for controlling the morphology of polyester particles. Given the importance of particle morphology in cell-material interactions, our findings may aid in the field's ability to control biological responses with biocompatible particulate systems.

## **3.2 Materials and Methods**

### *3.2.1 Materials*

75:25 poly(D,L-lactide-co-glycolide) (PLG) with a lauryl ester end group and an inherent viscosity of 0.79 dL/g and ester terminated polycaprolactone (PCL) with an inherent viscosity of 1.24 g/dL were purchased from Evonik (Birmingham, AL). Dichloromethane (DCM), resveratrol (RSV), poly(vinyl alcohol) (PVA) (MW 13,000–23,000, 87–89% hydrolyzed), poly(L-lactide) (PLLA) with an ester end group and an inherent viscosity of 1.1 dL/g, pinosylvin and coumarin 6 were purchased from Sigma (St.

Louis, MO). Ethyl acetate (EA) was purchased from Macron Fine Chemicals (Center Valley, PA) and trans-stilbene was purchased from TCI Chemicals (Portland, OR). Piceattanol was purchased from Cayman (Ann Arbor, MI). Methanol (MeOH) and acetone were purchased from BDH Chemicals (Radnor, PA). Ethanol (ETOH) was purchased from Decon Laboratories (King of Prussia, PA). Dimethyl sulfoxide (DMSO) was purchased from Fisher (Hampton, NH). Ultrapure water was obtained from a Thermo Scientific Barnstead Nanopure system.

### *3.2.2 Polymer Particle Fabrication*

Polymer particles were prepared using a single oil-in-water emulsification/solvent extraction method as described previously with modifications<sup>95</sup>. Briefly, polymer was dissolved in organic solvent at a concentration that would achieve a final organic phase concentration of 6% (wt/wt), hereafter simply “6%”. If a stilbene was included, it was dissolved in cosolvent and added to the organic phase for final concentrations and cosolvent proportions listed in Table 3.1. For the emulsion, 0.6 mL of organic phase was added dropwise into 4 mL of an aqueous solution of 1% (wt/v) polyvinyl alcohol (PVA), hereafter simply “1%”, and homogenized at 7000rpm for 30s using a Kinematica PT3100D homogenizer. Solvent extraction was then conducted by adding the homogenization mixture to 16 mL of ultrapure water and then stirring the mixture for 5 hours. This allows the organic solvent to extract and evaporate and the resulting particles to harden. The particles were then passed through a 40  $\mu$ m filter (Greiner Bio-one), collected via centrifugation at 1750xg and washed 4 times in ultrapure water. Washed particles were frozen at -20°C and subsequently lyophilized overnight with a Labconco freeze dryer. Recovered particles were stored under vacuum in a dry environment at room temperature.

For coumarin 6 loaded particles, all conditions were the same as the first formulation in Table 3.1, except coumarin 6 was added to the organic phase at 0.5 mg/mL.

**Table 3.1.** Conditions used for particle formulations.

<b>Primary Solvent</b>	<b>Cosolvent</b>	<b>Stilbene</b>	<b>Stilbene concentration</b>	<b>Volume % of cosolvent</b>	<b>Polymer</b>
DCM	<b>ETOH</b>	Resveratrol	10 mg/mL	25%	PLG
DCM	<b>MEOH</b>	Resveratrol	10 mg/mL	25%	PLG
DCM	<b>Acetone</b>	Resveratrol	10 mg/mL	25%	PLG
DCM	ETOH	Resveratrol	<b>4 mg/mL</b>	<b>25%</b>	PLG
DCM	ETOH	Resveratrol	<b>0 mg/mL</b>	<b>25%</b>	PLG
DCM	ETOH	Resveratrol	<b>4 mg/mL</b>	<b>10%</b>	PLG
DCM	ETOH	Resveratrol	10 mg/mL	25%	<b>PCL</b>
DCM	ETOH	Resveratrol	10 mg/mL	25%	<b>PLLA</b>
DCM	ETOH	<b>Piceattanol</b>	10 mg/mL	25%	PLG
DCM	ETOH	<b>Pinosylvin</b>	10 mg/mL	25%	PLG
DCM	ETOH	<b>Trans-Stilbene</b>	10 mg/mL	25%	PLG
<b>EA</b>	<b>None</b>	Resveratrol	10 mg/mL	0%	PLG

DCM: dichloromethane; EA: ethyl acetate; ETOH: ethanol; MEOH: methanol; PLG: poly(lactide-co-glycolide); PCL: polycaprolactone; PLLA: poly(L-lactide).



### 3.2.3 Video microscopy of particle formation

Particle formation was visualized under a Nikon Eclipse Ci microscope after the emulsion process had taken place. After homogenization, 10  $\mu\text{L}$  of the emulsion was transferred onto a glass slide. This was then observed under the microscope while images were acquired every second for 5 minutes, which was a sufficiently long time that no more particle formation was observed. Videos were made with a frame rate of 10 images per second.

### 3.2.4 Powder X-Ray Diffraction

A Rigaku MiniFlex X-ray diffractometer with high sensitivity 1D silicon strip detector (D\teX Ultra) was used to detect the presence of crystalline structure within the particles. 10 mg of samples were spread on zero-background holders for analysis. PXRD was performed over a range of  $5\text{--}80^\circ 2\theta$  at room temperature at a scan rate of  $2^\circ/\text{min}$ . An x-ray source with Cu target at 30kV and 15mA was used to generate Cu  $K\alpha$  x-rays ( $\lambda=1.54059\text{\AA}$ ) for analysis. Diffraction was recorded as intensity vs.  $2\theta$ . Peak fitting was performed using Fityk curve fitting program<sup>116</sup>.

### 3.2.5 Sessile Drop

To qualitatively determine interfacial tension of the emulsion system, a sessile drop experiment of the aqueous and organic phases was employed. 4 mL of aqueous phase (1% PVA) was added to a 20 mL scintillation vial. Into this, 0.3 mL of organic phase was carefully added to the bottom of the vial. Images were then taken from a level surface and relative height and angle of contact analyzed.

### *3.2.6 Scanning Electron Microscopy (SEM) and Light Microscopy (LM)*

Carbon adhesive tape was attached to aluminum SEM stubs, and particles were spread onto the stubs. Compressed air was applied briefly to the particles to create a monolayer on the carbon tape. Particles were sputtered with gold 3 times for 60 seconds in a Denton Desk II Vacuum sputter coater. Images were taken using a TESCAN Vega3 Scanning Electron Microscope at 10kV.

Light and fluorescence microscopy images of particles were taken on an EVOS FL microscope at 20x magnification. Particles were prepared in ultrapure water and suspended at a concentration of 0.25 mg/mL. 400  $\mu$ L of these suspensions was added to a well of a 48-well plate and allowed to settle prior to image acquisition. Fluorescence images were taken on the green GFP (470nm) fluorescence setting.

### *3.2.7 Measurement of Particle Size*

Particle size was found by analyzing light microscopy images using ImageJ software. Briefly, three representative images were taken of each particle condition and converted to binary (B/W) colors. The Particle Analysis plugin in ImageJ was used to measure particle diameter. We report the mean particle diameter and the coefficient of variation (CV%), which is the standard deviation divided by the mean. We validated this method previously<sup>68</sup> by accurately measuring the size of purchased polystyrene beads.

### *3.2.8 Mass Yield and Resveratrol Loading*

Mass yield was calculated by dividing the mass of recovered particles by the mass of polymer and resveratrol emulsified. Particle mass yield was calculated according to equation 1.

$$Mass\ Yield\ (\%) = \left( \frac{M_{PT}}{M_{Pol} + M_{RE}} \right) * 100 \quad (1)$$

Where  $M_{PT}$  is the mass of particles recovered from the emulsion,  $M_{Pol}$  is the mass of polymer added to the emulsion, and  $M_{RE}$  is the mass of resveratrol added to the emulsion.

Resveratrol content was determined by dissolving 1 mg of particles in 1 mL DMSO and measuring absorbance at 330 nm using a Spectramax 190 UV-Vis spectrophotometer. A 10-point standard curve was prepared by dissolving 1 mg of empty particles and a known mass of resveratrol in DMSO. Resveratrol concentration was determined by comparing the unknown samples to the standard curve. Resveratrol loading ( $\mu\text{g}/\text{mg}$ ) was calculated by dividing the mass of resveratrol extrapolated from the standard curve by the mass of particles dissolved in DMSO. Resveratrol loading was calculated by equation 2.

$$Loading\ \left( \frac{\mu\text{g}}{\text{mg}} \right) = \frac{M_R}{M_P} \quad (2)$$

Where  $M_P$  is the mass of particles dissolved in DMSO and  $M_R$  is the mass of resveratrol measured in those particles.

### 3.2.9 Calculation of surface area

Surface area of particles was determined by the Brunauer Emmet Teller (BET) gas adsorption method<sup>117</sup> using krypton adsorption isotherms measured using a Micromeritics ASAP 2020 physisorption instrument. Approximately 250 mg of particles were weighed out in a glass sample tube and degassed for 12 hours at 30°C. Krypton adsorption measurements were then carried out at 77K up to  $P/P_0 = 0.3$ . BET transformation of the Kr adsorption isotherms was fit with linear regression over appropriate range. Linear fitting of BET transform plot was considered acceptable above an  $R^2$  of 0.999. We validated that our protocol would provide accurate, reproducible measurements by analyzing 250 mg of a low surface area silica standard ( $0.20 \pm 0.03\ \text{m}^2/\text{g}$ ) provided by Micromeritics in three

independent experiments (Table 3.2.) The average value for the three trials fell within the reported range of the low SA alumina standard. Surface area measurements of polymer particles were then run 1 or 2 times for each condition.

**Table 3.2.** Surface area measurements of low surface area silica standard

<b>Trial # (Date)</b>	<b>BET Surface area (m<sup>2</sup>/g)</b>
1 (11/16/19)	0.1703±0.0045
2 (11/21/19)	0.1730±0.0014
3 (11/22/19)	0.1757±0.0014

### *3.2.10 Differential centrifugation of nonspherical particles*

Particles were separated by size based on the principle that large particles sediment more readily than small particles. For our system, we found that 10 minutes of centrifugation at 1xg sedimented 25 µm particles while 30xg sedimented 6 µm particles and 250xg sedimented 2 µm particles and smaller. We suspended 50 mg of nonspherical particles in 40mL water in a 50mL centrifugation tube and centrifuged at 1xg for 10 minutes. The supernatant was then collected and centrifuged for 10 minutes at 30xg. Finally, the supernatant of the second spin was centrifuged at 250xg for 10 minutes. This produced particles in size ranges of 2 µm – 6 µm, 6 µm – 25 µm, and 25 µm and larger. Particle sizing is described earlier in the methods.

## **3.3 Results**

### *3.3.1 Observing particle formation with video microscopy.*

Previously, we reported that the addition of resveratrol to the oil phase of a DCM/PLG/PVA/H<sub>2</sub>O emulsion using ethanol as co-solvent led to the formation of

nonspherical particles with creased or wrinkled surfaces<sup>68</sup>. To visualize the process by which the oil droplets become nonspherical particles, we imaged particle formation using video microscopy. This was achieved by forming the emulsion and then rapidly transferring a small sample to a glass slide for observation and video recording. We found that in emulsions with resveratrol, droplets buckled and crumpled as they decreased in volume, presumably as DCM and ethanol diffuse out of the droplet. In contrast, droplets formed without resveratrol maintained spherical geometry as their volume decreased (Fig 3.1). SEM images confirm that particles made with DCM or DCM and ethanol are spherical, while most particles made with resveratrol are highly crumpled (Figure 3.1, fourth column). The video microscopy indicates that when resveratrol is incorporated into the emulsion, the droplet deviates from its spherical form as volume is decreased leading to a crumpled morphology.

### *3.3.2 XRD analysis*

We next sought to determine if the resveratrol was crystalline in the particles made with the small molecule. To determine this, we conducted X-ray diffraction (Figure 3.2, PLG+RSV, blue line). For comparison, we also investigated free resveratrol (RSV, black line), particles made without resveratrol (PLG, orange line), and a physical mixture of the two (PLG+RSV Mixed, yellow line). Particles made with resveratrol had a loading of 65  $\mu\text{g}/\text{mg}$  or 6.5%, and thus, the physical mixture was 6.5% resveratrol by mass.

The diffractogram for free resveratrol indicated it was crystalline with several sharp diffraction peaks at 7.0, 16.7, 19.6 and 28.6° among others. The amorphous nature of the particles made without resveratrol was evidenced by a broad peak between 10 and 25°. The physical mixture of resveratrol and particles exhibited several diffraction peaks (including

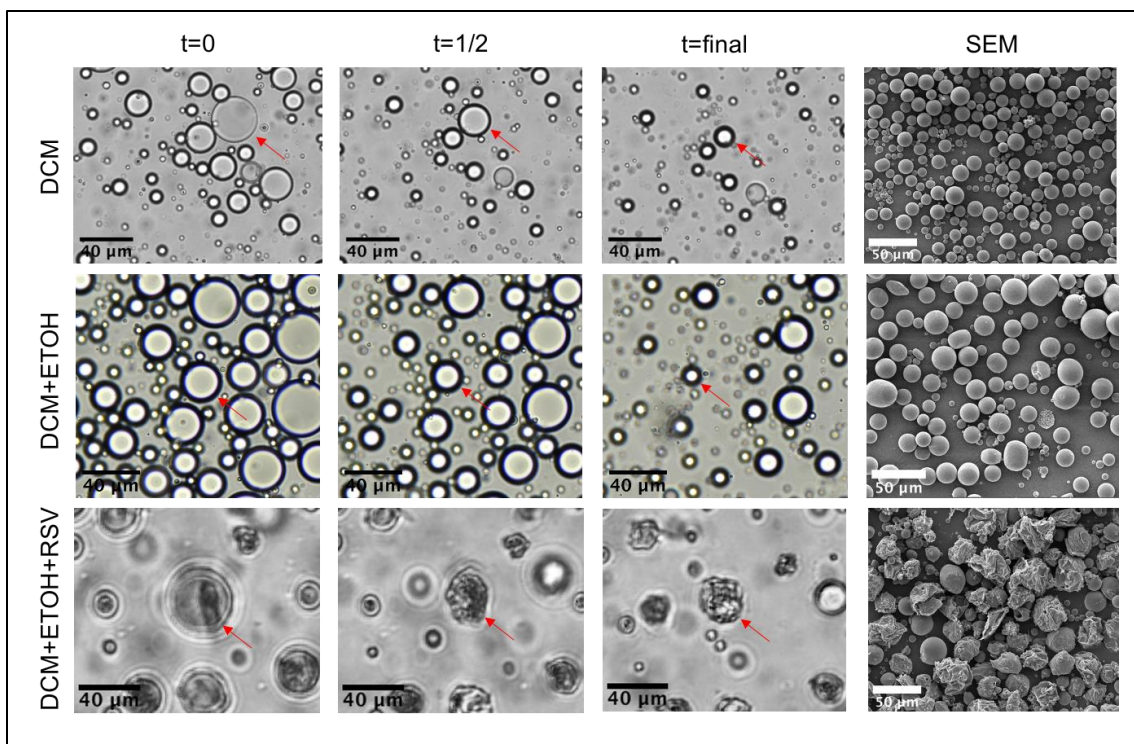


**Figure 3.1. Images from video microscopy of particle formation with corresponding SEM images.** The results of three emulsions are shown. For all cases, the concentration of PLG in the oil phase is 6% and the concentration of PVA in the aqueous phase is 1%. The formulation of the oil phase varies by row. The top row is 100% DCM. The middle row is 75% DCM and 25% ethanol (ETOH). The bottom row is 75% DCM, 25% ETOH and 10 mg/mL resveratrol (RSV). Frames are shown from the beginning of video acquisition ( $t=0$ ), midway through the video ( $t=1/2$ ) and at the end of the video when particle size has stabilized ( $t=final$ ). Red arrows indicate the same droplet over time for each condition. SEM images of the particles are shown in the right-hand column.

7.1, 16.9, 19.9, 29.0°), indicating crystalline resveratrol could be detected at the weight percent used (6.5%). The diffractogram for the particles made with resveratrol exhibited peaks at 7.0, 16.8, 19.6 and 28.7°, similar to those observed in the physical mixture (albeit they were smaller). The data suggest that a small amount of the resveratrol may be crystalline in the particles made with the small molecule.

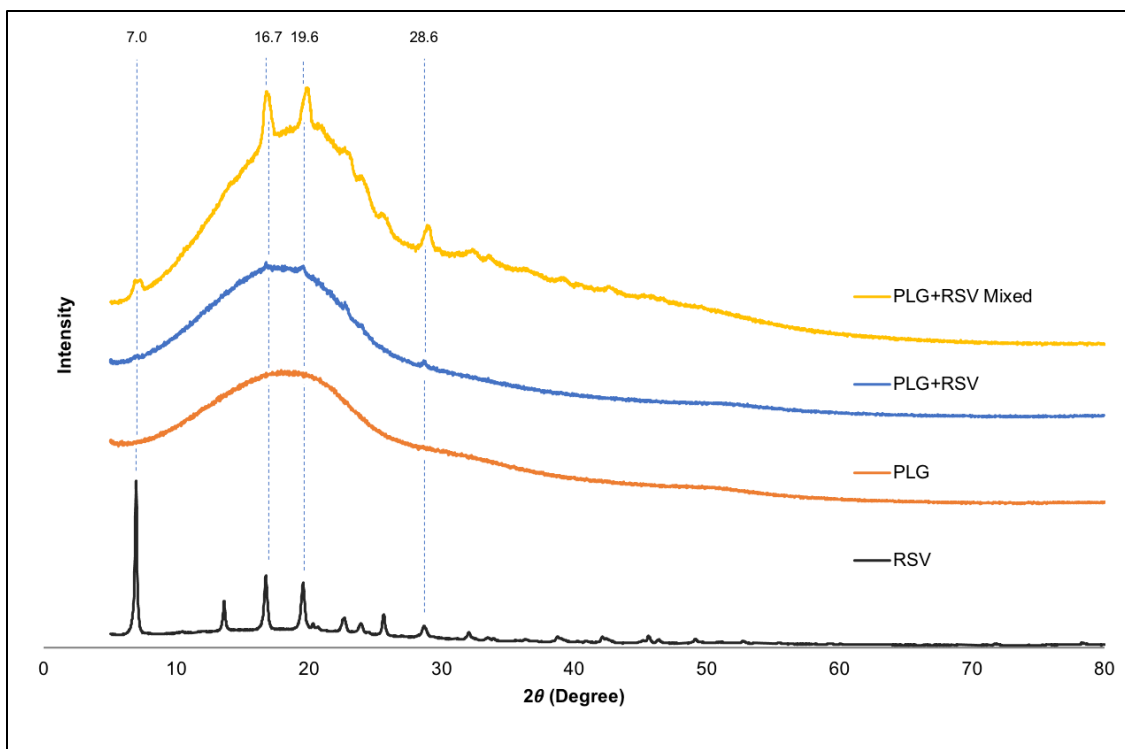


**Figure 3.2. X-ray diffraction of resveratrol and PLG particles.** Diffractogram of free resveratrol (RSV, black curve), PLG particles (PLG, orange curve), particles made with resveratrol with a loading of 65  $\mu\text{g}/\text{mg}$  (PLG+RSV, blue curve) and a physical mixture of particles and resveratrol that was 6.5% resveratrol by mass (PLG+RSV Mixed, yellow curve). Curves are displayed as Intensity vs.  $2\theta$ . Diffraction peaks shared by the particles containing resveratrol (blue curve), the physical mixture of particles and resveratrol (yellow curve,) and free resveratrol (black curve) are indicated with dotted blue lines with the corresponding  $2\theta$  measurement reported directly above the line.

### 3.3.3 Sessile drop analysis of interfacial tension

Decreasing interfacial tension of an emulsion can lead to deviations from spherical morphology<sup>101,111</sup>. To determine if resveratrol was affecting interfacial tension, we employed the sessile drop method to study the shape of a drop of the organic phase in the aqueous phase. In this method, the height of the drop is directly proportional to the interfacial tension between the two phases<sup>118</sup>. Figure 3.3A shows that PLG dissolved in DCM pipetted into an aqueous solution of PVA forms a sessile drop on the bottom of the vial. Fig 3.3B indicates that when the organic phase (PLG+DCM) contains 25% ethanol

the drop decreases in height, indicating the interfacial tension is decreased, which is consistent with another study<sup>97</sup>. In Figure 3.3C, resveratrol is added to the organic phase containing DCM, PLG and ethanol. The resveratrol can be seen diffusing into the aqueous phase as a white precipitate. The drop containing resveratrol appears to have a similar height to the drop containing only DCM and PLG (Fig. 3.3A), suggesting the addition of resveratrol nullifies the decrease in interfacial tension caused by the ethanol.

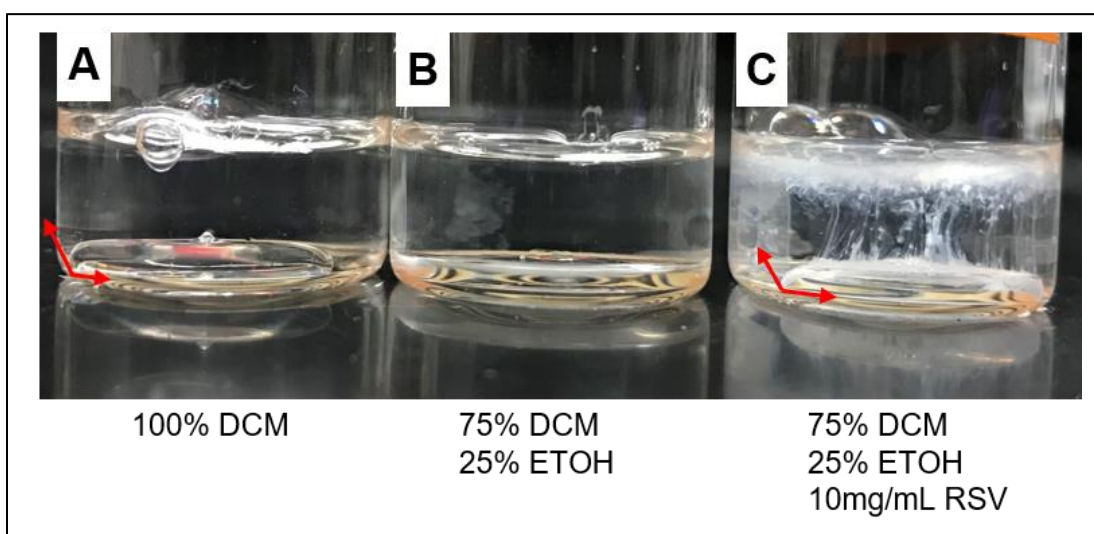


**Figure 3.3. Effect of ethanol and resveratrol on sessile drop formation.** Image of sessile drops formed by pipetting the organic phase into aqueous solution of PVA. Aqueous phase is 1% PVA in water. The organic phase is 6% PLG dissolved in **A)** 100% DCM, **B)** 25% ethanol 75% DCM and **C)** 25% ethanol 75% DCM and 10 mg/mL resveratrol. Arrows delineate the organic droplet against the bottom of the vial.

#### *3.4 Effect of hydroxyl group number and placement on particle morphology*

Resveratrol is a trans-stilbene derivative where hydroxyl groups reside at the 3, 5, and 4' positions relative to the double bond (Figure 3.4C). We hypothesized that hydroxyl group number and placement would impact particle morphology. Thus, we produced particles with trans-stilbene, which has no OH groups, pinosylvin, which lacks the 4' OH



group of resveratrol, and piceatannol, which has an additional OH group at the 3' position when compared to resveratrol (Figure 3.4). We found that incorporation of trans-stilbene or pinosylvin into the emulsion resulted in spherical particles. In contrast, incorporation of piceatannol largely inhibited particle formation. The mass yield of particles dropped from 60% (for trans-stilbene) to 12% for piceatannol, making it difficult to study the piceatannol particles via microscopy (Figure 3.4D). The particles that did form in the presence of piceatannol appeared irregular in shape. We conclude that the degree of hydroxyl substitution impacts emulsion stability. Furthermore, of the trans-stilbene derivatives investigated, the number and placement of hydroxyl groups in resveratrol appear to be optimal for inducing crumpled particle morphology at the conditions tested.

#### *3.3.5 Relative contributions of ethanol and resveratrol on particle morphology*

We next investigated the relative contributions of ethanol and resveratrol on particle morphology. Decreasing the resveratrol concentration from 10 mg/mL (used to make the particles depicted in Figure 3.1 and 3.4C) to 4 mg/mL, while maintaining the ethanol concentration at 25%, led to particles that were mostly spherical; however, we did observe a small population of particles with crumpled morphology (Figure 3.5 A,D, red arrows). Particles made this way had relatively low resveratrol loading, 1.5  $\mu$ g/mL. Particles made with 25% ethanol, but no resveratrol were spherical, indicating resveratrol is required for particle crumpling (Figure 3.5 B,E). Interestingly, when ethanol concentration was decreased to 10% while maintaining resveratrol at 4 mg/mL, particles were also spherical (Figure 3.5 C,F) and had a resveratrol loading of 4 mg/mL, which was 2.6-fold higher compared to the conditions in Figure 3.5 A,D. The data suggests that resveratrol loading

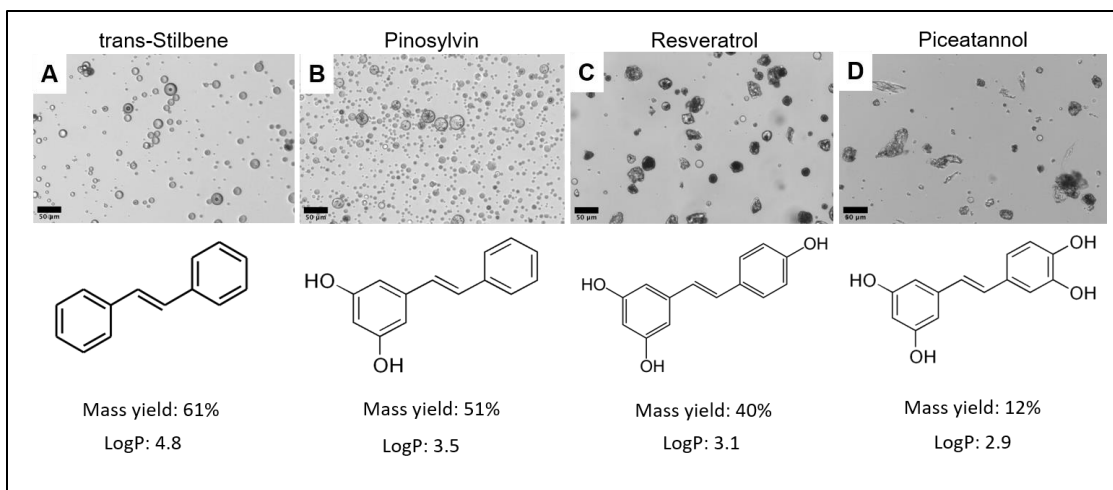


**Figure 3.4. Effect of resveratrol-like molecules on particle morphology.** Particles were made with an organic phase that was 25% ethanol, 75% DCM, and 6% PLG. In addition, the organic phase contained a stilbene at 10 mg/mL. The stilbenes investigated were (A) trans-stilbene, (B) pinosylvin, (C) resveratrol, or (D) piceatannol. Light microscopy images are shown along with the stilbene's structure and logP. The mass yield of particles is also listed. Scale bars indicate 50 µm.

may not be the defining factor that dictates particle morphology and that ethanol may enhance resveratrol's effect on particle buckling and crumpling.

### 3.3.6 The effect of cosolvent on particle morphology

Here, we sought to understand the effect of cosolvent on particle morphology. To accomplish this, we fabricated particles using either ethanol, methanol, or acetone as the cosolvent. All three solvents are able to solubilize resveratrol to a similar degree (50 mg/mL, Table 3.3). One difference between these three solvents is their solubility in water, which is also reflected by their LogP values (Table 3.3). Specifically, methanol is about twice as soluble in water as acetone, and ethanol's solubility resides in between methanol and acetone. An additional difference is that PLG is soluble in acetone at 6%, but not in ethanol or methanol (Table 3.3).

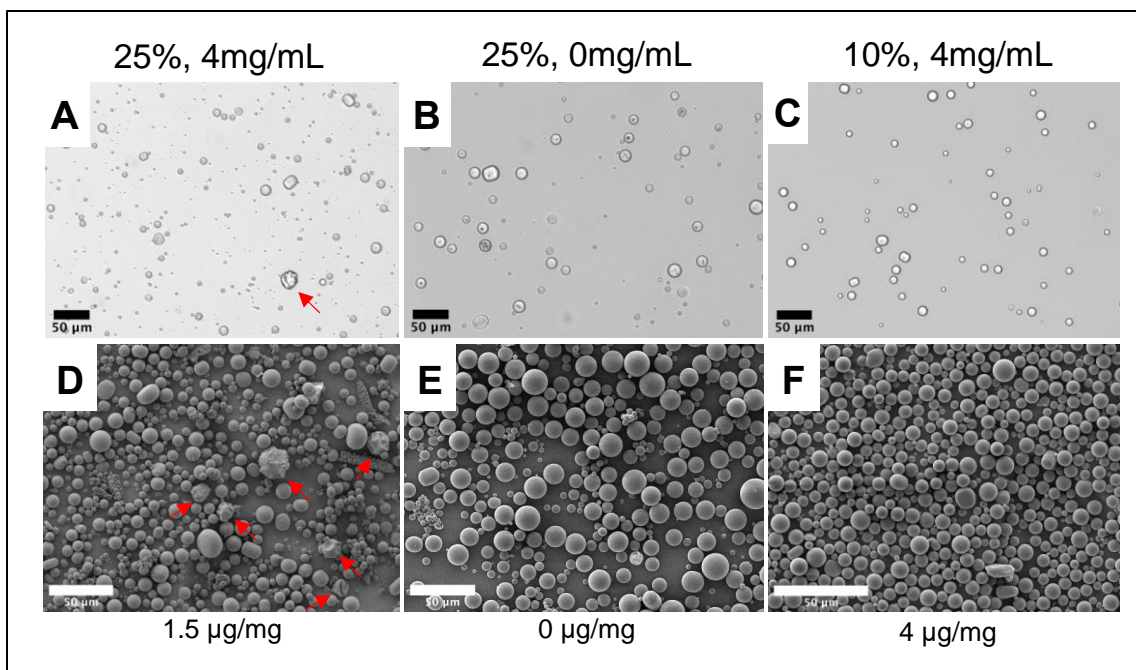


**Figure 3.5. Relative contributions of ethanol and resveratrol on particle morphology.** (A-C) Light microscopy images and (D-F) SEM images of particles made with differing amounts of resveratrol and ethanol in the oil phase. (A,D) 25% ethanol and 4 mg/mL resveratrol, (B,E) 25% ethanol and 0 mg/mL resveratrol, (C,F) 10% ethanol and 4 mg/mL resveratrol. Red arrows indicate crumpled particles. Scale bars indicate 50  $\mu\text{m}$ .

Utilizing ethanol as the cosolvent resulted in many highly crumpled particles and some smaller particles that were spherical (Figure 3.6A,D). Resveratrol content of the particles made with ethanol was 65  $\mu\text{g}/\text{mg}$ . Utilizing methanol as the cosolvent also resulted in crumpled particles and a population of spherical particles that tended to be smaller than the nonspherical particles (Figure 3.6B,E). Resveratrol content of particles made with methanol was 50  $\mu\text{g}/\text{mg}$ . Finally, when acetone was used as the cosolvent, particle morphology resembled collapsed spheres, with deep indentations (Figure 3.6C,F). Once again, spherical particles were also observed, but they tended to be smaller than the nonspherical particles. Resveratrol content of particles made with acetone was 18  $\mu\text{g}/\text{mg}$ . In addition, particles made with methanol or acetone, but without resveratrol, were

**Table 3.3. Solvent Properties** <sup>119–121</sup>

<b>Solvent</b>	<b>RSV Solubility (mg/mL)</b>	<b>6% PLG solubility</b>	<b>Solubility in Water</b>	<b>LogP</b>
Methanol	50	No	31.21 M	-0.77
Ethanol	50	No	21.71 M	-0.31
Acetone	50	Soluble	17.22 M	-0.24
Ethyl Acetate	10	Soluble	0.91 M	0.73
Dichloromethane	None	Soluble	0.15 M	1.25

spherical (data not shown), which was the case when ethanol, but no resveratrol was used (Figure 3.1).

To quantify the differences in morphology between the particles formed with the three cosolvents, we calculated surface area using krypton gas adsorption measurements and BET theory. Particles made with ethanol, methanol, and acetone had specific surface areas of 1.2, 0.91, and 0.71 m<sup>2</sup>/g, respectively. The data indicates the crumpled morphology achieved with ethanol has 70% higher specific surface area than the collapsed spheres made with acetone. In addition, we find surface area correlates with resveratrol content.

### *3.3.7 Effect of ethyl acetate as the organic solvent on particle morphology*

The data up to this point led us to hypothesize that the two solvent system involving DCM and a cosolvent was causing nonspherical particle formation. Thus, we searched for a solvent able to solubilize both PLG and resveratrol. We found that resveratrol was soluble up to 10 mg/mL in ethyl acetate containing 6% PLG (Table 3.3). In addition, ethyl acetate has been used to make PLG particles using PVA as the emulsifier<sup>122</sup>. Particles fabricated

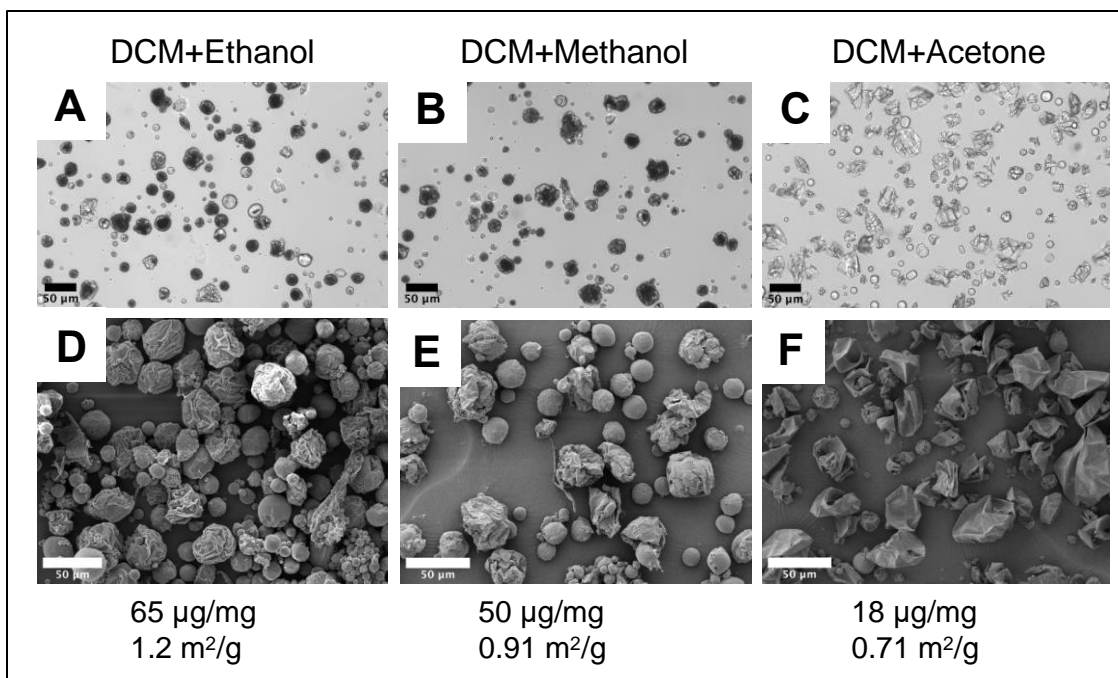


**Figure 3.6. The effect of cosolvent on particle morphology.** Representative images of PLG particles made with organic phases that were: **(A,D)** 25% ethanol and 75% DCM, **(B,E)** 25% methanol and 75% DCM, and **(C,F)** 25% acetone and 75% DCM. **(A-C)** are light microscopy images and **(D-F)** are SEM. The oil phase contained 6% PLG and 10 mg/mL RSV. The aqueous phase contained 1% PVA. Scale bars indicate 50 µm. Resveratrol loading is listed for each formulation in µg/mg. Surface area was determined by BET theory applied to Krypton adsorption isotherms and is listed in m²/g.

using ethyl acetate containing the same concentrations of resveratrol (10 mg/mL) and PLG (6%) as the DCM/ethanol system were smooth and spherical instead of crumpled (Figure 3.7). Particles made with ethyl acetate had similar loading to the highest loaded particles made with DCM and ethanol (57 µg/mg vs 65 µg/mg), but a lower surface area (0.78 m²/g vs 1.2 m²/g). This was expected because the particles made with ethyl acetate were spherical. Thus, we conclude that particle buckling that leads to the crumpled morphology is specific to when particles are made with resveratrol, and DCM is used with a cosolvent.

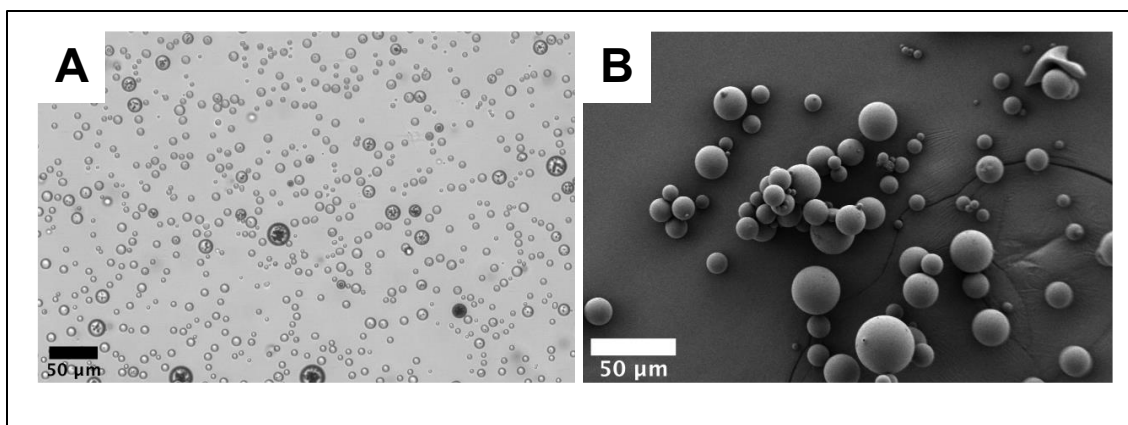


**Figure 3.7. Effect of Ethyl Acetate on particle morphology.** Light microscope (A) and SEM (B) images of resveratrol loaded particles made with ethyl acetate as the organic solvent. The oil phase contained 10 mg/mL resveratrol and 6% PLG. The aqueous phase contained 1% PVA. Resveratrol loading was 57  $\mu\text{g}/\text{mg}$  and the surface area was calculated to be 0.78  $\text{m}^2/\text{g}$ . Scale bars indicate 50  $\mu\text{m}$ .

### 3.3.8 Production of nonspherical particles using polycaprolactone and poly(L-lactide)

We were interested if crumpled particles could be produced from other polyesters that have been FDA approved for use in medical devices and drug delivery systems. We found that nonspherical particle formation could be achieved using polycaprolactone (PCL) or poly(L-lactide) (PLLA), which is demonstrated in Figure 3.8 A and C. To confirm that resveratrol was required for nonspherical particle formation, we made particles without resveratrol (blank particles) and confirmed they were spherical (Figure 3.8 B,D). Interestingly, the PCL particles were larger than the PLLA particles, which were similar in size when compared to PLG particles made without resveratrol. The PCL particles were probably larger because the PCL used has a higher inherent viscosity than the other two polymers and will naturally form larger droplets in the emulsion<sup>58</sup>.

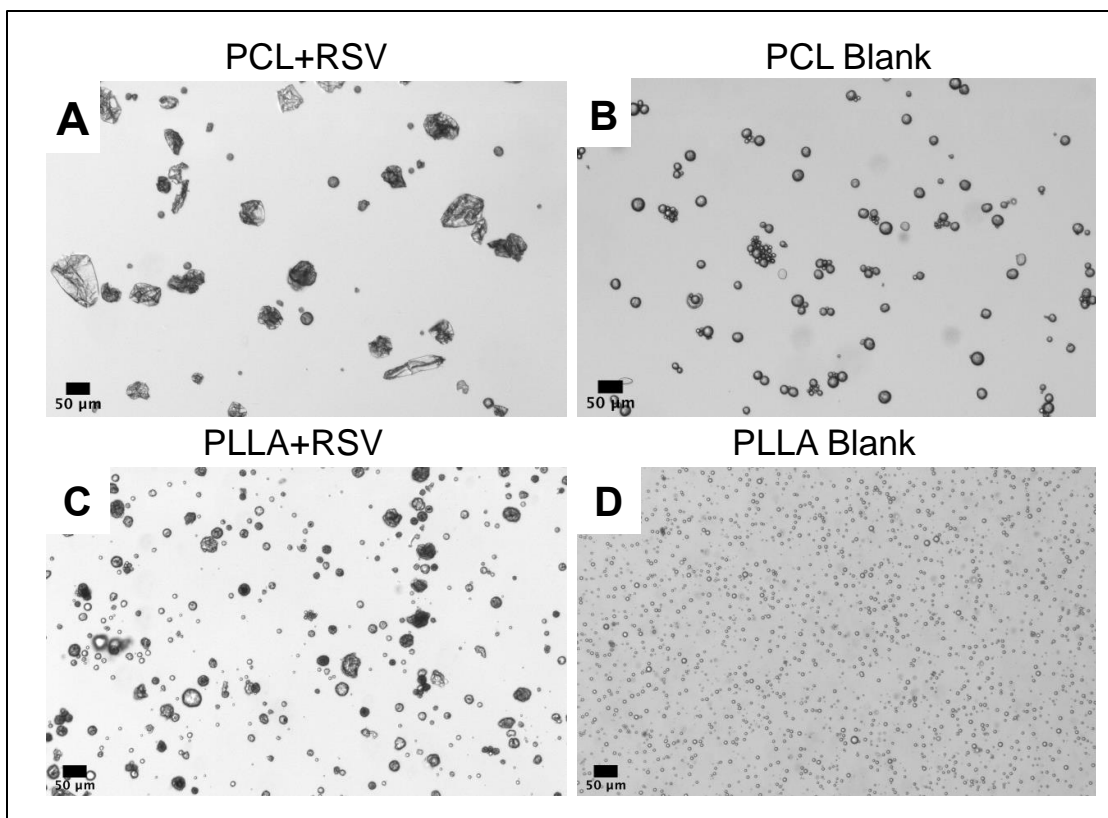


**Figure 3.8. Morphology of polycaprolactone (PCL) and poly(L-lactide) (PLLA) particles made with resveratrol.** Representative images of particles made with an oil phase consisting of (A,C) 25% ethanol and 75% DCM and 10 mg/mL of resveratrol or (B,D) 100% DCM with no resveratrol. (A,B) were made with an oil phase that was 6% PCL and (C,D) were made with an oil phase that was 6% PLLA. The aqueous phase of the emulsion contained 1% PVA. Scale bars indicate 50  $\mu$ m.

### 3.3.9 Incorporation of coumarin 6 into resveratrol loaded particles

One application of nonspherical particles is drug delivery, and we investigated if a hydrophobic agent could be encapsulated in the crumpled particles formed with resveratrol. As proof of concept, we added coumarin 6, a hydrophobic fluorochrome, to the oil phase containing ethanol, DCM, PLG and resveratrol. These particles formed with the same crumpled morphology as particles produced without coumarin 6 (compare Figure 3.9A with 6A) and were highly fluorescent (Figure 3.9B), indicating coumarin 6 was successfully encapsulated. Encapsulating coumarin 6 in the absence of resveratrol resulted

in smooth particles, demonstrating that coumarin 6 does not have an effect on particle morphology (Figure 3.9 C,D). These results suggest that hydrophobic bioactive agents could be encapsulated into the crumpled particles for drug delivery applications.

### *3.10 Separation of nonspherical particles by size*

Particle size impacts drug release kinetics<sup>103</sup>. Size also dictates how a biological system will interact with the particle. For example, particles smaller than 6 microns are readily phagocytosed by macrophages, while larger particles are left to reside in the extracellular space<sup>69</sup>. To demonstrate that nonspherical particles could be sorted based on size, differential centrifugation was employed to separate particles made with 25% ethanol and 75% DCM and 10 mg/mL of resveratrol. The process successfully separated 3 size ranges, as can be seen in Fig. 3.10. Centrifugation at 1xg collected particles above 25  $\mu\text{m}$  (Figure 3.10A). A subsequent round of centrifugation at 30xg collected particles between 6  $\mu\text{m}$  and 25  $\mu\text{m}$  (Figure 3.10B). A final round of centrifugation at 250xg collected particles that were less than 6  $\mu\text{m}$  (Figure 3.10C). The images suggest that the frequency of crumpled particles may decrease as size decreases.

## **3.4 Discussion**

The O/W emulsion/solvent extraction technique is a simple and scalable method for producing polymer particles and has been used in the fabrication of several FDA approved polymer particle therapies<sup>54</sup>. However, it is challenging to produce particles of nonspherical morphology, as O/W emulsions preferentially produce spherical particles. Here we present a facile method for producing nonspherical PLG particles by adding resveratrol and a cosolvent to the oil phase of a DCM/PLG/PVA/H<sub>2</sub>O emulsion. While



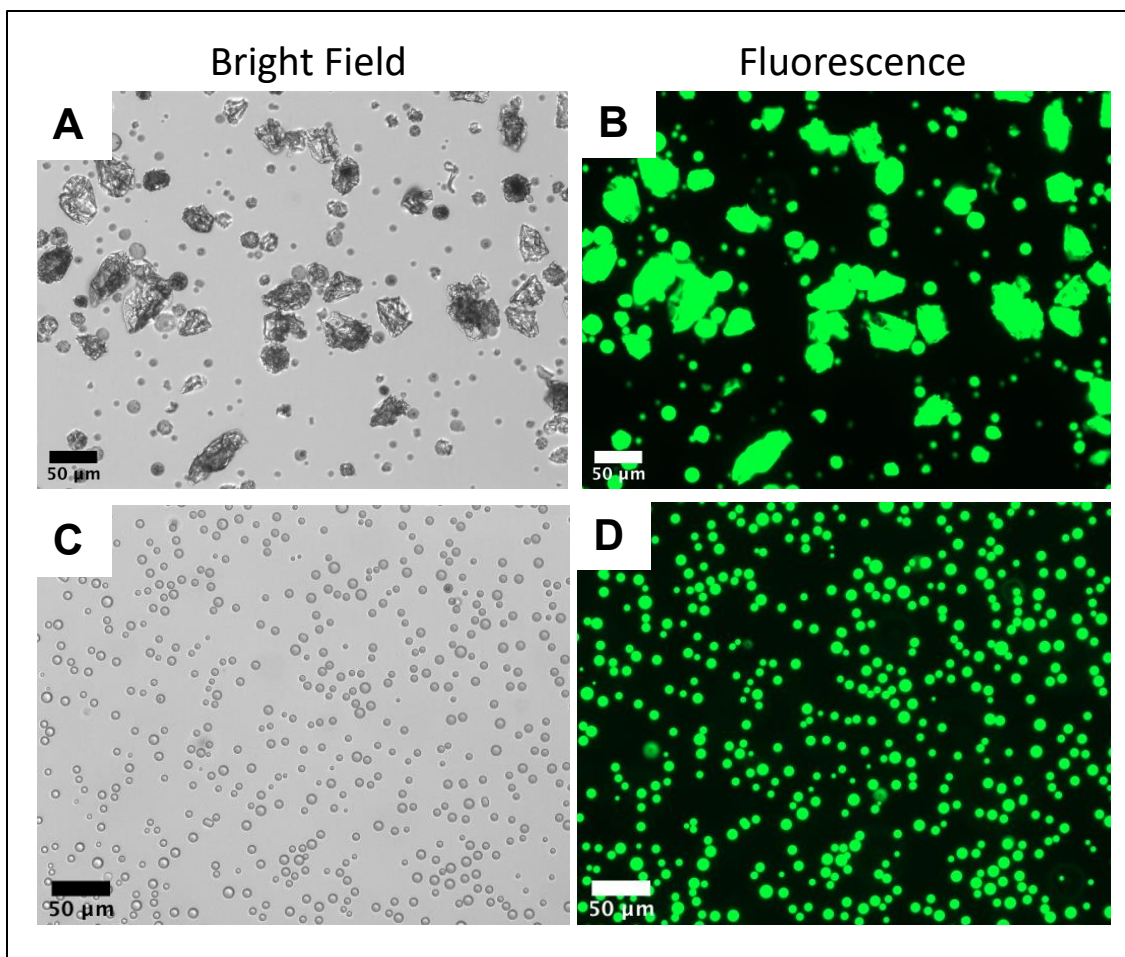


**Figure 3.9. Coumarin 6 can be encapsulated into crumpled particles formed with resveratrol.** Particles were fabricated with an oil phase consisting of 25% ethanol, 75% DCM, 6% PLG, and 0.5 mg/mL coumarin 6 with (A, B) or without (C,D) 10 mg/mL resveratrol. Scale bar indicates 50 μm.

addition of resveratrol and ethanol produce particles with a “crumpled paper” morphology, addition of resveratrol and acetone produce particles with a morphology that resembles deflated or indented spheres. We demonstrate broad applicability of the technique by producing nonspherical particles out of polycaprolactone and poly(L-lactide) in addition to PLG. Importantly, PCL and PLL are slower degrading polymers compared to PLG. Using polymers with varying degradation times can be used to modulate release rates for

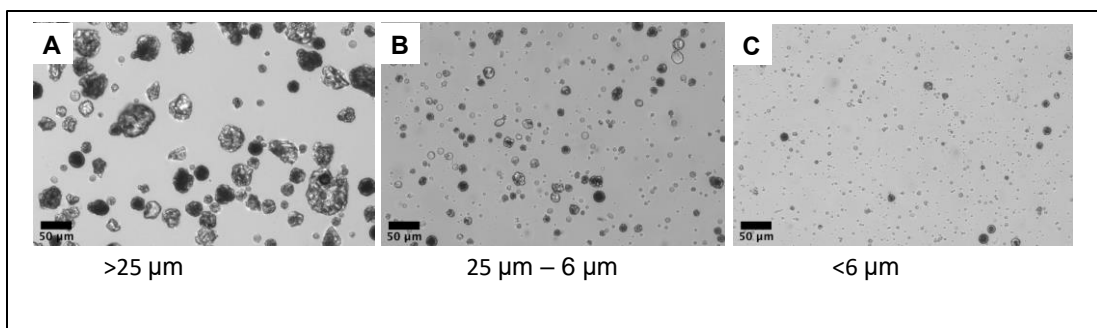


**Figure 3.10. Nonspherical particles can be separated by size using differential centrifugation.** Particles were fabricated with an oil phase consisting of 25% ethanol, 75% DCM 6% PLG, and 10 mg/mL resveratrol. The aqueous phase was 1% PVA. Particles were separated by size using differential centrifugation. Particles were first centrifuged at 1xg (A), then at 30xg (B), and finally at 250xg (C) each for 10 minutes. These steps produced particles that were 25  $\mu\text{m}$  and greater (A), 25  $\mu\text{m}$  – 6  $\mu\text{m}$  (B), and less than 6  $\mu\text{m}$  (C).

drug delivery applications<sup>123</sup>. In addition, we co-encapsulate resveratrol with a hydrophobic fluorescent dye, coumarin 6, which produces fluorescent nonspherical particles. This result suggests hydrophobic bioactive agents could be encapsulated into the crumpled particles for drug delivery applications. A previous study co-encapsulated nonspherical particles with fluorescent molecules with a lithography approach<sup>124</sup>, but the benefit of our system is that the O/W emulsion/solvent extraction is more scalable. Finally, we show that using differential centrifugation we can purify large particles (>25  $\mu\text{m}$  particles) that could act as drug depots or smaller particles (less than 6  $\mu\text{m}$ ) that could be endocytosed for intracellular drug delivery applications<sup>125,126</sup>.

To our knowledge, no other studies have reported production of crumpled or highly deformed spherical particles using the O/W emulsion/solvent extraction technique<sup>70</sup>. Many nonspherical particles have been produced using microfluidics, photopolymerization and lithography. A wide variety of shapes have been made using these methods such as rods, discs, rings, and wrinkled particles<sup>62,64,70</sup>. These methods have been successful in

controlling morphology; however, those fabrication processes are not currently used to make FDA approved controlled release formulations<sup>54</sup> and they are less efficient than the O/W emulsion/solvent extraction in terms of making large quantities of particles for industrial purposes.

Video microscopy revealed that addition of resveratrol and ethanol to the dispersed phase of the emulsion caused the spherical droplets to buckle as they decreased in volume leading to a crumpled morphology. Generally, droplets in these emulsions (i.e. DCM/PLG/PVA/H<sub>2</sub>O) remain spherical up until the polymers precipitate and the particle forms. This is likely because there is sufficient mobility for the polymer chains to reorganize and condense as droplet volume decreases (due to diffusion of DCM out of the droplet). The buckling behavior observed when resveratrol and ethanol are added to the emulsion is reminiscent of when a thin, spherical elastic shell is deformed by applying external pressure or reducing the volume<sup>127</sup>. This phenomenon can be visualized with a ping pong ball. When pressed on at a single location, with sufficient force, the shell indents. If the ball is pressed on at multiple points with sufficient force, the shell crumples with multiple indentations. It is unclear why the emulsion droplets crumple with the addition of resveratrol and ethanol. The literature is rich with reports of encapsulating small molecules in PLG particles<sup>102–105</sup> and, to our knowledge, crumpled morphology was not observed, even when ethanol was added to a DCM/PLG/PVA/H<sub>2</sub>O emulsion used to encapsulate dexamethasone<sup>97</sup>. It does appear that the hydroxyl groups are optimally positioned on resveratrol to induce the crumpled morphology because switching out resveratrol for pinosylvin, which lacks the 4' hydroxyl group, led to spherical particles, while using piceatannol with the additional 3' hydroxyl decreased particle yield to 12%, indicating

particle formation was disrupted in some way. We think that resveratrol somehow restricts chain motion of the polymers at the oil–water interface. The reduction in their fluidity would introduce a shear modulus that could lead to buckling behavior as the droplet decreases in volume<sup>128</sup>. XRD of the highly crumpled particles suggest that there may be small amounts of crystalline resveratrol. Perhaps these crystalline regions form at the oil–water interface during solvent extraction and restrict polymer chain motion as the droplet shrinks. In support of this idea, a white precipitate is seen forming at the oil water interface in the sessile drop experiment. Another possibility is that resveratrol molecules, rather than crystals, restrict chain motion during droplet shrinkage. We propose that resveratrol might accomplish this by hydrogen bonding with carbonyl groups in the PVA.

Cosolvent appears to play an important role in resveratrol-induced particle crumpling. We believe this role is to transport resveratrol to the oil–water interface. Addition of resveratrol to the DCM/PLG/PVA/H<sub>2</sub>O emulsion with the aid of ethanol, methanol, or acetone all led to particle crumpling (albeit varying degrees, discussed below). In contrast, when ethyl acetate was used instead of DCM, a cosolvent was not needed and particles remained spherical. Furthermore, there is a dose dependence of cosolvent on particle crumpling. When the oil phase contained 10% ethanol and 4 mg/mL resveratrol, only spherical particles were observed; however, when ethanol was increased to 25%, particle crumpling was detected in a small population of particles. We propose that as the cosolvent leaves the droplet, some portion of the resveratrol is redistributed from the bulk of the droplet to the surface, and greater redistribution is achieved by increasing cosolvent concentration. Interestingly, particles made with 25% ethanol, which exhibited a low frequency of particle crumpling, contained less resveratrol (2.5x less) than the those made

with 10% ethanol. It is tempting to conclude that resveratrol content and particle crumpling can be decoupled as long as sufficient resveratrol is transported to the oil-water interface. However, we caution that the resveratrol measurements are an average value for the entire batch of particles and may not reflect the true loading of the small population of crumpled particles, which could have much higher resveratrol content than the smooth particles.

The cosolvent used had a dramatic effect on particle morphology in some cases. By switching out ethanol for acetone we produced particles resembling deflated spheres with few, large indentations rather than spheres that were highly crumpled. The shape of a deformed thin spherical shell, which can vary from a sphere with a single indentation to sphere with many indentations, which appears highly crumpled, depends on deformation rate, extent of volume change, and the Foppl-von Karman (FvK) number<sup>127</sup>. The FvK number is the ratio of shell radius to shell thickness scaled by Poisson's ratio. Essentially, shells with a larger FvK deform more readily and, thus, require a smaller volume change in order to deform. Modeling indicates that for a given FvK and volume change, a large deformation rate leads to the simultaneous formation of many indentations that culminate in a high degree of crumpling, while a sufficiently slow deformation rate results in a single indentation<sup>127</sup>. In fact, the modeling suggests there is a lower limit on deformation rate that must be achieved otherwise only 1 or 2 indentations result<sup>127</sup>, and the morphology resembles that of the particles made with acetone. We propose that deformation rate (i.e. change in droplet volume) may be different for droplets formed with ethanol versus acetone because ethanol has a higher solubility in water (Table 3.3) and could possibly leave the droplet faster. Following this logic, using ethanol as a co-solvent leads to droplet deformation rates that support multiple indentations and a highly crumpled surface when

the particle forms, while using acetone leads to relatively slower deformation rates that cause fewer indentations and a deflated sphere morphology.

The hypothesis that crumpled particle morphology correlates with cosolvent solubility with water is not supported by the methanol data. Indeed, methanol is more soluble in water than ethanol or acetone. Furthermore, the difference in water solubility is actually greater between methanol and ethanol than ethanol and acetone (Table 3.3). Despite this, particles made with methanol had less surface area compared to particles made by ethanol, indicating they were less crumpled or there was a lower frequency of droplets that crumpled. Thus, factors other than cosolvent miscibility with water must also be important in determining particle morphology. We found that surface area correlates with resveratrol content among the particles made with the three different cosolvents. Particles made with ethanol had a resveratrol content of 65  $\mu\text{g}/\text{mg}$  and a surface area of 1.2  $\text{m}^2/\text{g}$ . Particles made with methanol contained 23% less resveratrol and had a corresponding 25% decrease in surface area compared to the particles made with ethanol. However, particles made with acetone contained 72% less resveratrol than those made with ethanol but exhibited only a 40% decrease in surface area. We believe this data indicates that some cosolvents are better at transporting and/or retaining resveratrol at the oil–water interface at critical levels that support droplet deformation as it shrinks, with both ethanol and acetone outperforming methanol in this regard.

Many of the nonspherical particles observed were greater than 20  $\mu\text{m}$  in size, ranging up to almost 50  $\mu\text{m}$ . Potential biomedical applications for particles in this size range include acting as a drug depot or acting as a matrix for cell attachment and growth. PLG microspheres loaded with naltrexone have been FDA approved, and have an average

diameter around 60  $\mu\text{m}$ <sup>129</sup>. The naltrexone particles are smooth and spherical and provide nearly a zero-order release profile over 4 weeks. It is established that particle morphology impacts drug release<sup>70</sup>. While it is unknown how the morphologies produced herein would impact drug release profiles, we expect that drug release would be increased (compared to spherical particles with similar size and drug loading) due to increased surface area. It has also been reported that 40  $\mu\text{m}$  particles with wrinkled surfaces promote greater cell adhesion, when used as matrices for fibroblast culture, compared to smooth particles<sup>64</sup>. Thus, crumpled drug delivery depots might be leveraged to target cell populations in tissues based on their propensity to adhere to the crumpled surface.

Intracellular delivery of bioactive factors is an important aspect of drug delivery, especially when modulating the immune system<sup>130–133</sup>. While many of the nonspherical particles produced herein are too large for endocytosis, we believe that the emulsion conditions can be modified to produce smaller, nonspherical particles with ridges and flat surfaces that might impact cell uptake and intracellular delivery of bioactive factors. For example, decreasing polymer molecular weight and increasing homogenization speeds produces smaller droplets that will condense into smaller particles<sup>58</sup>. However, it is important to consider that the small particles were less likely to be crumpled or indented in the present work. This was not surprising because smaller droplets have a smaller FvK number and thus are more resistant to crumpling<sup>127</sup>. The resistance of small droplets to crumpling has also been reported for Pickering emulsions, in which the droplet surface is solid<sup>134</sup>. For thin, elastic shells with small FvK numbers, slow deformation rates were more effective at producing indentations<sup>127</sup>. Thus, focusing on acetone as the cosolvent may be a promising avenue to develop small, nonspherical particles for intracellular drug delivery.

A final consideration is the effect of resveratrol delivery from the particle, since it is required to modulate particle shape. When given orally, resveratrol has been found to be an antioxidant<sup>23</sup>, anti-inflammatory<sup>23</sup>, or an exercise mimetic<sup>26</sup>. Resveratrol is available as a supplement in pill form and high doses (150 mg, six times/day, for thirteen doses) were well tolerated in a clinical trial<sup>28</sup>. In vitro, it is found that concentrations of 50–100  $\mu$ M do not induce toxicity while inducing lipid mobilization in adipocytes and downregulation of inflammatory signaling in macrophages<sup>25,135</sup>. For comparison, if 1 mg of the highly crumpled particles (resveratrol loading of 65  $\mu$ g/mg) released their resveratrol content into 100 mL of water (or tissue) instantaneously, the concentration would be less than 3  $\mu$ M. Thus, while resveratrol toxicity would need to be investigated for each biological system in which the particles were applied, we believe it is plausible the resveratrol would be well tolerated and could possibly synergize with other drug payloads. In addition, resveratrol can also act as a preservative and increases the stability of  $\alpha$ -tocopherol encapsulated in whey protein particles subjected to oxidizing conditions<sup>136</sup>. However, if resveratrol loading is undesirable, our previous research demonstrates we can decrease loading by up to 60% with a 1-minute ethanol wash<sup>68</sup>. How this wash affects the loading of other bioactive factors will need to be carefully studied as we move this technology forward.

### **3.5. Conclusion**

Addition of resveratrol, with the aid of a cosolvent, to an emulsion of dichloromethane and poly(lactide-co-glycolide) in aqueous polyvinyl alcohol leads to the production of nonspherical particles following solvent extraction. Particle shape can be modulated by cosolvent type with ethanol yielding highly crumpled particles and acetone leading to particles that resemble deflated spheres. In addition, spherical particles can be



obtained if ethyl acetate is used in lieu of dichloromethane and a cosolvent. The method extends to polycaprolactone and poly(l-lactic acid) and is compatible with the encapsulation of a hydrophobic fluorescent dye, suggesting hydrophobic bioactive agents could be encapsulated. Video microscopy revealed that oil droplets crumple as they decrease in volume during solvent extraction when resveratrol and ethanol were present. Crumpling did not occur when droplets contained ethanol without resveratrol and geometry remained spherical until the particles formed. This crumpling behavior is similar to when a thin elastic shell is deformed and suggests that the surface of the droplets containing ethanol and resveratrol may not be sufficiently fluid to maintain a spherical morphology as the droplet decreases in volume. Resveratrol's hydroxyl groups appear to be optimally positioned to induce the nonspherical particles because the crumpling is lost with the removal of the 4' hydroxyl group or the addition of a 3' hydroxyl group. Based on all the data, we propose that resveratrol inhibits chain motion of polymers at the droplet's surface that must reorganize in order to maintain a spherical geometry and the function of the cosolvent is to redistribute resveratrol from the droplet's bulk to its surface. To our knowledge, no other studies have reported production of crumpled or highly deformed spherical particles using the oil in water emulsion/solvent extraction technique. Since particle morphology impacts drug release kinetics and how biological systems engage with a biomaterial, this method could be used to fine-tune FDA approved polymer-based controlled release therapies already on the market or enable the development of novel particle-based systems to control or study cell biology.

# CHAPTER 4

## DEVELOPMENT OF MODIFIED PVA FOR SURFACE FUNCTIONALIZING PLG MICROPARTICLES FOR MACROPHAGE TARGETING AND SIGNALING<sup>3</sup>

### 4.1 Introduction

Macrophages are professional phagocytes that exist throughout the body. They perform a wide variety of tasks, from phagocytic removal of pathogens to regulating homeostasis<sup>14</sup>. There are many activated states of macrophages, however, it is traditionally thought that they exist on a spectrum of phenotypes, from pro-inflammatory (M1) to anti-inflammatory (M2)<sup>17</sup>. M1 phenotype is triggered in response to an infection and M2 phenotype is triggered when wound healing is needed. Macrophages play an important role in many inflammatory diseases, and strategies that seek to “reprogram” their phenotype to address an inflammatory disease have gained interest over recent years<sup>16</sup>.

Mannose receptor (MR) is a c-type lectin found primarily on macrophages and dendritic cells and has recently been considered a target for inducing anti-inflammatory (M2) phenotype in macrophages<sup>20,137</sup>. Although traditionally known as a phagocytic receptor activated by pathogens, mannose receptor is not associated with the inflammatory

---

<sup>3</sup> Isely, C., Atube, K.J., Cheung, C.V., Steege, C., Stevens, A.C., Pelechia, P., and Gower, R.M. To be submitted to *Biomacromolecules*

response that other pattern recognition receptors have, such as toll-like receptor 4<sup>138</sup>. In fact, it was found that mannose-capped lipoarabinomannan (a polymer of mannose) could upregulate the nuclear receptor PPAR gamma in macrophages, which is thought to inhibit inflammatory signals<sup>139,140</sup>. Another study found that clustering of the mannose receptor via konjac glucomannan nanoparticles could induce an M2 phenotype, specifically upregulating IL-10 production<sup>21</sup>, once again suggesting the anti-inflammatory nature of MR. Despite these promising results, few other studies have looked at activating MR to induce anti-inflammation in macrophages, and none to our knowledge have used components in FDA approved particle systems such as the O/W emulsion process. Hence strategies that aim to activate mannose receptor with mannose decorated particles made with the O/W emulsion process could have promise in treating inflammatory diseases.

Previous groups have functionalized particles for macrophage targeting<sup>79,141,142</sup>. None of these groups used PLG microparticles, however. PLG microparticles are excellent candidates for delivery of mannose to MR on macrophages because PLG has a track record of FDA approval, the emulsion fabrication process is well suited for making particles around 2-3 microns and can be scaled for pharmaceutical production<sup>44</sup>. We hypothesize that polylactide-co-glycolide (PLG) microparticles can be surface functionalized with mannose and these particles can bind the mannose receptor to promote anti-inflammatory effects in macrophages.

The oil in water (O/W) single emulsion solvent extraction process is the most widely used for fabricating PLG microparticles<sup>52,58</sup>. Poly(vinyl alcohol) (PVA) is the most common emulsifier used, and it ends up coating the surface of the particle after it is freeze dried<sup>74</sup>. We propose that conjugating molecules to PVA used in the emulsion process is a

convenient strategy for functionalizing the surface of particles, as it allows for easy characterization and PVA inserts on the surface of particles spontaneously during particle formation<sup>74</sup>. This approach, to our knowledge has not been applied in studies by other groups.

Isothiocyanates have traditionally been used in biomaterials to functionalize proteins or other materials with abundant amine groups, however, isothiocyanates also react with alcohols, such as PVA<sup>106</sup>. In the present study, we sought to test the isothiocyanates that could be used to react with PVA to produce bioactive effects in vitro. Herein, we developed PVA modified with fluorescein isothiocyanate (FITC), rhodamine isothiocyanate (RITC), and mannopyranosyl phenyl isothiocyanate (MITC).

Attaching mannose in particular to the surface of particles could have implications in many inflammatory diseases, and we predicted it could have implications for muscle atrophy due to activation of the mannose receptor producing anti-inflammatory responses. Muscle atrophy is the loss of muscle in response to a disease, disuse or simply aging<sup>9</sup>. Sarcopenia specifically, which is muscle atrophy that results from aging, was estimated to cost the U.S. \$40 billion alone in hospitalizations in 2014<sup>143</sup>. Muscle atrophy is characterized by a decrease in muscle fiber size, and often coincides with an increase in inflammation<sup>12</sup>. Targeting macrophages and inducing an anti-inflammatory and pro-regenerative phenotype is therefore an appealing strategy for treating muscle atrophy. Here, we test the ability of mannose decorated (MITC) particles to bind to macrophages and colocalize with the mannose receptor compared to particles without mannose. As a measure of muscle growth, we test the ability of media conditioned with macrophages treated with

MITC particles to increase the formation of C2C12 myotubes, the building blocks of muscle tissue fibers.

## **4.2 Materials and Methods**

### *4.2.1 Materials*

50:50 poly (D,L-lactide-co-glycolide) (PLG) with an ester end group and a MW of 7,000-17,000 were purchased from Evonik (Birmingham, AL). Poly (vinyl alcohol) (PVA) (MW 13,000–23,000, 87–89% hydrolyzed), dichloromethane (DCM), coumarin 6, and fluorescein isothiocyanate isomer 1 (FITC) were purchased from Sigma (St. Louis, MO). Rhodamine b isothiocyanate (RITC) was purchased from Cayman. Ethanol (ETOH) was purchased from Decon Laboratories (King of Prussia, PA). Dimethyl sulfoxide (DMSO) was purchased from Fisher (Hampton, NH). Ultrapure water was obtained from a Thermo Scientific Barnstead Nanopure system. RAW 264.7 macrophages and C2C12 myoblasts were obtained from ATCC (TIB-71) (CRL-1772). Dulbecco's Modified Eagle's Medium (DMEM) with 4.5 g/L glucose and L-glutamine was purchased from Corning Cellgro (Corning, NY). Trypsin with 0.25% EDTA, Fetal Bovine Serum (FBS) and Pen/Strep were purchased from Fisher (Hampton, NH).

### *4.2.2 Modified Poly (Vinyl Alcohol) Synthesis*

Modified PVA was prepared by dissolving 100 mg of PVA into 10mL of DMSO along with an amount of the isothiocyanate molecule (fluorescein isothiocyanate, rhodamine isothiocyanate or mannopyranosyl phenyl isothiocyanate) that corresponded to a mole percentage of OH groups present on the backbone of the polymer (0.1, 1 and 10% for example). This mixture was reacted at varying times from 5-24 hours and varying temperatures from 25°C to 80°C as listed in Table 4.1. After reaction, the modified PVA

was added to dialysis tubing with 3.5 kDa MWCO and allowed to dialyze for 3 days in 5L of ultrapure water, with exchanges of water twice a day. After this, the PVA product was frozen and lyophilized overnight. Final dried product was weighed, and mass yield was calculated via equation 1:

$$\text{Mass Yield (\%)} = \left( \frac{M_{\text{ITC-PVA}}}{M_{\text{PVA}} + M_{\text{ITC}}} \right) * 100 \quad (1)$$

Where  $M_{\text{ITC-PVA}}$  is the final mass of modified PVA,  $M_{\text{PVA}}$  is the initial mass of PVA and  $M_{\text{ITC}}$  is the initial mass of isothiocyanate.

#### 4.2.3 *Fourier Transform Infrared Spectroscopy*

FTIR of PVA and modified PVA was collected on a PerkinElmer Spectrum 100 machine. About 5 mg of sample was spread on the sample holder and data recorded from 650-4000  $\text{cm}^{-1}$ . Transmittance was plotted against wavenumber ( $\text{cm}^{-1}$ ). Peaks were analyzed qualitatively.

#### 4.2.4 *Nuclear Magnetic Resonance Characterization*

$^1\text{H-NMR}$  of PVA and modified PVA was carried out using a Bruker Avance IIIHD 400 MHz spectrometer. 10 mg of samples were dissolved in 0.7 mL of DMSO- $d_6$ . 32 scans were taken with a 20ppm window centered at 6.175 ppm. 4 second acquisition time with 1 second recovery delay and 30-degree pulse widths was used.

#### 4.2.5 *Polymer Particle Fabrication*

Polymer particles were prepared using a single oil-in-water emulsification solvent extraction method. Briefly, 50:50 PLG was dissolved in dichloromethane at a concentration that would achieve a final organic phase concentration of 4% (wt/wt). For the emulsion, 0.6 mL of organic phase was added dropwise into 4 mL of an aqueous solution of 0.2% (wt/v) polyvinyl alcohol (PVA) or modified PVA, and homogenized at 11000rpm for 5

minutes using a Kinematica PT3100D homogenizer. Solvent extraction was then conducted by adding the emulsion to 80 mL of ultrapure water and then stirring the mixture for 1 hour. This allowed the dichloromethane to extract and evaporate and the resulting particles to harden. The particles were then passed through a 40  $\mu\text{m}$  filter (Greiner Bio-one), collected via centrifugation at 250xg (to collect particles 2  $\mu\text{m}$  and larger) and washed 4 times in ultrapure water. Washed particles were frozen at  $-20^{\circ}\text{C}$  and subsequently lyophilized overnight with a Labconco freeze dryer. Recovered particles were stored under vacuum in a dry environment at room temperature. For coumarin 6 loaded particles, all conditions were the same except coumarin 6 was added to the organic phase at 0.3 mg/mL.

#### *4.2.6 Light Microscopy (LM)*

Light and epifluorescence microscopy images of particles were taken on an EVOS FL microscope at 20x magnification. Particles were prepared in ultrapure water and suspended at a concentration of 0.25 mg/mL. 400  $\mu\text{L}$  of these suspensions was added to a well of a 48-well plate and allowed to settle prior to image acquisition. Fluorescence images were taken on the green GFP (470nm) or red RFP (560nm) fluorescence settings.

#### *4.2.7 Particle Size Measurements*

Particle size was found by analyzing light microscopy images using ImageJ software. Briefly, three representative images were taken of each particle condition and converted to binary (B/W) colors. The Particle Analysis plugin in ImageJ was used to measure particle diameter. We report the mean particle diameter and the coefficient of variation (CV%), which is the standard deviation divided by the mean. We validated this method previously by accurately measuring the size of purchased polystyrene beads<sup>68</sup>.

#### 4.2.8 Mass Yield

Mass yield was calculated by dividing the mass of recovered particles by the mass of polymer and resveratrol emulsified. Particle mass yield was calculated according to equation 2.

$$\text{Mass Yield (\%)} = \left( \frac{M_{PT}}{M_{Pol} + M_{RE}} \right) * 100 \quad (2)$$

Where  $M_{PT}$  is the mass of particles recovered from the emulsion,  $M_{Pol}$  is the mass of polymer added to the emulsion, and  $M_{RE}$  is the mass of resveratrol added to the emulsion.

#### 4.2.9 Cell Culture

RAW 264.7 macrophages (ATCC TIB-71) were subcultured via the ATCC protocol. Briefly, cells were seeded at 625,000 cells in T-25 flasks in 3 mL of complete media (DMEM supplemented with 1mM sodium pyruvate, 1500 mg/mL sodium bicarbonate, 1% penicillin-streptomycin, and 10% fetal bovine serum). This was allowed to grow for 2 days or until cells became about 60-70% confluent. Cells were then rinsed with PBS and 1 mL of Trypsin with 0.25% EDTA was added for 5 minutes at 37°C. Trypsin was then diluted into 2 mL of complete media, cells were scraped with a rubber policeman and added to a 15 mL centrifuge tube. An aliquot of this solution is diluted with Trypan blue and used to count the cells with a hemacytometer. The rest is centrifuged at 1500 rpm for 5 minutes. The cell pellet is reconstituted in complete media and seeded into flasks and plates as needed. Cells were seeded at 25,000/cm<sup>2</sup>.

C2C12 myoblasts (ATCC CRL-1772) were subcultured via the ATCC protocol. Cells were seeded into T-25 flasks at 125,000 in 3mL of complete media (DMEM supplemented with 1% penicillin-streptomycin and 10% fetal bovine serum). When cells were 60-70% confluent, they were rinsed with PBS and 1 mL of trypsin was added for 5



minutes at 37°C. Trypsin was diluted into 2 mL of complete media and cells were collected into a 15 mL centrifuge tube. Cells were counted as described above and centrifuged at 1500 rpm for minutes. Cell pellet was reconstituted in complete media and seeded into flasks and plates as needed.

#### 4.2.10 Particle Binding Assay

RAW 264.7 macrophages were cooled to 4°C and then incubated with coumarin 6-containing MITC or blank particles for 10, 20 and 30 minutes at 0.3, 1.5 and 3 µg per well. Unbound particles were then washed away with ice cold PBS. To visualize particle binding *in situ*, cells were fixed in 10% Formalin, stained with Hoescht at a 1:2000 dilution and imaged with a EVOS fluorescent microscope. To quantify particle binding, cells were not fixed, but incubated with DMSO to solubilize the bound coumarin 6 particles. The DMSO was then collected and added to a 96 well plate. Fluorescence in the DMSO was measured in a black 96 well plate with a Biotek plate reader. A serial dilution of fluorescent particles was made in DMSO to make a standard curve of fluorescent intensity vs µg/mL of particles dissolved. This resulted in a linear relationship shown in equation 3.

$$\text{Fluorescence intensity} = m * \left( \frac{\mu\text{g}}{\text{mL}} \text{particles} \right) + b \quad (3)$$

Where m is the slope and b is the y intercept of the linear regression. Concentration of particles (µg/mL) bound was calculated by interpolating the standard curve and mass of particles bound was calculated by multiplying by the volume (mL) of DMSO used to extract the particles (0.1mL).

#### 4.2.11 Mannose Receptor Colocalization

Colocalization of MR in macrophages was studied in response to particle treatment. RAW 264.7 cells were cultured as described above and cells were seeded in 24 well plates.

Particles were added 24 hours later at a 1:10 cell:particle ratio. Particles were incubated for 3 hours at 37°C. Cells were washed thoroughly 3 times in PBS. Cells were fixed in 10% formalin for 30 minutes. Blocking was done in 1% BSA for 1 hour and cells washed twice in PBS. MR antibody (Abcam) was added at 10 µg/mL for 1 hour at RT and cells washed twice in 1% BSA in PBS. Secondary antibody (Alexa Fluor 555) was added at 8 µg/mL for 1 hour at RT and cells washed twice in 1% BSA in PBS. Hoescht was added at 1:2000 dilution for 5 minutes. Cells were imaged on an EVOS FL microscope on the DAPI, GFP and RFP settings. Quantification of colocalization was done in ImageJ. Green and red color were thresholded. Yellow color was set to the hue range of 15-58 in ImageJ. Area of green and area of yellow were analyzed and the yellow area divided by the green area was calculated. Conditions used were: cells only, cells treated with blank particles and cells treated with MITC particles.

#### *4.2.12 RAW 264.7 Conditioned Media on C2C12 Myoblast Differentiation*

RAW cells were seeded in T-25 flasks at 25,000 cells/cm<sup>2</sup> on day 0 and particles added on day 1. On day 2, conditioned media was collected and frozen. C2C12 cells were plated at 5,000/cm<sup>2</sup> and differentiation began on day 1. Conditioned media in a 50:50 ratio with differentiation media was added on day 2, 3 and 4. On day 5, myotubes were fixed with formalin for 30 min and blocked in 10% goat serum with 0.3% Triton X. Then, Myosin Heavy Chain primary antibody was added at 10 µg/mL for 1 hour. Next, Alexa Fluor 555 secondary antibody was added at 1:200 dilution for 1 hour. Cells were counterstained with Hoescht at 1:2000 dilution for 5 minutes. Cells were then imaged on the RFP channel on an EVOS FL microscope. Number of nuclei per myotube per frame for three independent wells were counted with imageJ. Myotubes counted were set as

having more than 3, 6, or 9 nuclei to demonstrate three different ways of defining myotubes.

#### *4.2.13 Statistics*

Prism graphpad software was used to carry out statistical analysis. Error bars represent standard deviation. Where appropriate, unpaired t-test, one-way ANOVA and two-way ANOVA with Tukey's multiple comparison test were used to compare differences in the means.  $P < 0.05$  was used as an indication of statistical significance.

### **4.3 Results**

#### *4.3.1 Synthesis of Modified PVA*

FITC, RITC and MITC modified PVA was synthesized via a one-step reaction as shown in Figure 4.1A. The reaction proceeded in DMSO for 5-24 hours at varying temperatures, and after 3 days of dialysis the modified PVA was recovered via lyophilization, seen in Figure 4.1B. FITC was added at 0.1, 1 and 10% by mol OH group and RITC was added at 1% by mol OH group. The recovered products were colored as can be seen in Figure 4.1C, suggesting a successful reaction of the components. We ran 16 trials of modified PVA reactions seen in Table 4.1. We varied the ITC group, the ITC mol % added, the reaction time, the temperature, and the solvent used, and the mass yield was measured by weighing the product. The % OH conjugated by running NMR analysis.

#### *4.3.2 Characterizing FITC modified PVA.*

FITC modified PVA was characterized with FTIR and NMR shown in Figure 4.3. FTIR of PVA showed the characteristic OH peak around 3350 cm which was not present in the FITC (Figure 4.2A). FTIR of FITC alone showed the characteristic cyano (NCS) peak around 2000, which was not present in the PVA and notably not in the FITC-PVA,

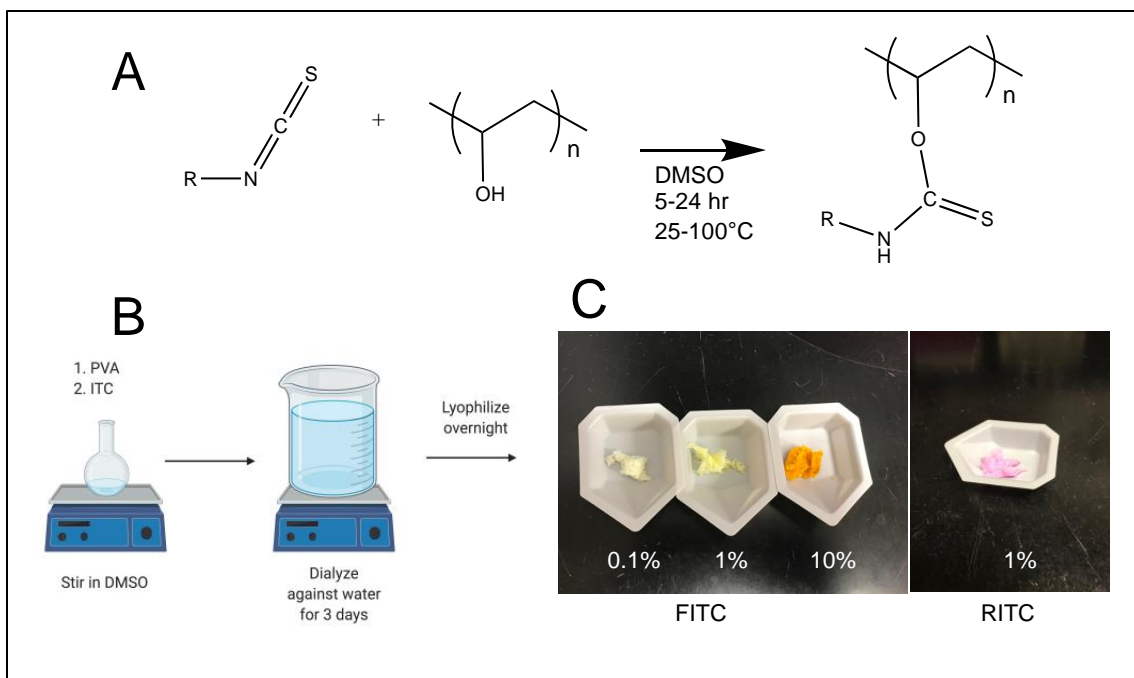


**Figure 4.1. Synthesis of Modified PVA.** **A)** Isothiocyanate (ITC) modifiers were attached to PVA via a one-step reaction. **B)** PVA and ITC were added to DMSO for 5 hours at room temperature and then dialyzed against water in tubing with MWCO of 3.5 kDa. **C)** Images showing FITC modified PVA at 0.1, 1 and 10% by mol OH conjugation and RITC modified PVA at 1% by mol OH conjugation.

**Table 4.1.** Reaction trials of ITC modifiers with PVA

Trial #	ITC	ITC %	Rxn Time	Temp	Solvent	Mass yield	% OH conjugated (from NMR)	conversion
1	FITC	0.1%	5 hr	RT	DMSO	37%	0	0%
2	FITC	1%	5 hr	RT	DMSO	29%	0.07	7%
3	FITC	10%	5 hr	RT	DMSO	25%	8	80%
4	MITC	1%	5 hr	RT	DMSO	51%	0.11	11%
5	MITC	10%	5 hr	RT	DMSO	55%	0.13	1.3%
6	MITC	20%	5 hr	RT	DMSO	19%	0.16	0.8%

<b>7</b>	MITC	5%	24 hr	RT	DMSO	46%	0	0%
<b>8</b>	MITC	5%	24 hr	RT	DMSO/H <sub>2</sub> O	53%	0	0%
<b>9</b>	MITC	5%	24 hr	60C	DMSO	54%	0.19	3.8%
<b>10</b>	MITC	5%	24 hr	60C	DMSO/H <sub>2</sub> O	66%	0.08	1.6%
<b>11</b>	MITC	5%	5 hr	60C	DMSO	36%	0.05	1.0%
<b>12</b>	MITC	5%	24 hr	80C	DMSO	21%	1.7	34%
<b>13</b>	MITC	5%	24 hr	80C	DMSO	28%	0.87	17.4%
<b>14</b>	MITC	5%	24 hr	80C	DMSO	28%	0.91	18.2%
<b>15</b>	MITC	5%	24 hr	100C	DMSO	34%	1.3	26%
<b>16</b>	MITC	5%	24 hr	100C	DMSO	28%	1.03	21%
<b>17</b>	RITC	1%	5 hr	25C	DMSO	35%	0.4%	40%

suggesting a successful reaction, because a monothiourethane bond should replace the isothiocyanate bond. The FITC modified PVA had the 3350 OH peak and the 1600 C=C peak seen in FITC, suggesting FITC had been attached. NMR characterization showed PVA had proton peaks in the 2 ppm region, characteristic of the carbon backbone (Figure 4.2B). FITC spectra showed peaks in the 7-10 ppm region characteristic of the phenyl rings. 10% FITC-PVA (Table 4.1, Trial 3) contained both of these peaks, and integration of the two showed a ratio of 24:200 which corresponded to 8% of the OH a conversion of 80% of the FITC by mole. This data indicates that FITC attachment to PVA proceeds readily at room temperature with high conversions of 80%.

#### 4.3.3. Characterizing MITC modified PVA

MITC was reacted with PVA in the same manner as FITC and RITC. Initially, we found 0% conversion of MITC with PVA, which was surprising because 80% conversion

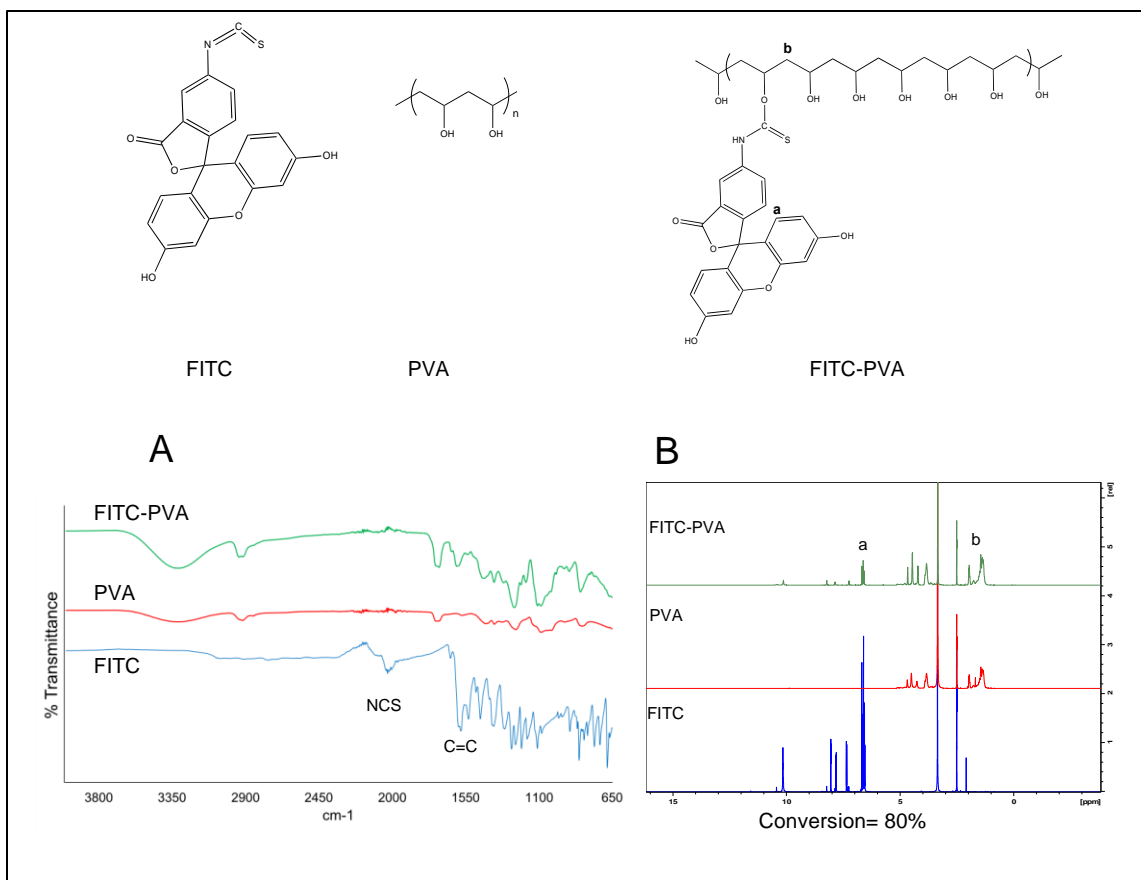


**Figure 4.2. Characterization of FITC-PVA.** **A)** FITC modified PVA (green), PVA (red), and FITC (blue) were analyzed with FTIR spectroscopy. Carbonyl shift at 1600 was highlighted in green representing the carbonyl present on the FITC molecule (circled in green). **B)** NMR spectra of FITC-PVA, PVA and FITC. Characteristic protons in FITC and PVA are marked with a and b respectively and labeled on the inset structure. Integration of these two peaks suggested 80% conversion of FITC.

was found with FITC. It was found that increasing the temperature of the reaction bath increased the conversion of MITC, suggesting a temperature dependence, seen in Table 4.1 and Figure 4.3B. Figure 4.3A is an NMR spectra of PVA, MITC and MITC PVA from Trial 15 in Table 4.1. MITC was characterized similarly to FITC, phenyl protons were compared to PVA backbone protons.

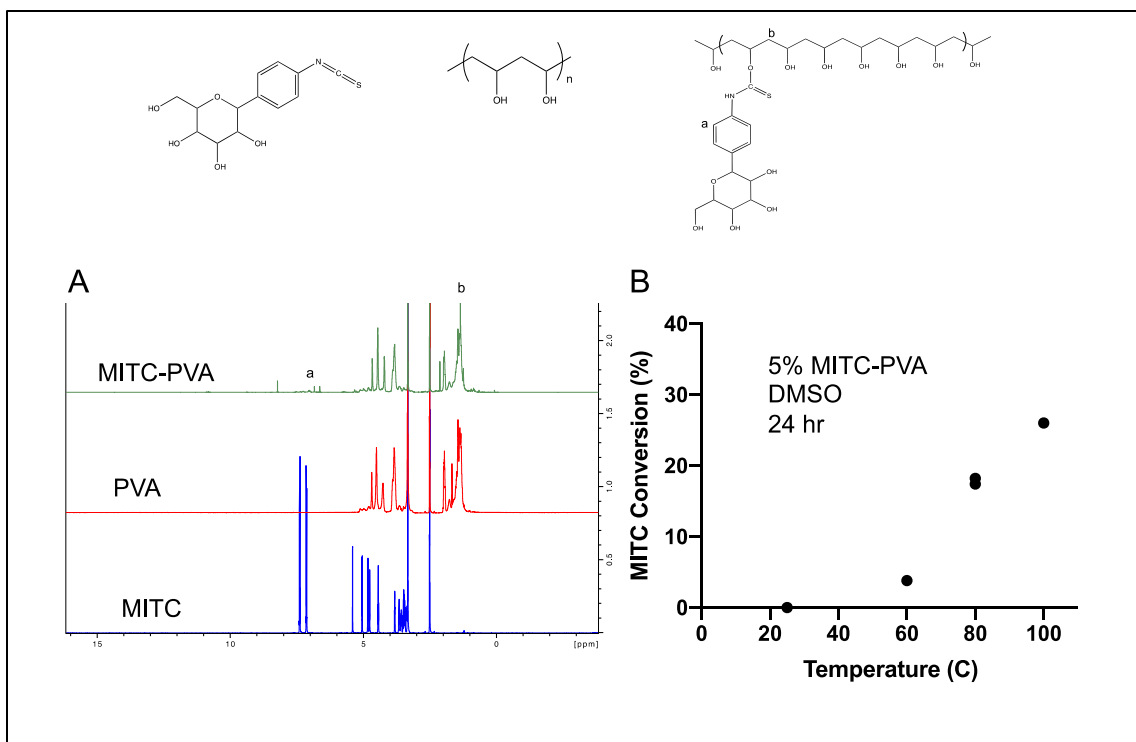


**Figure 4.3. Characterization of MITC-PVA.** A) NMR spectra of MITC-PVA (green), PVA (red) and MITC (blue). Characteristic protons of MITC and PVA are labeled with a and b respectively. B) Plot of MITC conversion vs. temperature for 5 different reaction trials from Table 4.1.

### 4.3 PLG particle fabrication

Microparticles were fabricated using an oil in water single emulsion as previously described, shown graphically in Figure 4.4A. Fabrication parameters such as homogenization and centrifugation speed were optimized previously<sup>71</sup> to make particles with diameters of 2-4  $\mu\text{m}$  and low polydispersity. FITC-labeled PLG particles were imaged under confocal microscopy and cross-section z-slices of the particles showed a ring around the particles, demonstrating visually that the fluorescent PVA was coating the surface of (Figure 4.4B). Similarly, RITC-labeled PVA particles had red signal under epifluorescence microscopy, showing solid circles instead of rings due to the fact that all

of the z-direction was collected (Figure 4.4B). Particles were also imaged under bright field microscopy seen in Figure 4.4C. Particle diameter was 3.5  $\mu\text{m}$  for blank, 3.7  $\mu\text{m}$  for FITC, 3.7  $\mu\text{m}$  for RITC, and 2.8  $\mu\text{m}$  for MITC. Epifluorescent images of particles loaded with coumarin 6 are shown in Figure 4.4D. Coefficient of variation (CV) was less than 40% for all conditions, indicating low polydispersity. Mass yield varied between 40% and 60% for all conditions without a clear trend. MITC-PVA, PVA, MITC-PVA C6 and PVA C6 particles were used for future cell studies.

#### *4.3.5 Cold binding of particles with macrophages*

RAW 264.7 cells were treated with blank and MITC particles loaded with coumarin 6 at 0.3, 1.5 and 3  $\mu\text{g}$  per well for 10, 20, and 30 min at 4°C. Wells were washed with PBS three times, DMSO was added to each well and fluorescence was quantified. Mass bound was calculated from a standard curve of coumarin 6 particles and was plotted against time for each dose as seen in Figure 4.5. We found that MITC significantly increased the mass of particles bound at the 0.3  $\mu\text{g}$  dose, but not at 1.5  $\mu\text{g}$ . At 3  $\mu\text{g}$  dose MITC increased binding at 20 min but not at 10 or 30 min. This confirms that particles were successfully functionalized with mannose and have bioactive effects with macrophages. This data also suggests that it may be important for mannose functionalized particles to be used at low concentrations.

#### *4.3.6 MITC particles are more associated with mannose receptor*

RAW 264.7 macrophages were treated with 3  $\mu\text{g}$  MITC C6 and blank C6 particles (No MITC) for 3 hours at 37°C and were fixed and stained with MR antibody and counterstained with Hoescht. As seen in Figure 4.6, MR (red) was well expressed throughout the cells in all conditions. In untreated cells (Figure 4.6A) there were distinct



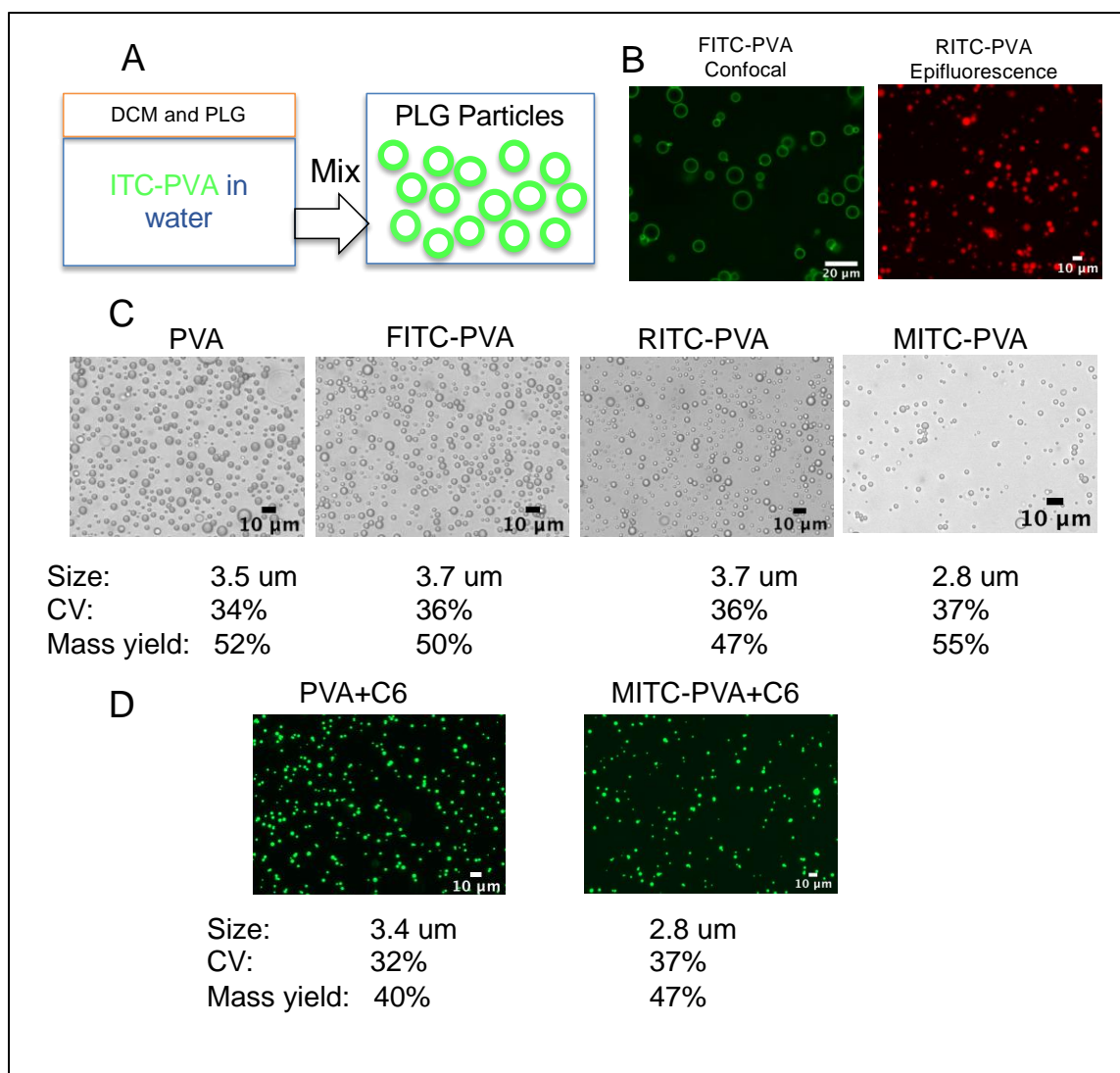


**Figure 4.4. Imaging of PLG particles made with modified PVA.** A) Diagram of O/W emulsion process for PLG particles. B) Confocal image of FITC-labeled PLG particles and Epifluorescent image of RITC-labeled PLG particles. C) Bright field images of modified PVA particles and D) Epifluorescent images of coumarin-6 loaded particles.

regions high in MR spread throughout the cell. Blank and MITC particles were readily taken up by macrophages (Figure 4.6B and C). MITC particles appear visually to colocalize with the MR stain to a greater extent than blank particles, suggesting receptor binding was occurring. Quantification of colocalization via ImageJ suggesting MITC was having an effect as well, with a p value of 0.0568 (Figure 4.6D).

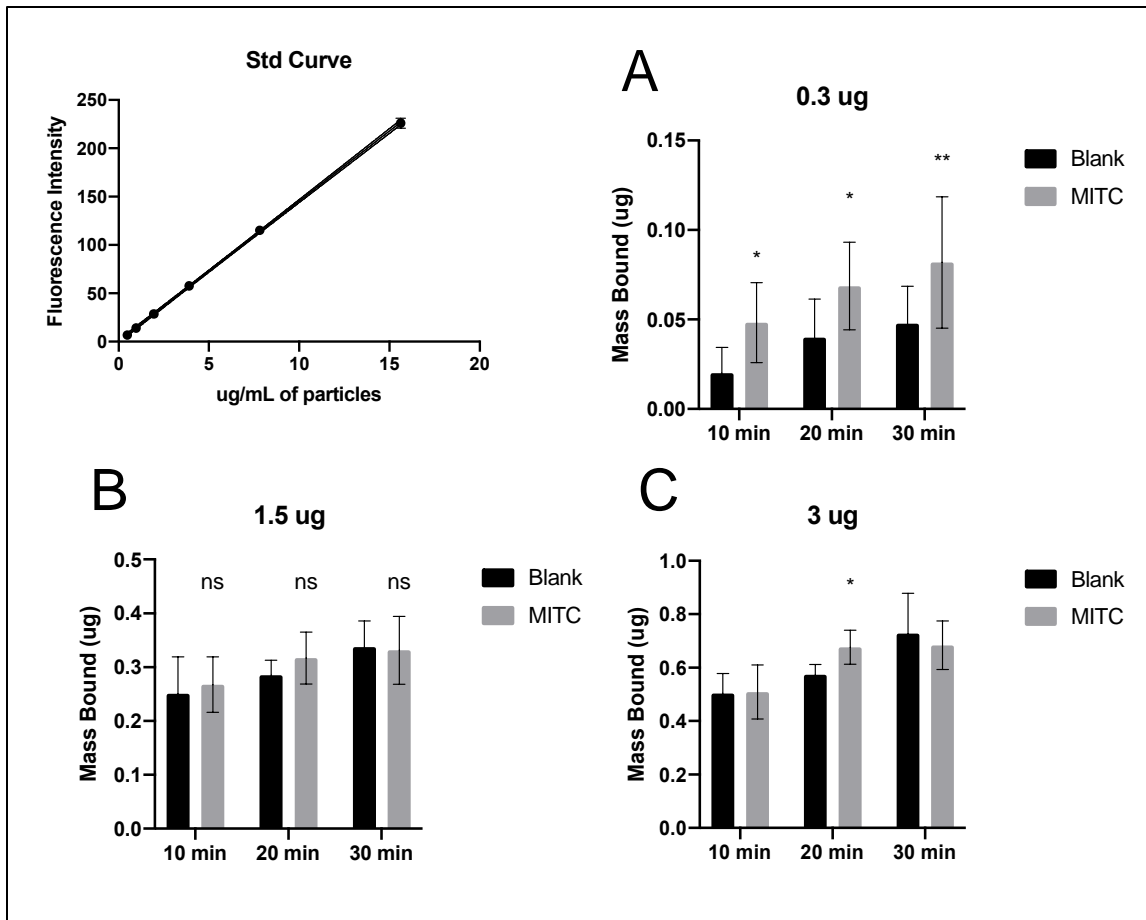


**Figure 4.5. Binding of MITC particles by RAW cells.** RAW 264.7 cells were treated with blank and MITC particles for 10, 20, and 30 minutes at 3 doses: 0.3 (A) 1.5 (B) and 3  $\mu$ g (C) of particles. Particles were loaded with coumarin 6, and at each timepoint cells were washed 3x with PBS and DMSO was added to the well to extract the coumarin 6 dye. Mass bound was quantified by reading the fluorescence of each well on a plate reader and comparing to a standard curve of coumarin 6 loaded particles. Data was analyzed with a Two Way ANOVA, and \* =  $p < 0.05$ , \*\* =  $p < 0.01$  in the Blank vs MITC comparison for each condition with a multiple comparisons test. Error bars are standard deviation.

#### 4.3.7 Macrophage conditioned media affects myotube formation

RAW cells were treated with particles for 24 hours. Media was collected and mixed 50:50 with C2C12 differentiation media and C2C12 myoblasts were treated with this “conditioned” media for 3 days. On the fourth day, C2C12 cells were fixed and stained

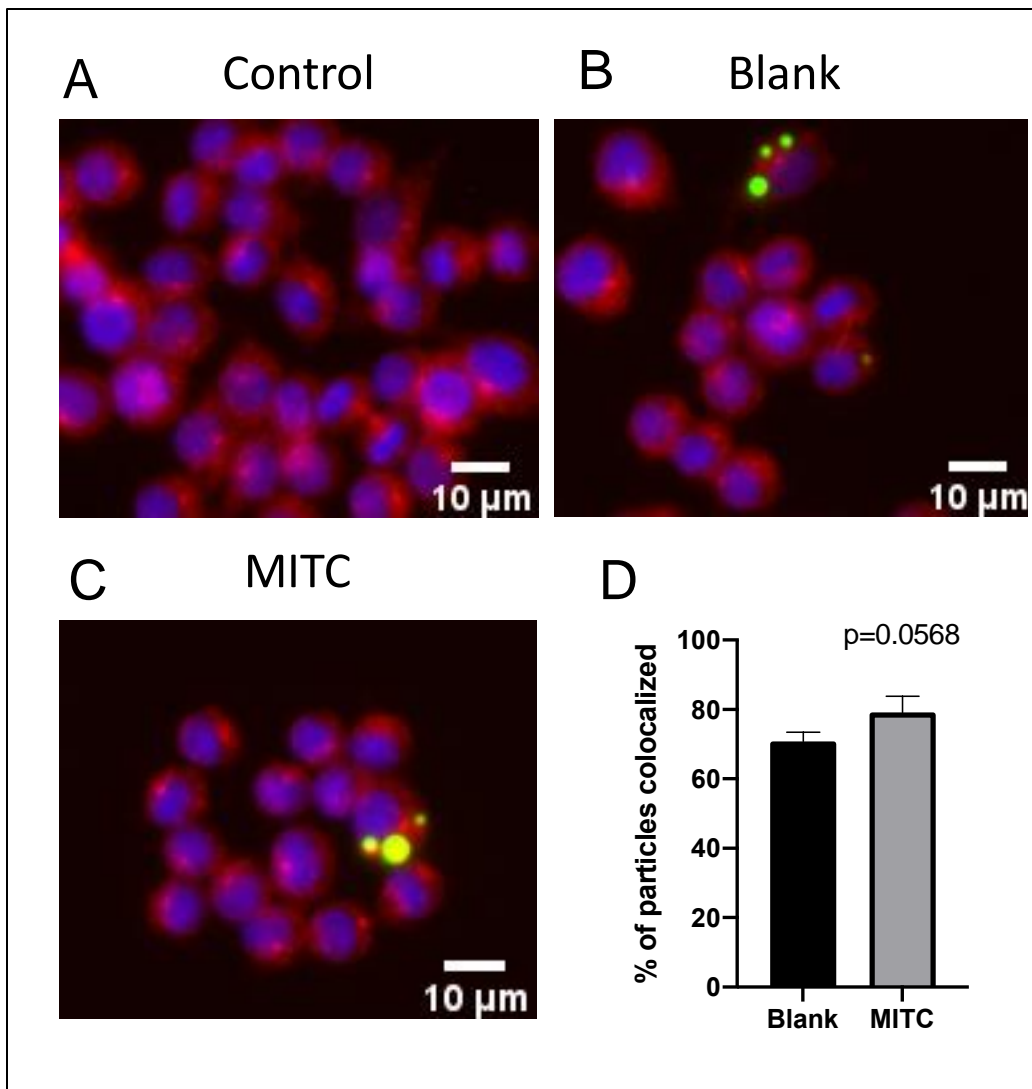


**Figure 4.6. Colocalization of MR with MITC-PVA particles.** Raw 264.7 cells were treated with A) no particles, B) blank particles and C) MITC particles for 3 hours. D) Quantification of the percentage of particles with yellow colocalization by area. Data was analyzed with an unpaired t-test.

with myosin heavy chain, a marker for myotube formation. As seen in Figure 4.7A, multi-nucleated myotubes were stained with myosin heavy chain, and undifferentiated cells were not. Cells treated with media only (Figure 4.7A media) were short and did not have many nuclei, whereas cells treated with macrophage conditioned media appeared larger and had more nuclei. Myotubes treated with particle conditioned media appeared larger, and myotubes treated with macrophage+particle treated media appeared largest. Indeed,

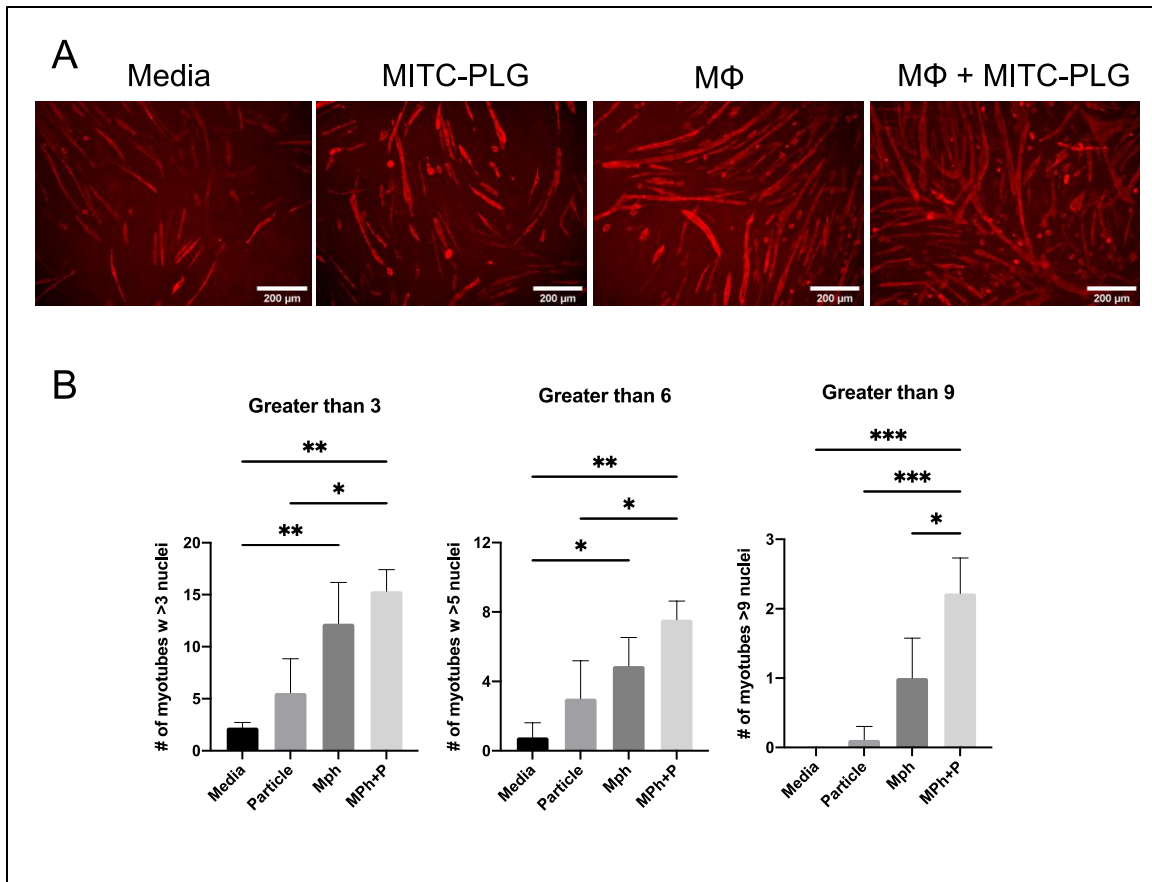


**Figure 4.7. Effect of macrophage and particle conditioned media on myotube formation.** A) Myotubes treated with media alone, media conditioned with MITC-PVA particles, media conditioned with macrophages and media conditioned with macrophages treated with MITC-PVA were stained with myosin heavy chain seen in the red channel of an EVOS FL microscope. B) Quantification of the number of myotubes per well per frame with greater than 3, 6 and 9 nuclei. One-way ANOVA was conducted with a Tukey's multiple comparisons test where \* =  $p < 0.05$ , \*\* =  $p < 0.01$ , \*\*\* =  $p < 0.001$ ,

quantification of the number of nuclei per myotube per frame confirmed these trends (Figure 4.7B). Quantifying myotubes set at having greater than 9 nuclei revealed that MITC particle treated macrophage media had a statistically significant increase compared to macrophage media treated alone.

#### 4.4 Discussion

In this study we find that PVA can be modified with three different isothiocyanate derivatives. In RAW 264.7 macrophages, mannose modified PVA particles bind to the surface and colocalize with MR to a higher extent than do particles without mannose. In addition, media conditioned with macrophages treated with mannose modified PVA particles promote myotube formation.

An important area of research in polymer particle design is surface functionality. Many methods for surface functionalization have been shown in the literature, including passively adsorbing ligands to the surface of particles, conjugating ligands to PVA using EDC, NHS, and CDI chemistry, and PEGylation<sup>59,66</sup>. After particles are formed, characterization can be a challenge. An approach that would be useful is conjugating and characterizing the product prior to particle formation. To that end, we proposed that PVA could be modified, characterized, and then localized to the surface of polymer particles during the O/W emulsion process. Here we show that PVA can be modified with isothiocyanate chemistry with three different isothiocyanate derivatives, and characterization can be completed prior to particle formation.

The three isothiocyanate derivatives were first tested at 25°C for 5 hours. 10% FITC-PVA had highest conversion (80% conversion) as measured by NMR and MITC had the lowest conversion at 25°C at 0%. Interestingly, MITC conversion was temperature dependent, and required increasing temperature to 100°C to achieve higher conversion. This may be because of the more hydrophilic nature of MITC being less soluble in DMSO. We achieved 1.3% OH conjugation at 100°C reacting for 24 hours for a conversion of 26%.

In this study FITC and RITC-PVA coated the surface of 50:50 low MW PLG particles and could be visualized under confocal and epifluorescent microscopy. Particles formed were between 2-4 microns with relatively low dispersity (CV<40%). Rings seen under confocal microscopy confirm that PVA is localized on the surface of particles. ITC-modified PVA was shown to coat the surface of particles via microscopy, and was conjugated to PVA to a high extent, however, we sought to demonstrate bioactive effects with mannose decorated particles by affecting macrophages in vitro.

In a cold binding study, MITC particles bound macrophages to a higher extent than blank particles. This only occurred at the low particle dose (0.3  $\mu$ g). One reason that only low doses increased binding may be that higher doses promote more nonspecific binding, thus reducing any effect seen by MITC. Low doses of particles may also be more clinically relevant, because as particles get administered in the body it is likely only low numbers of particles will interact with each cell. As a point of comparison, one study showed that mannose coated particles improved binding compared to blank particles, however, this only occurred when the particles were capped with a methoxy and not a hydroxyl<sup>142</sup>. They suggested that hydroxy binds more readily than methoxy. PLG particles are coated with PVA hydroxyl groups, and this could be why blank particles bind to a high extent and no effects are seen at high particle doses. Blank particles may also bind other receptors, such as TLR4.

At 3  $\mu$ g dose and at 37C MITC particles were found to colocalize to a higher extent than blank particles with RAW 264.7 macrophages. This suggested to us that mannose decorated particles had functional effects and were associating with MR as we predicted. A previous study showed that nanoparticles induced “nanoclusters” of MR could be

produced upon treatment with mannan functionalized nanoparticles<sup>21</sup>. In the present study particle signal and MR signal colocalized, and although “nanoclusters” were not observed, we cannot rule out that a similar clustering effect was occurring.

To demonstrate that MITC particles were converting macrophages into an anti-inflammatory phenotype, we treated macrophages with particles, then treated differentiating C2C12 myoblasts with macrophage conditioned media. We show myotubes induced with MITC particles treated macrophage media had more nuclei than myotubes treated with just macrophage media. This suggested that MITC particles were inducing a change in the secretome of macrophages that was favorable to myotube formation. Macrophages produce many factors that could be beneficial to myotube formation, such as IL-10, TGF-beta, PDGF, and IGF-1<sup>14</sup>. Future studies will be conducted to determine which of these factors, or other factors could be producing this increase in myotube formation

#### **4.5 Conclusion**

This study demonstrates that isothiocyanate chemistry can be used to functionalize PVA, that it can be used to coat PLG particles and can have therapeutic benefits in terms of muscle atrophy. Three isothiocyanate derivatives, FITC, RITC and MITC were attached to PVA at high concentrations. MITC reaction was temperature dependent, with a high conversion achieved at 100°C. Particles were successfully coated with modified PVA as evidenced by fluorescent microscopy and by MITC binding of macrophages. In addition, MITC particles colocalized with MR in macrophages and induced myotube formation in macrophage conditioned media. Taken together, this data suggests that this one-step reaction for attaching ligands to PLG particles could be useful in many instances where

ligand attachment is needed, and PLG particles decorated in mannose in this way can have positive implications for the treatment of muscle atrophy.



## CHAPTER 5

### CONCLUDING REMARKS AND FUTURE DIRECTIONS

#### 5.1 Concluding Remarks

Biodegradable polymer particles have proven incredibly useful for treating a variety of diseases over the last few decades, as evidenced by the number of particle formulations that have been FDA approved and rise in number of publications this field has generated<sup>33</sup>. However, more research is still needed into the field of O/W emulsions for polymer microparticle fabrication continue to achieve more FDA approvals. Although the O/W emulsion system is simple conceptually, it has many parameters that affect response variables and achieving consistent manufacturing has been a challenge. In addition, many inflammatory diseases may benefit from polymer particle drug delivery, however, some avenues of investigation, such as resveratrol and mannose incorporation into polymer particles, require more research. The objective of this dissertation was to test the effects of incorporating the polyphenol resveratrol and the sugar mannose into the particle design for treatment of inflammatory diseases, and to better understand the effects of fabrication parameters on response variables such as morphology and surface functionality.

In Chapter 2 it was shown that resveratrol could be incorporated effectively into PLG microparticles. Resveratrol encapsulation required the addition of ethanol as cosolvent in the system, and resulted in nonspherical particle morphology, as demonstrated

by SEM imaging. These resveratrol particles induced lipolysis as shown by an oil red o assay on 3T3-L1 adipocytes, suggesting potential of these particles as an anti-obesity formulation. The nonspherical particles showed sustained resveratrol release over 42 days, however, the release was somewhat variable. It was determined that resveratrol particle size was controlled by homogenization time and speed. Smaller particles made with less resveratrol had more uniform release profiles. A major finding was that resveratrol was surface loaded. This was demonstrated by the higher burst release of smaller particles, the higher removal of resveratrol by ethanol of smaller particles, and the disruption of FITC-PVA signal by resveratrol under confocal microscopy. The implication of resveratrol being surface loaded is important in designing drug delivery systems. Longer release applications would require larger particles such as those with a 10-micron diameter or larger because we demonstrated there is a lower burst release. Evidence of surface loading and nonspherical morphology of resveratrol particles led to studies of the mechanism of nonspherical particle formation.

As a result of the finding that resveratrol caused nonspherical morphology in PLG particles in Chapter 2, we set about understanding this effect further. Studies on the morphology change suggested it was dependent on PVA concentration in the aqueous phase and resveratrol concentration. In Chapter 3, light microscopy videos of particle formation demonstrate that PLG particles crumple during the formation process. The videos suggested that a shell was forming around particles and as the solvent was removed the shell was collapsing. In addition, it was found that nonspherical morphology of particles was dependent on cosolvent selection and concentration of cosolvent in the organic phase.

This led to the conclusion that resveratrol was surface active. In fact, other stilbene molecules did not convey the same morphology change; it was unique to resveratrol.

Surface functionality is another parameter of interest in fabrication of polymer microparticles. There have been many efforts to functionalize the surface of polymer particles in the literature. In particular, NHS, EDC, CDI chemistry have been used previously<sup>72</sup>, which have all shown very promising results in many articles as efficient methods for attaching ligands. In this dissertation a novel approach was taken to functionalize the surface of PLG particles, i.e. modification of PVA. Modifying the PVA which coats the surface of particles to provide surface functionality was discussed in Chapters 2 and 4. Isothiocyanate chemistry was used to attach FITC, RITC and MITC on to PVA. Being fluorophores, FITC and RITC attachment provided fluorescent visualization of PVA, and acted as a fluorescent tag for PVA via microscopy. This was demonstrated in Chapter 2 when resveratrol interactions with PVA could be visualized through decreases in PVA signal in confocal microscopy.

In Chapter 4, it was demonstrated that MITC attachment to PVA provided bioactive functionality to PLG particles. This was demonstrated through particle binding at 4°C, through colocalization of particles with MR at 37C and through MITC particle inducing macrophage secretory activity that promoted myotube formation. The premise of this therapy would be that injection of mannose-decorated particles into muscle would work by inducing secretion of muscle-regenerative factors from macrophages. These results demonstrated that modifying PVA for surface functionalization is not only useful for determining surface characteristics of particles but also as a method for achieving bioactive

effects in cells. We propose that our modified PVA method is a simpler method of surface ligand attachment than other chemistries currently used in the literature.

Taken together, the results of this dissertation provide several main innovations to the polymer microparticle field. Namely: i) a potential microparticle system for the delivery of resveratrol for the treatment of obesity, ii) a simple method for tuning morphology of polymer microparticles by adding resveratrol in O/W emulsion solvent extraction systems, iii) a new method for functionalizing the surface of polymer particles made with the O/W emulsion solvent extraction method by modifying PVA with isothiocyanate chemistry, and iv) using mannose decorated particles to target macrophages in treatment in muscle atrophy. These innovations in understanding how components of the O/W emulsion solvent extraction system affect surface properties could have far-reaching effects in the design of new controlled release systems for FDA approval, and could have a direct impact on a growing sector of the pharmaceutical industry.

## **5.2 Future Directions**

The results of this dissertation indicate that particles created here show promise. However, there is still work to be done to move the technology forward. Namely, i) using resveratrol particles in mouse studies for the treatment of mice fed a high-fat diet, ii) seeing how morphology of particles affect the performance in vivo, iii) attaching new ligands to the surface of PLG particles, for example other sugar molecules beyond mannose, and iv) testing mannose-presenting particles in mouse studies for the treatment of mice with muscle atrophy.

In this work it was shown that resveratrol-loaded microparticles can be added to adipocytes and promote lipid mobilization. Although other systems have added resveratrol

to polymer particles<sup>144</sup>, it has not been shown previously that they can have these effects on adipocytes. Because of these promising results, we predict that resveratrol particles can decrease the fat mass of mice on a high-fat diet compared to blank particles. Future studies should look at the effect of dose and time on fat mass and glucose tolerance in C57/BL6 mice fed a high-fat diet. The high-fat diet model for obesity has been used previously by our lab, and could be implemented to test microparticle effects on mice<sup>145,146</sup>.

In this work we show that resveratrol causes nonspherical morphology upon addition to the O/W emulsion solvent extraction method. Nonspherical morphology of polymer microparticles has been shown before in the literature, but the innovation of our system is that it requires only the addition of a natural compound (resveratrol) in the emulsion system to achieve morphology changes. Future studies could look at how “crumpled” and “deflated beach ball” particles shown in Chapter 3 compare to smooth particles in the attachment to various cell types, such as fibroblast cells<sup>64</sup>. It is possible that increased interaction with target cells could increase the amount of drug that reaches its destination. The implication here is that by simply adding resveratrol to an FDA-approved system could improve targeted delivery of the drug to cells of interest.

Design of modified PVA also has important implications in the drug delivery field. Current methods for surface functionalization often involve complex chemistry applied to particles post-fabrication. The method presented of modifying PVA pre-fabrication and simply dissolving it in the aqueous phase to achieve particle surface functionality could be applied to any molecule with an isothiocyanate group. Future studies should determine if this technology is possible with other molecules useful in MR targeting such as fucose and n-acetylglucosamine<sup>147</sup>. One important consideration for the results in Chapter 4 of this

dissertation is that the PVA is decorated with mono-mannose, and it is possible that di-mannose or tri-mannose would have stronger effects in vitro. In fact, the mannose receptor responds more strongly to higher density mannose, such as the polymer mannan<sup>148</sup>. Future studies should determine if conjugating PVA with di-mannose, tri-mannose or mannan have a stronger effect than mono-mannose.

Collectively, the future directions suggested here could have impacts on the usefulness of resveratrol particles to treat obesity and mannose-decorated particles to treat muscle atrophy. The O/W emulsion solvent extraction system is a straightforward and scalable process and is already used in FDA-approved systems. The results shown here can easily be implemented in these systems by simply adding resveratrol to the oil phase or modifying PVA used in the aqueous phase to have significant effects on particle properties. The groundwork is laid here for future researchers to now implement these innovations into new and improved biodegradable polymer microparticle systems.

## REFERENCES

1. Okin, D. & Medzhitov, R. Evolution of Inflammatory Diseases. *Curr. Biol.* **22**, R733–R740 (2012).
2. Rodríguez-Hernández, H., Simental-Mendía, L. E., Rodríguez-Ramírez, G. & Reyes-Romero, M. A. Obesity and Inflammation: Epidemiology, Risk Factors, and Markers of Inflammation. *Int. J. Endocrinol.* **2013**, 1–11 (2013).
3. *Muscle Atrophy*. vol. 1088 (Springer Singapore, 2018).
4. 2013 AHA/ACC/TOS Guideline for the Management of Overweight and Obesity in Adults. *Circulation* **37**.
5. Adult Obesity Facts. (2021).
6. Spiegelman, B. M. & Flier, J. S. Adipogenesis and Obesity: Rounding Out the Big Picture. *Cell* **87**, 377–389 (1996).
7. Rodgers, R. J., Tschop, M. H. & Wilding, J. P. H. Anti-obesity drugs: past, present and future. *Dis. Model. Mech.* **5**, 621–626 (2012).
8. Boss, O. & Bergenhem, N. Adipose targets for obesity drug development. *Expert Opin. Ther. Targets* **10**, 119–134 (2006).
9. Bonaldo, P. & Sandri, M. Cellular and molecular mechanisms of muscle atrophy. *Dis. Model. Mech.* **6**, 25–39 (2013).
10. Cruz-Jentoft, A. J. & Sayer, A. A. Sarcopenia. *The Lancet* **393**, 2636–2646 (2019).

11. Janssen, I., Shepard, D. S., Katzmarzyk, P. T. & Roubenoff, R. The Healthcare Costs of Sarcopenia in the United States: ECONOMIC COST OF SARCOPENIA. *J. Am. Geriatr. Soc.* **52**, 80–85 (2004).
12. Tidball, J. G. Regulation of muscle growth and regeneration by the immune system. *Nat. Rev. Immunol.* **17**, 165–178 (2017).
13. Morley, J. E. Pharmacologic Options for the Treatment of Sarcopenia. *Calcif. Tissue Int.* **98**, 319–333 (2016).
14. Wynn, T. A., Chawla, A. & Pollard, J. W. Macrophage biology in development, homeostasis and disease. *Nature* **496**, 445–455 (2013).
15. Mantovani, A., Biswas, S. K., Galdiero, M. R., Sica, A. & Locati, M. Macrophage plasticity and polarization in tissue repair and remodelling: Macrophage plasticity and polarization in tissue repair and remodelling. *J. Pathol.* **229**, 176–185 (2013).
16. Martinez, F. O. Macrophage activation and polarization. *Front. Biosci.* **13**, 453 (2008).
17. Mosser, D. M. The many faces of macrophage activation. *J. Leukoc. Biol.* **73**, 209–212 (2003).
18. Dean, J. H., Cornacoff, J. B., Barbolt, T. A., Gossett, K. A. & LaBrie, T. Pre-clinical toxicity of Il-4: A model for studying protein therapeutics. *Int. J. Immunopharmacol.* **14**, 391–397 (1992).
19. *Cytokine therapies: novel approaches for clinical indications*. (Blackwell Pub. on behalf of the New York Academy of Sciences, 2009).
20. Gazi, U. & Martinez-Pomares, L. Influence of the mannose receptor in host immune responses. *Immunobiology* **214**, 554–561 (2009).
21. Gan, J. *et al.* Producing anti-inflammatory macrophages by nanoparticle-triggered clustering of mannose receptors. *Biomaterials* **178**, 95–108 (2018).



22. Burns, J., Yokota, T., Ashihara, H., Lean, M. E. J. & Crozier, A. Plant Foods and Herbal Sources of Resveratrol. *J. Agric. Food Chem.* **50**, 3337–3340 (2002).
23. de la Lastra, C. A. & Villegas, I. Resveratrol as an antioxidant and pro-oxidant agent: mechanisms and clinical implications. *Biochem. Soc. Trans.* **35**, 1156–1160 (2007).
24. Mercken, E. M., Carboneau, B. A., Krzysik-Walker, S. M. & de Cabo, R. Of mice and men: The benefits of caloric restriction, exercise, and mimetics. *Ageing Res. Rev.* **11**, 390–398 (2012).
25. Picard, F. *et al.* Sirt1 promotes fat mobilization in white adipocytes by repressing PPAR- $\gamma$ . *Nature* **429**, 771–776 (2004).
26. Baur, J. A. & Sinclair, D. A. Therapeutic potential of resveratrol: the in vivo evidence. *Nat. Rev. Drug Discov.* **5**, 493–506 (2006).
27. Lasa, A., Churrua, I., Eseberri, I., Andrés-Lacueva, C. & Portillo, M. P. Delipidating effect of resveratrol metabolites in 3T3-L1 adipocytes. *Mol. Nutr. Food Res.* **56**, 1559–1568 (2012).
28. Almeida, L. *et al.* Pharmacokinetic and safety profile of trans-resveratrol in a rising multiple-dose study in healthy volunteers. *Mol. Nutr. Food Res.* **53**, S7–S15 (2009).
29. Walle, T., Hsieh, F., DeLegge, M., Oatis, J. & Walle, U. K. HIGH ABSORPTION BUT VERY LOW BIOAVAILABILITY OF ORAL RESVERATROL IN HUMANS. *Drug Metab. Dispos.* **32**, 1377–1382 (2004).
30. Langer, R. New methods of drug delivery. *Science* **249**, 1527–1533 (1990).
31. KREUTER, J. Nanoparticles and microparticles for drug and vaccine delivery. *J. Anat.* **189**, 503–505 (1996).

32. Yun, Y. H., Lee, B. K. & Park, K. Controlled Drug Delivery: Historical perspective for the next generation. *J. Controlled Release* **219**, 2–7 (2015).
33. Rosen, H. & Abribat, T. The rise and rise of drug delivery. *Nat. Rev. Drug Discov.* **4**, 381–385 (2005).
34. Global Markets and Technologies for Advanced Drug Delivery Systems. (2015).
35. Uhrich, K. E., Cannizzaro, S. M., Langer, R. S. & Shakesheff, K. M. Polymeric Systems for Controlled Drug Release. *Chem. Rev.* **99**, 3181–3198 (1999).
36. Makadia, H. K. & Siegel, S. J. Poly Lactic-co-Glycolic Acid (PLGA) as Biodegradable Controlled Drug Delivery Carrier. *Polymers* **3**, 1377–1397 (2011).
37. Danhier, F. *et al.* PLGA-based nanoparticles: An overview of biomedical applications. *J. Controlled Release* **161**, 505–522 (2012).
38. Anderson, L. C., Wise, D. L. & Howes, J. F. An injectable sustained release fertility control system. *Contraception* **13**, 375–384 (1976).
39. Anderson, J. M. & Shive, M. S. Biodegradation and biocompatibility of PLA and PLGA microspheres. *Adv. Drug Deliv. Rev.* **64**, 72–82 (2012).
40. Gopferich, A. Mechanisms of polymer degradation and erosion. *Biomaterials* **17**, 12 (1996).
41. Park, T. G. Degradation of poly(lactic-co-glycolic acid) microspheres: effect of copolymer composition. *Biomaterials* **16**, 1123–1130 (1995).
42. Park, T. G. Degradation of poly(d,l-lactic acid) microspheres: effect of molecular weight. *J. Controlled Release* **30**, 161–173 (1994).
43. Approval Package for Lupron Depot, 4 Months, 30 mg, Leuprolide Acetate. Application Number: 020517/S002. (1997).

44. Park, K. *et al.* Injectable, long-acting PLGA formulations: Analyzing PLGA and understanding microparticle formation. *J. Controlled Release* **304**, 125–134 (2019).
45. O'Donnell, P. B. & McGinity, J. W. Preparation of microspheres by the solvent evaporation technique. *Adv. Drug Deliv. Rev.* **28**, 25–42 (1997).
46. Berkland, C., Kim, K. K. & Pack, D. W. Fabrication of PLG microspheres with precisely controlled and monodisperse size distributions. **73**, 59–74 (2001).
47. Allison, S. D. Analysis of initial burst in PLGA microparticles. *Expert Opin. Drug Deliv.* **5**, 615–628 (2008).
48. Berkland, C., King, M., Cox, A., Kevin, K. & Pack, D. W. Precise control of PLG microsphere size provides enhanced control of drug release rate. *J. Controlled Release* **82**, 137–147 (2002).
49. Mitragotri, S. In Drug Delivery, Shape Does Matter. *Pharm. Res.* **26**, 232–234 (2009).
50. Han, F. Y., Thurecht, K. J., Whittaker, A. K. & Smith, M. T. Bioerodable PLGA-Based Microparticles for Producing Sustained-Release Drug Formulations and Strategies for Improving Drug Loading. *Front. Pharmacol.* **7**, (2016).
51. Berkland, C., King, M., Cox, A., Kim, K. (Kevin) & Pack, D. W. Precise control of PLG microsphere size provides enhanced control of drug release rate. *J. Controlled Release* **82**, 137–147 (2002).
52. Jain, R. A. The manufacturing techniques of various drug loaded biodegradable poly(lactide-co-glycolide) (PLGA) devices. *Biomaterials* **21**, 2475–2490 (2000).
53. Wang, Y., Li, P., Truong-Dinh Tran, T., Zhang, J. & Kong, L. Manufacturing Techniques and Surface Engineering of Polymer Based Nanoparticles for Targeted Drug Delivery to Cancer. *Nanomaterials* **6**, 26 (2016).

54. Wischke, C. & Schwendeman, S. P. Principles of encapsulating hydrophobic drugs in PLA/PLGA microparticles. *Int. J. Pharm.* **364**, 298–327 (2008).
55. Freitas, S., Merkle, H. P. & Gander, B. Microencapsulation by solvent extraction / evaporation: reviewing the state of the art of microsphere preparation process technology. *J. Controlled Release* **102**, 313–332 (2005).
56. Dlugi, A. M., Miller, J. D. & Knittle, J. Lupron\*\*TAP Pharmaceuticals, North Chicago, Illinois. depot (leuprolide acetate for depot suspension) in the treatment of endometriosis: a randomized, placebo-controlled, double-blind study ††Supported by a grant from TAP Pharmaceuticals, North Chicago, Illinois. *Fertil. Steril.* **54**, 419–427 (1990).
57. Syed, Y. Y. & Keating, G. M. Extended-Release Intramuscular Naltrexone (VIVITROL®): A Review of Its Use in the Prevention of Relapse to Opioid Dependence in Detoxified Patients. *CNS Drugs* **27**, 851–861 (2013).
58. Li, M., Rouaud, O. & Poncelet, D. Microencapsulation by solvent evaporation: State of the art for process engineering approaches. *Int. J. Pharm.* **363**, 26–39 (2008).
59. Mohamed, F. & van der Walle, C. F. Engineering Biodegradable Polyester Particles With Specific Drug Targeting and Drug Release Properties. *J. Pharm. Sci.* **97**, 71–87 (2008).
60. Hamdy, S., Haddadi, A., Hung, R. W. & Lavasanifar, A. Targeting dendritic cells with nano-particulate PLGA cancer vaccine formulations. *Adv. Drug Deliv. Rev.* **63**, 943–955 (2011).
61. Champion, J. A. & Mitragotri, S. Role of target geometry in phagocytosis. *Proc. Natl. Acad. Sci.* **103**, 4930–4934 (2006).

62. Champion, J. A., Katare, Y. K. & Mitragotri, S. Particle shape: A new design parameter for micro- and nanoscale drug delivery carriers. *J. Controlled Release* **121**, 3–9 (2007).
63. Li, W.-I., Anderson, K. W. & Deluca, P. P. Kinetic and thermodynamic modeling of the formation of polymeric microspheres using solvent extraction/evaporation method. *J. Controlled Release* **37**, 187–198 (1995).
64. Li, M. *et al.* Wrinkling Non-Spherical Particles and Its Application in Cell Attachment Promotion. *Sci. Rep.* **6**, 30463 (2016).
65. Kumari, A., Yadav, S. K. & Yadav, S. C. Biodegradable polymeric nanoparticles based drug delivery systems. *Colloids Surf. B Biointerfaces* **75**, 1–18 (2010).
66. Langer, R. Drug delivery and targeting. **392**, 6 (1998).
67. Davidov-Pardo, G. & McClements, D. J. Resveratrol encapsulation: Designing delivery systems to overcome solubility, stability and bioavailability issues. *Trends Food Sci. Technol.* **38**, 88–103 (2014).
68. Isely, C. *et al.* Development of microparticles for controlled release of resveratrol to adipose tissue and the impact of drug loading on particle morphology and drug release. *Int. J. Pharm.* **568**, 118469 (2019).
69. Veisheh, O. *et al.* Size- and shape-dependent foreign body immune response to materials implanted in rodents and non-human primates. *Nat. Mater.* **14**, 643–651 (2015).
70. Jindal, A. B. The effect of particle shape on cellular interaction and drug delivery applications of micro- and nanoparticles. *Int. J. Pharm.* **532**, 450–465 (2017).
71. Isely, C., Stevens, A. C., Tate, G. L., Monnier, J. R. & Gower, R. M. Fabrication of biodegradable particles with tunable morphologies by the addition of resveratrol to oil in water emulsions. *Int. J. Pharm.* **590**, 119917 (2020).

72. Nicolas, J., Mura, S., Brambilla, D., Mackiewicz, N. & Couvreur, P. Design, functionalization strategies and biomedical applications of targeted biodegradable/biocompatible polymer-based nanocarriers for drug delivery. *Chem Soc Rev* **42**, 1147–1235 (2013).
73. Kamaly, N., Xiao, Z., Valencia, P. M., Radovic-Moreno, A. F. & Farokhzad, O. C. Targeted polymeric therapeutic nanoparticles: design, development and clinical translation. *Chem. Soc. Rev.* **41**, 2971 (2012).
74. Lee, S. C., Oh, J. T., Jang, M. H. & Chung, S. I. Quantitative analysis of polyvinyl alcohol on the surface of poly ( D , L -lactide-co-glycolide ) microparticles prepared by solvent evaporation method : effect of particle size and PVA concentration. *J. Controlled Release* **59**, 123–132 (1999).
75. Wei, Z. Mannose\_ Good player and assister in pharmacotherapy. 6 (2020).
76. Geijtenbeek, T. B. H. & Gringhuis, S. I. Signalling through C-type lectin receptors: shaping immune responses. *Nat. Rev. Immunol.* **9**, 465–479 (2009).
77. Barratt, G., Tenu, J.-P., Yapo, A. & Petit, J.-F. Preparation and characterisation of liposomes containing mannosylated phospholipids capable of targeting drugs to macrophages. *Biochim. Biophys. Acta BBA - Biomembr.* **862**, 153–164 (1986).
78. Yu, S. S. *et al.* Macrophage-Specific RNA Interference Targeting via “Click”, Mannosylated Polymeric Micelles. *Mol. Pharm.* **10**, 975–987 (2013).
79. Phanse, Y. *et al.* Functionalization of polyanhydride microparticles with di-mannose influences uptake by and intracellular fate within dendritic cells. *Acta Biomater.* **9**, 8902–8909 (2013).

80. Shilakari Asthana, G., Asthana, A., Kohli, D. V. & Vyas, S. P. Mannosylated Chitosan Nanoparticles for Delivery of Antisense Oligonucleotides for Macrophage Targeting. *BioMed Res. Int.* **2014**, 1–17 (2014).
81. Langcake, P. & Pryce, R. J. The production of resveratrol by *Vitis vinifera* and other members of the Vitaceae as a response to infection or injury. *Physiol. Plant Pathol.* **10** (1976).
82. Bishayee, A. Cancer Prevention and Treatment with Resveratrol: From Rodent Studies to Clinical Trials. *Cancer Prev. Res. (Phila. Pa.)* **2**, 409–418 (2009).
83. De la Lastra, C. A. & Villegas, I. Resveratrol as an anti-inflammatory and anti-aging agent: Mechanisms and clinical implications. *Mol. Nutr. Food Res.* **49**, 405–430 (2005).
84. Gülçin, İ. Antioxidant properties of resveratrol: A structure–activity insight. *Innov. Food Sci. Emerg. Technol.* **11**, 210–218 (2010).
85. Szkudelska, K. & Szkudelski, T. Resveratrol, obesity and diabetes. *Eur. J. Pharmacol.* **635**, 1–8 (2010).
86. Chang, C.-C., Lin, K.-Y., Peng, K.-Y., Day, Y.-J. & Hung, L.-M. Resveratrol exerts anti-obesity effects in high-fat diet obese mice and displays differential dosage effects on cytotoxicity, differentiation, and lipolysis in 3T3-L1 cells. *Endocr. J.* **63**, 169–178 (2016).
87. Amri, A., Chaumeil, J. C., Sfar, S. & Charrueau, C. Administration of resveratrol : What formulation solutions to bioavailability limitations? *J. Controlled Release* **158**, 182–193 (2012).

88. Kapetanovic, I. M., Muzzio, M., Huang, Z., Thompson, T. N. & McCormick, D. L. Pharmacokinetics, oral bioavailability, and metabolic profile of resveratrol and its dimethylether analog, pterostilbene, in rats. *Cancer Chemother. Pharmacol.* **68**, 593–601 (2011).
89. Alberdi, G. *et al.* Changes in white adipose tissue metabolism induced by resveratrol in rats. *Nutr. Metab.* **8**, 29 (2011).
90. Spogli, R. *et al.* Solid Dispersion of Resveratrol Supported on Magnesium DiHydroxide (Resv@MDH) Microparticles Improves Oral Bioavailability. *Nutrients* **10**, 1925 (2018).
91. Gokce, E. H. *et al.* Wound healing effects of collagen-laminin dermal matrix impregnated with resveratrol loaded hyaluronic acid-DPPC microparticles in diabetic rats. *Eur. J. Pharm. Biopharm.* **119**, 17–27 (2017).
92. Trotta, V. *et al.* Brain targeting of resveratrol by nasal administration of chitosan-coated lipid microparticles. *Eur. J. Pharm. Biopharm.* **127**, 250–259 (2018).
93. Gower, R. M. *et al.* Modulation of leukocyte infiltration and phenotype in microporous tissue engineering scaffolds via vector induced IL-10 expression. *Biomaterials* **35**, 2024–2031 (2014).
94. Liu, J. M. H. *et al.* Transforming growth factor-beta 1 delivery from microporous scaffolds decreases inflammation post-implant and enhances function of transplanted islets. *Biomaterials* **80**, 11–19 (2016).
95. Murphy, K. P. *et al.* Resveratrol Delivery from Porous Poly(lactide- *co* -glycolide) Scaffolds Promotes an Anti-Inflammatory Environment within Visceral Adipose Tissue. *ACS Appl. Mater. Interfaces* **10**, (2018).



96. Cayman Chemical. Product Information trans-Resveratrol (CAS 510-36-0).
97. Rawat, A. & Burgess, D. J. Effect of ethanol as a processing co-solvent on the PLGA microsphere characteristics. *Int. J. Pharm.* **394**, 99–105 (2010).
98. Ito, F. *et al.* Study of types and mixture ratio of organic solvent used to dissolve polymers for preparation of drug-containing PLGA microspheres. *Eur. Polym. J.* **45**, 658–667 (2009).
99. Sahoo, S. K., Panyam, J., Prabha, S. & Labhasetwar, V. Residual polyvinyl alcohol associated with poly (D,L-lactide-co-glycolide) nanoparticles affects their physical properties and cellular uptake. *J. Controlled Release* **82**, 105–114 (2002).
100. Berg, J. C. *An Introduction to Interfaces and Colloids: The Bridge to Nanoscience*. (WORLD SCIENTIFIC, 2009). doi:10.1142/7579.
101. Liu, S., Deng, R., Li, W. & Zhu, J. Polymer Microparticles with Controllable Surface Textures Generated through Interfacial Instabilities of Emulsion Droplets. *Adv. Funct. Mater.* **22**, 1692–1697 (2012).
102. Berkland, C., Kim, K. & Pack, D. W. PLG Microsphere Size Controls Drug Release Rate Through Several Competing Factors. *Pharm. Res.* **20**, 1055–1062 (2003).
103. Chen, W., Palazzo, A., Hennink, W. E. & Kok, R. J. Effect of Particle Size on Drug Loading and Release Kinetics of Gefitinib-Loaded PLGA Microspheres. *Mol. Pharm.* **14**, 459–467 (2017).
104. Dawes, G. J. S. *et al.* Size effect of PLGA spheres on drug loading efficiency and release profiles. *J. Mater. Sci. Mater. Med.* **20**, 1089–1094 (2009).

105. Raman, C., Berkland, C., Kevin, K. & Pack, D. W. Modeling small-molecule release from PLG microspheres: effects of polymer degradation and nonuniform drug distribution. **103**, 149–158 (2005).
106. Iwakura, Y. & Okada, H. THE KINETICS OF THE REACTION OF ORGANIC ISOTHIOCYANATES WITH 1-OCTANOL IN *o* -DICHLOROBENZENE. *Can. J. Chem.* **40**, 2369–2375 (1962).
107. Miazgowski, T. *et al.* Visceral fat reference values derived from healthy European men and women aged 20-30 years using GE Healthcare dual-energy x-ray absorptiometry. *PLOS ONE* **12**, e0180614 (2017).
108. VIVITROL® (naltrexone for extended-release injectable suspension). (2018).
109. Ogawa, Y., Yamamoto, M., Okada, H., Yashiki, T. & Shimamoto, T. A new technique to efficiently entrap leuprolide acetate into microcapsules of polylactic acid or copoly(lactic/glycolic) acid. *Chem. Pharm. Bull. (Tokyo)* **36**, 1095–1103 (1988).
110. Su, Z.-X. *et al.* Biodegradable poly(D, L-lactide-co-glycolide) (PLGA) microspheres for sustained release of risperidone: Zero-order release formulation. *Pharm. Dev. Technol.* **16**, 377–384 (2011).
111. Hussain, M. *et al.* Biodegradable Polymer Microparticles with Tunable Shapes and Surface Textures for Enhancement of Dendritic Cell Maturation. *ACS Appl. Mater. Interfaces* **11**, 42734–42743 (2019).
112. Lee, B. K., Yun, Y. & Park, K. PLA micro- and nano-particles. *Adv. Drug Deliv. Rev.* **107**, 176–191 (2016).

113. Banerjee, A., Qi, J., Gogoi, R., Wong, J. & Mitragotri, S. Role of nanoparticle size, shape and surface chemistry in oral drug delivery. *J. Controlled Release* **238**, 176–185 (2016).
114. Mohamed, F. & van der Walle, C. F. PLGA microcapsules with novel dimpled surfaces for pulmonary delivery of DNA. *Int. J. Pharm.* **311**, 97–107 (2006).
115. Ulery, B. D., Nair, L. S. & Laurencin, C. T. Biomedical applications of biodegradable polymers. *J. Polym. Sci. Part B Polym. Phys.* **49**, 832–864 (2011).
116. Wojdyr, M. *Fityk* : a general-purpose peak fitting program. *J. Appl. Crystallogr.* **43**, 1126–1128 (2010).
117. Brunauer, S., Emmett, P. H. & Teller, E. Adsorption of Gases in Multimolecular Layers. *J. Am. Chem. Soc.* **60**, 309–319 (1938).
118. Rotenberg, Y., Boruvka, L. & Neumann, A. W. Determination of surface tension and contact angle from the shapes of axisymmetric fluid interfaces. *J. Colloid Interface Sci.* **93**, 169–183 (1983).
119. Riddick, J. A., Bunger, W. B., Sakano, T. & Weissberger, A. *Organic solvents: physical properties and methods of purification*. (Wiley, 1986).
120. Banerjee, Sujit. Solubility of organic mixtures in water. *Environ. Sci. Technol.* **18**, 587–591 (1984).
121. Schneider, G. M. A. L. Horvath: Halogenated Hydrocarbons. Solubility - Miscibility with Water, Marcel Dekker, Inc., New York, Basel 1982. 889 Seiten, Preis: 310 SFr. *Berichte Bunsenges. Für Phys. Chem.* **87**, 289–289 (1983).

122. Sah, H. Microencapsulation techniques using ethyl acetate as a dispersed solvent: effects of its extraction rate on the characteristics of PLGA microspheres. *J. Controlled Release* **47**, 233–245 (1997).
123. Hines, D. J. & Kaplan, D. L. Poly(lactic-co-glycolic) Acid-Controlled-Release Systems: Experimental and Modeling Insights. *Crit. Rev. Ther. Drug Carrier Syst.* **30**, 257–276 (2013).
124. Rolland, J. P. *et al.* Direct Fabrication and Harvesting of Monodisperse, Shape-Specific Nanobiomaterials. *J. Am. Chem. Soc.* **127**, 10096–10100 (2005).
125. Champion, J. A., Walker, A. & Mitragotri, S. Role of Particle Size in Phagocytosis of Polymeric Microspheres. *Pharm. Res.* **25**, 1815–1821 (2008).
126. Kissel, T. *et al.* Parenteral depot-systems on the basis of biodegradable polyesters. *J. Controlled Release* **16**, 27–41 (1991).
127. Vliegenthart, G. A. & Gompper, G. Compression, crumpling and collapse of spherical shells and capsules. *New J. Phys.* **13**, 045020 (2011).
128. Witten, T. A. Stress focusing in elastic sheets. *Rev. Mod. Phys.* **79**, 643–675 (2007).
129. Andhariya, J. V. *et al.* Development of in vitro-in vivo correlation of parenteral naltrexone loaded polymeric microspheres. *J. Controlled Release* **255**, 27–35 (2017).
130. Liu, Q. *et al.* Use of Polymeric Nanoparticle Platform Targeting the Liver To Induce Treg-Mediated Antigen-Specific Immune Tolerance in a Pulmonary Allergen Sensitization Model. *ACS Nano* **13**, 4778–4794 (2019).
131. Shae, D. *et al.* Endosomolytic polymersomes increase the activity of cyclic dinucleotide STING agonists to enhance cancer immunotherapy. *Nat. Nanotechnol.* **14**, 269–278 (2019).

132. Son, S. *et al.* Sugar-Nanocapsules Imprinted with Microbial Molecular Patterns for mRNA Vaccination. *Nano Lett.* **20**, 1499–1509 (2020).
133. Zhang, F. *et al.* Genetic programming of macrophages to perform anti-tumor functions using targeted mRNA nanocarriers. *Nat. Commun.* **10**, 3974 (2019).
134. Datta, S. S., Shum, H. C. & Weitz, D. A. Controlled Buckling and Crumpling of Nanoparticle-Coated Droplets. *Langmuir* **26**, 18612–18616 (2010).
135. Cullberg, K. B., Foldager, C. B., Lind, M., Richelsen, B. & Pedersen, S. B. Inhibitory effects of resveratrol on hypoxia-induced inflammation in 3T3-L1 adipocytes and macrophages. *J. Funct. Foods* **7**, 171–179 (2014).
136. Wang, L. *et al.* Effect of resveratrol or ascorbic acid on the stability of  $\alpha$ -tocopherol in O/W emulsions stabilized by whey protein isolate: Simultaneous encapsulation of the vitamin and the protective antioxidant. *Food Chem.* **196**, 466–474 (2016).
137. Allavena, P., Chieppa, M., Monti, P. & Piemonti, L. From Pattern Recognition Receptor to Regulator of Homeostasis: The Double-Faced Macrophage Mannose Receptor. *Crit. Rev. Immunol.* **24**, 179–192 (2004).
138. Zhang, J. *et al.* Negative regulatory role of mannose receptors on human alveolar macrophage proinflammatory cytokine release in vitro. 10.
139. Rajaram, M. V. S. *et al.* *Mycobacterium tuberculosis* Activates Human Macrophage Peroxisome Proliferator-Activated Receptor  $\gamma$  Linking Mannose Receptor Recognition to Regulation of Immune Responses. *J. Immunol.* **185**, 929–942 (2010).
140. Heming, M. *et al.* Peroxisome Proliferator-Activated Receptor- $\gamma$  Modulates the Response of Macrophages to Lipopolysaccharide and Glucocorticoids. *Front. Immunol.* **9**, 893 (2018).

141. Hatami, E. *et al.* Mannose-decorated hybrid nanoparticles for enhanced macrophage targeting. *Biochem. Biophys. Rep.* **17**, 197–207 (2019).
142. D’Addio, S. M. *et al.* Optimization of cell receptor-specific targeting through multivalent surface decoration of polymeric nanocarriers. *J. Controlled Release* **168**, 41–49 (2013).
143. Goates, S. *et al.* ECONOMIC IMPACT OF HOSPITALIZATIONS IN US ADULTS WITH SARCOPENIA. **8**, 7 (2019).
144. Augustin, M. A., Sanguansri, L. & Lockett, T. Nano- and micro-encapsulated systems for enhancing the delivery of resveratrol: Enhanced resveratrol delivery by encapsulation. *Ann. N. Y. Acad. Sci.* **1290**, 107–112 (2013).
145. Hendley, M. A. *et al.* The host response to poly(lactide-co-glycolide) scaffolds protects mice from diet induced obesity and glucose intolerance. *Biomaterials* **217**, 119281 (2019).
146. Hendley, M. A. *et al.* Scaffold Implant Into the Epididymal Adipose Tissue Protects Mice From High Fat Diet Induced Ectopic Lipid Accumulation and Hyperinsulinemia. *Front. Bioeng. Biotechnol.* **8**, 562 (2020).
147. Kerrigan, A. M. & Brown, G. D. C-type lectins and phagocytosis. *Immunobiology* **214**, 562–575 (2009).
148. Yeeprae, W., Kawakami, S., Yamashita, F. & Hashida, M. Effect of mannose density on mannose receptor-mediated cellular uptake of mannosylated O/W emulsions by macrophages. *J. Controlled Release* **114**, 193–201 (2006).

## APPENDIX A

### PLG PARTICLE FABRICATION BEST PRACTICES

PLG particle fabrication is a central technique used in the Gower lab. It is a somewhat complicated process that can be very sensitive to small changes in the protocol. One thing to keep in mind is that small things in the protocol (like vortexing the PLG solution and evaporation time of the extraction bath) can actually have a big impact on the final microparticle product. As such, I would like to include some tips and tricks I have learned over the years. Li et al. 2008 is a great primer on this fabrication process<sup>58</sup>. The general PLG particle fabrication protocol is kept on the Gower lab drive, but what follows are some additional considerations I would like to mention.

First, any particle fabrication may end up being used in cell culture or an animal study. It is very important that aseptic conditions be used as much as possible. The homogenizer is cleaned before and after fabrication as follows: 5 minutes in acetone, 5 minutes in ethanol, 5 minutes in water and 5 minutes in water at 11,00rpm. Use fresh clean 20 mL scintillation vials for dissolving PLG and drug in the organic phase. Keep vials and centrifuge tubes closed and only open them in the hood when it is time to add what is inside to the emulsion. When it is time to do the wash steps, bring the beakers into the laminar flow hood. Filter and remove supernatant in there.

Second, quality of PVA is important. Make up a fresh PVA solution the day before fabrication. Dissolving PVA in water requires heat and takes a while to dissolve, so give

yourself a few hours for this process. Store PVA in the 4C refrigerator. I found that larger concentrations of PVA (2-5 wt/v%) do not store for a long time, in other words the PVA begins to precipitate out of solution after about a week. As a general rule, I would not use PVA that is over a week old. If possible, use PVA the day after you make it to avoid this issue. In terms of the concentration of PVA, it is not feasible to go higher than 5% wt/v with the 18,000 Da PVA we use in the lab. It will not dissolve easily and will also precipitate when it is cooled. Concentrations as low as 0.1% wt/v are feasible, but the emulsion will begin to lose stability and the particle size distribution will increase at this concentration.

Third, use new scintillation vials for every beaker of particles you make. I found that making a stock solution of particles and dipping in for every emulsion resulted in inconsistent mass yields and particle loading values. Make sure to vortex the vial right before you add it to the emulsion. Also, use a fresh 40 um filter for each condition you are doing during the wash step (you can re-use the filter for replicates of the same condition).

For washing the homogenizer use a glass slide jar and fill it with the solvents you are using (there is a jar that is used just for particle fabrication washing). Wash the homogenizer tip between fabrications of different conditions. This will prevent cross-contamination. Two washes for 30secs in acetone and one in water should be sufficient. This cleans any residue off the tip and also prevents cross contamination.

Particle size is dependent on PLG concentration in the organic phase, homogenization speed, and centrifugation speed. In particular, centrifugation speed can be used to “purify” a size of interest. Slower speeds do not settle the smallest particles, and you can “tighten” your size distribution by running at slower speeds to remove submicron



particles. This is a product of the stokes law for sedimentation which dictates that sedimentation rate is dependent on particle size, density and viscosity of the medium among several things. The speed to purify a certain size range is dependent on the instrument used and the distance needed to settle (length of your centrifugation tube). For example, in our system I found that 250xg settles 2 um particles efficiently when spun for 10 minutes in the large centrifuge in the basement lab (SWG009).

Homogenization speed can also control size, but I don't recommend running the homogenizer at speeds higher than 11,000 rpm. Higher speeds in our emulsion medium made loud noises in the homogenizer. As a result, adjusting PLG concentration is the other option for making different sizes. I found that it is not feasible to go to less than 1% wt/wt (PLG/DCM) in the system for two reasons. One is the mass yield is too low to be usable. And the second is that going lower did not produce significant changes in the size of the particles. As a result, with this process the smallest particles I was able to produce, all things considered, were between 1 and 2 microns. As such, this technique is not suitable for making nanoparticles, but modifications such as using a probe sonicator could make that possible in the future. Also, the largest particles I was able to produce were nearly 30 microns, and this could be achieved with high PLG % such as 12% wt/wt, low homogenization such as 7,000rpm and settling via gravity (let tube sit for 10 minutes on the lab bench and then remove supernatant). Resveratrol particles were usually larger than 30 um, but they were a special case as I outlined in this dissertation.

The length of time for evaporation/extraction and the bath volume are also very important to particle fabrication. Extraction rate can affect the drug loading of particles which was a major source of investigation of Maddie Spetz, a former student in the lab.


We initially added an emulsion with 0.6 mL of DCM 4 mL PVA to an extraction bath of 16 mL. This is a DCM vol% of 3 which is higher than its solubility in water (around 2%). As a result, we increased this to 80 mL in the extraction bath which ensures DCM is always soluble. In addition, we found that extracting for 1 hour was sufficient for evaporating away DCM (which is highly volatile) and 1 hour extraction is now the standard of practice.

Add organic solution slowly to the PVA during the emulsion step. PVA should be measured out and put in a 50 mL centrifuge tube and PLG solution should be handled with a Hamilton syringe. After you have vortexed the vial, take up the organic solution into the Hamilton syringe. Then start the homogenizer and begin adding the solution slowly into the 50 mL tube. It is most likely that the organic solution and PVA can be added at the same time and then begin homogenization. However, I never studied this possibility extensively so future students can take that question on if they wish. Most literature suggests adding the organic phase slowly.

These are my major pieces of wisdom. There are many parameters that can be controlled in this process and sometimes it is important to run your own experiments to understand how they affect the system. If you have any questions contact me at [chris.isely11@gmail.com](mailto:chris.isely11@gmail.com). If you are a future student in the lab, good luck with your experiments, and thank you for reading until the end!

## APPENDIX B

### MANUSCRIPT PERMISSIONS



**Development of microparticles for controlled release of resveratrol to adipose tissue and the impact of drug loading on particle morphology and drug release**

**Author:** Christopher Isely, Michael A. Hendley, Kendall P. Murphy, Safaa Kader, Prakasam Annamalai, Esmail Jabbari, R. Michael Gower

**Publication:** International Journal of Pharmaceutics

**Publisher:** Elsevier


**Date:** 10 September 2019

© 2019 Elsevier B.V. All rights reserved.

**Journal Author Rights**

Please note that, as the author of this Elsevier article, you retain the right to include it in a thesis or dissertation, provided it is not published commercially. Permission is not required, but please ensure that you reference the journal as the original source. For more information on this and on your other retained rights, please visit: <https://www.elsevier.com/about/our-business/policies/copyright#Author-rights>

BACK CLOSE WINDOW



**Fabrication of biodegradable particles with tunable morphologies by the addition of resveratrol to oil in water emulsions**

**Author:** Christopher Isely, Alexandra C. Stevens, Gregory L. Tate, John R. Monnier, R. Michael Gower

**Publication:** International Journal of Pharmaceutics

**Publisher:** Elsevier

**Date:** 30 November 2020

Published by Elsevier B.V.

**Journal Author Rights**

Please note that, as the author of this Elsevier article, you retain the right to include it in a thesis or dissertation, provided it is not published commercially. Permission is not required, but please ensure that you reference the journal as the original source. For more information on this and on your other retained rights, please visit: <https://www.elsevier.com/about/our-business/policies/copyright#Author-rights>

BACK CLOSE WINDOW

**Figure B.1 Copyright permissions for publications reprinted in this dissertation.**